COMMUNICATIONS

Dear reader,

The present volume of the journal Communications is devoted to the problems of biomedical engineering solved mainly by the University of Zilina and some of its partners. Biomedical engineering (BME) represents very broad interdisciplinary and progressively developing field of activities connected with technical problems of medicine. The scientific and educational program of BMI started at the Faculty of Electrical Engineering of the University of Zilina in the year 1999 after completing the Tempus Phare project, which was oriented to this topic. Scientific program of our Department of Electrical and Biomedical Engineering and cooperating departments of the faculty is concerned with problems of modelling of physiological processes by means of electromechanical analogy, influence of electromagnetic field on the human organism, medical informatics, processing of medical images and processing of biomedical signals. Problems of biomaterials are solved in cooperation with the Faculty of Mechanical Engineering of the University of Zilina. The main partner of Faculty of Electrical Engineering of the University of Zilina in the study and research programs of BME is the Jessenius Medical Faculty of the Comenius University in Martin. Our faculty cooperates also with the Institute of Measurement of the Slovak Academy of Science in Bratislava and other institutions. The main international partners are the University of Technology – RWTH Aachen, Germany, and the National University of Ireland in Dublin, Ireland, which gave us many valuable ideas both in the field of research and education. During the last ten years the University became with its program of biomedical instrumentation and information technologies the significant part of biomedical engineering research and educational system in the Slovak Republic.

We appreciate the possibility to present a brief review of some research results of the Faculty of Electrical Engineering of the University of Zilina and its partners in the field of BME and to offer cooperation with similarly oriented institutions.

Ivo Cap

Vladimir Blazek *

BIOMEDICAL TECHNOLOGY – 2011 AND BEYOND

Fundamental advances in knowledge and understanding across a range of specialized fields in medicine, biology, engineering and other natural sciences; the discovery of novel sensor concepts for non-invasive function diagnostics of diseases and abnormal developments at early stages; the development of cost-effective, automated measuring procedures that can be miniaturized to the cellular and molecular level; the implementation of new imaging techniques for optimized therapies and therapy-control – these are just some of the reasons for the rapid growth of biomedical technology as an independent field of study and research in the past decades.

Furthermore, in a contemporary health-policy context marked by health-insurances', patients' and society's demands for reduced health spending, the advances and high-quality, interdisciplinary knowledge available in biomedical technology today have a highly significant role to play in medico-technical process optimization and cost-benefit analyses.

There is increasing demand for highly competent staff with the interdisciplinary qualifications and open-mindedness needed to venture beyond the core areas – staff capable of realizing innovative, individual advances in a structured way, while also advancing the field as a whole. Thus the question as to the future prospects of biomedical technology and the young generation of students, researchers and professionals can be decisively answered: "exciting, promising and highly rewarding."

All in all, biomedical technology continues to be both an excellent profession and field of study and research at the intersection of animate and inanimate matter – though excellence always comes with responsibility.

1. Selective hindsight into the history of medical technology is beneficial for new excellence initiatives

Medicine, especially in the past five decades, has made highly significant progress and thereby achieved marked improvements in the diagnosis, treatment and prevention of different diseases. Biomedical technology, an autonomous and recognized field of study since the mid-twentieth century as well as a bridge between medicine and engineering sciences [1, 2], has contributed enormously to these advances. Thus, in Germany alone, the number of organ transplants (including live-donor transplants) since 2000 has increased by 25% since 2000 [3]. Nonetheless, some 12 000 patients in Germany are currently waiting for a donor organ. At present, medico-technical progress is a trend that continues unabated, and has led to the quality of life and life expectancy we enjoy today – unthinkable in former generations.

However, interdisciplinary thinkers and innovators in medical technology are nothing new. Over many centuries, a wide and diverse range of experimental, theoretical and technological discoveries have contributed to our present standard of living. Thus the ancient Egyptians already had an astonishing concept of the human vascular system. Homer, in his poetry, mentions blood vessel injuries; Hippocrates, the most-famed doctor of antiquity, was the first to describe the function of the aortic valves; Aristotle knew the aorta, the vena cava and its tributaries; while Claudius already recognized the existence of pulse waves in the second century B.C.

Nonetheless, many more centuries were needed for the functionalities of the human body to be discovered and understood. Thus in 1492, Leonardo da Vinci (1452–1519) drew the Vitruvian Man in one of his diaries, while around the same time Albrecht Dürer (1471–1528) undertook a first attempt to determine the proportions of the human body and render the movement of bodies in space by mathematical means – a far from trivial problem of descriptive spatial geometry. One can therefore justly identify Dürer as the founder of biometrics, although the term was used explicitly only in 1841 by Christoph Bernoulli (1782–1863).

The discovery and localization of the heart as motor of circulation and impulse-creating system was achieved around 1618 by William Harvey (1578–1657), who is therefore recognized as the founder of modern medicine. His calculation of the heart's pumping rate is the first significant application of mathematics in the physiology of circulation; but he too severely underestimated the heart's pumping capacity – he assumed that the left ventricle expelled approximately ½ an ounce (18 grams) of blood per minute. He multiplied this quantity by 1000 heart beats in half an hour and calculated a total of 500 ounces of blood. It appeared logical to him that such a quantity of blood could impossibly be produced somewhere in the body in such a short time and thus – through a simple quantitative examination – Harvey discovered the closed blood circulation system. Many more discoveries were to follow, which cannot all be listed here. Interested readers can find some of the most significant and highly instructive advances in the natural sci-

* **Vladimir Blazek**
Philips Chair of Medical Information Technology, Helmholtz Institute for Biomedical Engineering, RWTH Aachen University, Aachen, Germany
Email: blazek@hia.rwth-aachen.de

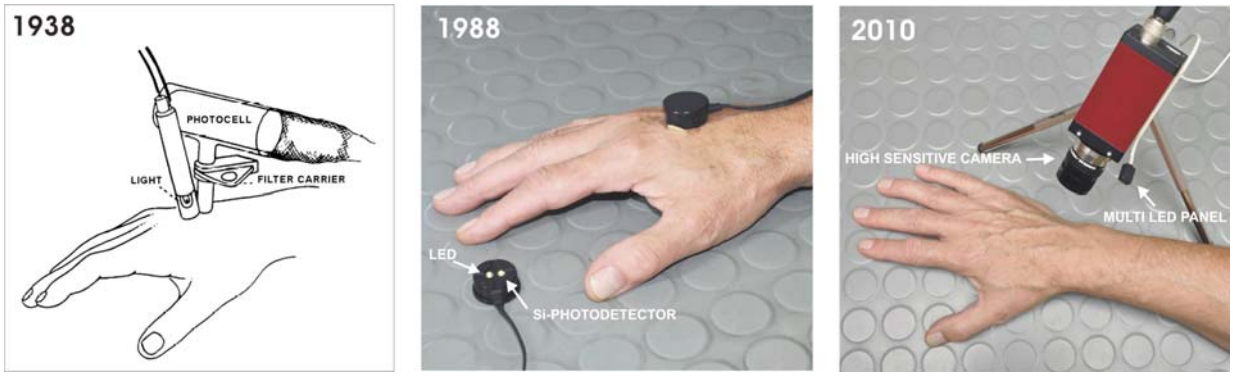

Fig. 1 Progress in photoplethysmography and its sensor concepts: First optoelectronic sensor by Hertzman [6] with incandescent lamp as polychromatic light source and selenium cell as photo detector (left); a PPG sensor on the market today (middle); new video camera-based PPGI sensor (right).

ences, which ultimately came to culminate in our present day medical system, summarized in the literature [4]

2. Exemplary technological and diagnostic progress: from the Hertzman Plethysmograph in 1938 to the contactless Photoplethysmographic Imager in 2011

As only one example of progress in biomedical diagnostic systems in recent years, this chapter presents recent advances and developments in classical photoplethysmography (PPG) and the role played by the novel camera-based, contactless photoplethysmography Imaging method (PPGI®) and the quantification of space-resolved dermal blood circulation changes in a resting state, as well as after defined pharmacological and mechanical skin irritations.

Optoelectronic sensor concepts have come to play an important role in functional blood circulation diagnosis because of their non-invasive and non-damming nature. They are generally accepted by patients not only during vascular screening-examinations since they cause neither pain, nor harmful radiation or ionizing phenomena. Analogously to classical PPG with skin attached discrete sensors, PPGI utilizes the fact that blood has a much higher absorption in the visible and near-infrared spectrum than the surrounding bloodless tissue. When illuminating the skin with a selective light source, a detector can assess the optical attenuation, which is modulated by the time-variable blood content.

Using a highly sensitive video camera as a detector array brings advantages over the current state-of-the-art technology: not only a non-invasive assessment of the dermal blood perfusion status can be performed in vivo – it is also contactless and spatially resolved. A wide spectrum of new applications of optoelectronic sensor systems in functional peripheral vascular diagnostics is hereby opened.

The experimental details and perfusion signal processing and visualization strategies by the PPGI system will be explained with some clinically relevant examples and perfusion protocols. The analysis of the PPGI video sequences can either be done interactively by selecting skin regions for which the skin perfusion is calculated, or automatic algorithms for functional mapping can be executed. Together with the necessary software tools, a sound basis for assessment, evaluation and visualization of space-resolved dermal perfusion changes is provided.

2.1. Hertzman's discovery in 1938

After the pioneering work by Matthes [5], Cartwright, Haxthausen and Molitor et al., Alrick B. Hertzman, Physiologist at St. Louis University School of Medicine, discovered a relationship between the intensity of backscattered polychromatic light and blood volume in the skin in 1938. His instruments consisted of three essential components still found in modern systems: a light source, a light detector (Fig. 1 left) and a registration unit. He called the device photoelectric plethysmograph and described his findings ([6], p. 336):

- "Volume pulse of the skin as an indicator of the state of the skin circulation at rest" and,
- "amplitude of volume pulse as a measure of the blood supply of the skin".

The basic principle behind the measurement of blood volume changes in the skin by means of PPG is the simple fact that hemoglobin in the blood absorbs infrared light many times more strongly than the remaining skin tissues (Fig. 2), [7–9]. For example, as blood pressure in the skin vessels decreases, the surface area of the vessels is reduced. This increases the average reflection in the measuring window under the sensor, so it will be recorded as an increase in PPG signal. Following this principle, the PPG signal reflects the blood volume changes in the cutaneous and partially also the subcutaneous vessel plexus and consists of a high constant part which is independent from the perfusion (light scattering in tissue), a smaller quasi static vein signal and a very small, periodical modulated arterial signal (Fig. 3). Therefore this non-invasive technique allows one to acquire functional data from the dermal venous and/or arterial circulation.

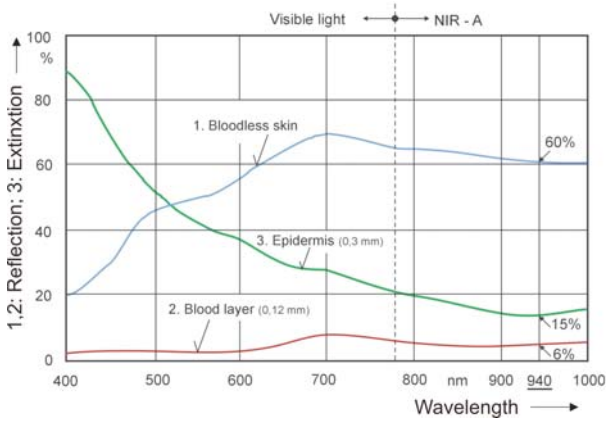

Fig. 2 Optical properties of human skin and blood in the visible and near-infrared area of the spectrum. Typical reflection spectra of anemic skin and of a 0.12 mm thick blood layer on glass are shown as well as an extinction spectrum of a 0.3 mm epidermal layer. The difference in reflectivity between the skin tissue and the blood is evident and results in a high optical contrast between skin and dermal vessel plexus. The optical attenuation of the epidermis is very high in the ultraviolet and blue regions and lowest at IR wavelengths of about 950 nm.

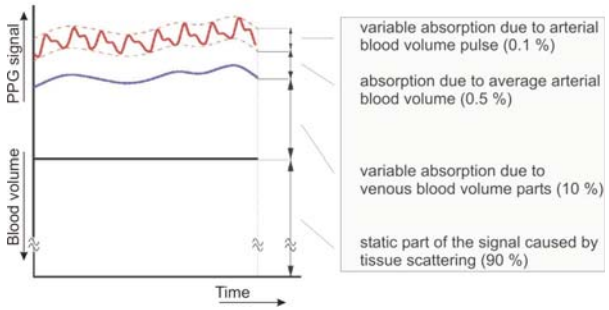

Fig. 3 Composition of the photoplethysmographic signal. The intensity of the backscattered light depends on the blood volume in arterial and venous vessels in the measuring zone. Reducing blood volume in the monitored area under the PPG sensor increases the PPG signal. A separation of venous and arterial parts of the detected signal is possible by electronic signal-filtering.

In contrast to the conventional PPG version with skin-attached discrete sensors (Fig. 1 in the middle), PPGI operates remotely, i.e. not in contact with the tissue. The measured large area of the skin is illuminated by quasi monochromatic LED light of selected wavelengths and is filmed by the camera from a distance of typically 50 cm. This detects small fluctuations in the tissue brightness, which is synchronous with the venous and / or arterial blood-volume dynamics. The fluctuations are caused by parts of the light which are reflected or transmitted towards the camera by passing the skin tissue.

2.2. The Photoplethysmographic Imager – functions and typical recordings

The PPG Imager was developed at the RWTH Aachen University [7–9] and is a computer-based system comprising both hardware and software parts (Figs. 4 and 5). The core of the PPGI

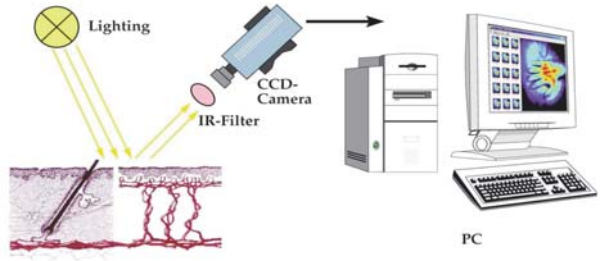

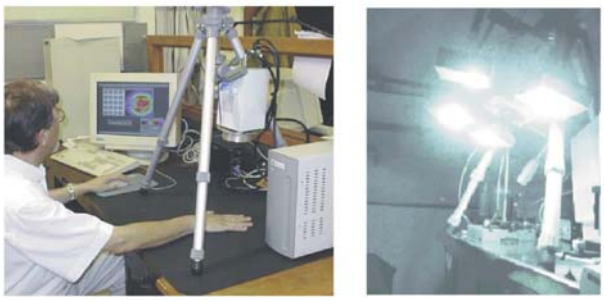

Fig. 4 Photoplethysmography Imaging setup. The skin is illuminated by a custom LED floodlight (different wavelengths can be selected), the backscattered light intensity dynamics are recorded by a high-sensitivity CCD camera.

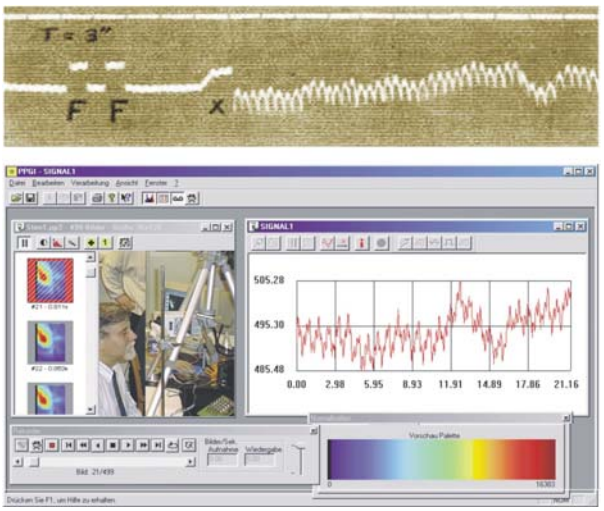

Fig. 5 Comparison of typical photoplethysmograms of the forehead taken in 1938 (above) and 2010 (below), illustrating progress in medical devices using modern computer aided detection and visualization strategies. To quantify plethysmograms in terms of arbitrary units, Hertzman [6] had to insert a filter in front of the detector manually (two F-marked signal steps in the registration below). Today calibration is fully automated [8].

is an imaging strategy capable of contactless recording, processing and displaying of image sequences of the selected skin area, so as to visualize the skin vessels and analyze dermal perfusion. The selected body area is illuminated by monochromatic light (multiple LED panels). In contrast to Hertzman's original device and all other plethysmographs on the market, we use green light to visualize the arterial skin perfusion, as this spectral range offers a good optical contrast between blood and skin tissue and the limited penetration of this light enables a targeted collection of perfusion dynamics in the microcirculation area of the skin [9]. The size of the observed skin/body region and the spatial resolution can be arbitrarily chosen, depending on the utilized camera lens and distance between camera and measuring object. To minimize motion artifacts, which can be created by the separation of the camera sensor from the skin, we prefer measurements in the recumbent patient; the selected skin region is fixed in a foam cup.

To detect the weak light modulation backscattered from the skin, which is caused by the arterial perfusion (dermal blood volume pulse), a high-sensitivity scientific camera has to be used. Our setup utilizes the UltraPix FE 250 camera from Life Science Resources because of its high dynamic range of 14 Bits and high readout speed of 5.5 MB/s. The sensor, a silicon frame-transfer black-white CCD chip with a pixel volume of 512 × 512, is sensitive in the visible and near infrared range of the spectrum. Typical PPGI recording lasts about 100 seconds, consisting of nearly 1.000 images of the same scenario and has a mean data volume of 700 MB.

In the 'interactive operator' system-mode, the observer can directly select one or more arbitrary regions of interest (ROI) in the test field after each video sequence. For these marked regions, the mean backscattered light intensity is calculated and displayed as a perfusion sensitive parameter over time. An example of (not spatially resolved) 1 ROI PPGI registration, which can be compared with the classical PPG-examination, is shown in Fig. 5.

A particular advantage of PPGI systems is the ability to freely select several skin areas in the same measurement scenario in order to analyze and visualize the spatial resolution in perfusion dynamics. A typical recording with three closely adjacent and corresponding PPGI signals can be seen in Fig. 6, done on a left hand with a small fresh wound in the skin of the middle finger. As can be seen, the perfusion patterns from healthy skin and the wound on the middle finger show significant differences. When looking only at the heart beat, it is slightly increased inside the wound; however, the slow rhythms of about 0.1 Hz are strongly reduced inside the wound. Not only is it possible to discriminate the wound and the healthy skin when comparing the different three regions, it is also apparent that the low perfusion pattern has strong local variation. Even the two ROIs on healthy skin at a distance of a few mm show evident differences in the 0.1 Hz band.

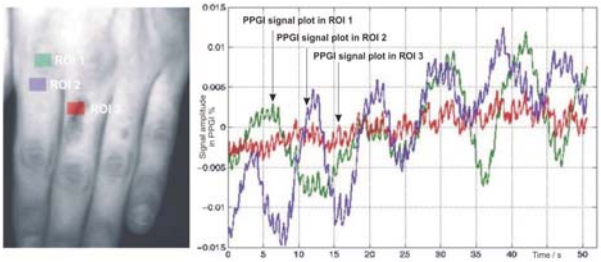

Fig. 6 PPGI recordings of a hand with a wound on the middle finger. Calculated photoplethysmograms (blood volume changes against time) in the three selected ROIs. The curves allow a direct comparison of blood perfusion in the healthy skin and the small fresh wound close by. The absence of lower frequency vasomotion rhythms in the wound-area is clearly visible.

2.2.1. Advanced signal processing provides new insights into the phenomenon of distributed dermal blood-circulation rhythmicity

When trying to analyze further the perfusion patterns with a classical Fourier transform (FT), not much new information is revealed. It is possible to recognize differences at low frequencies; however the resolution is quite limited. The frequency spectrum can't reveal much advanced information, the reason being that the FT is not well suited for analysis of transient signals.

However, using the Wavelet transform (WT), many new insights into the distributed perfusion patterns are obtained. An example of a WT of PPGI signals from Fig. 6 is shown in Fig. 7. Here, the evolution of different frequency components (vertical axis) can be directly recognized against time (horizontal axis). For the first time, the generated advanced PPGI signal visualization reveals that the slow rhythms in the skin perfusion are not stationary but fluctuate in amplitude and also slightly in frequency.

Apart from the strong temporal fluctuations in dermal perfusion, a new behavior of distributed spatial rhythm fluctuations was observed in our lab at IHF/RWTH Aachen University. This phenomenon, which can only be observed in animated video representations of the PPGI recordings, consists of "blood volume clouds" moving on the forehead in a coherent but complicated pattern [10, 11]. Fig. 8 tries to illustrate this with screenshots of a recording; for the animated video presentation please refer to the web page http://www.medit.hia.rwth-aachen.de/aw/cms/medit/Themen/forschung/~ttj/Photoplethysmographie_Imaging_PPGI_/?lang=en

2.2.2. Completely detached – assessment of human hemodynamics under micro-gravity

Astronauts complain about fluid shifts from their lower extremities to the head caused by weightlessness during flight in space. To study this phenomenon, RWTH Aachen University in cooperation with Charité University Berlin participated in two parabolic flight campaigns undertaken by the German Aerospace Centre (DLR) in September 2005 and June 2006 (the 7th and 8th DLR parabolic flight campaigns in Bordeaux and Cologne respectively). The characteristics of the rapid fluid shifts during hyper- and

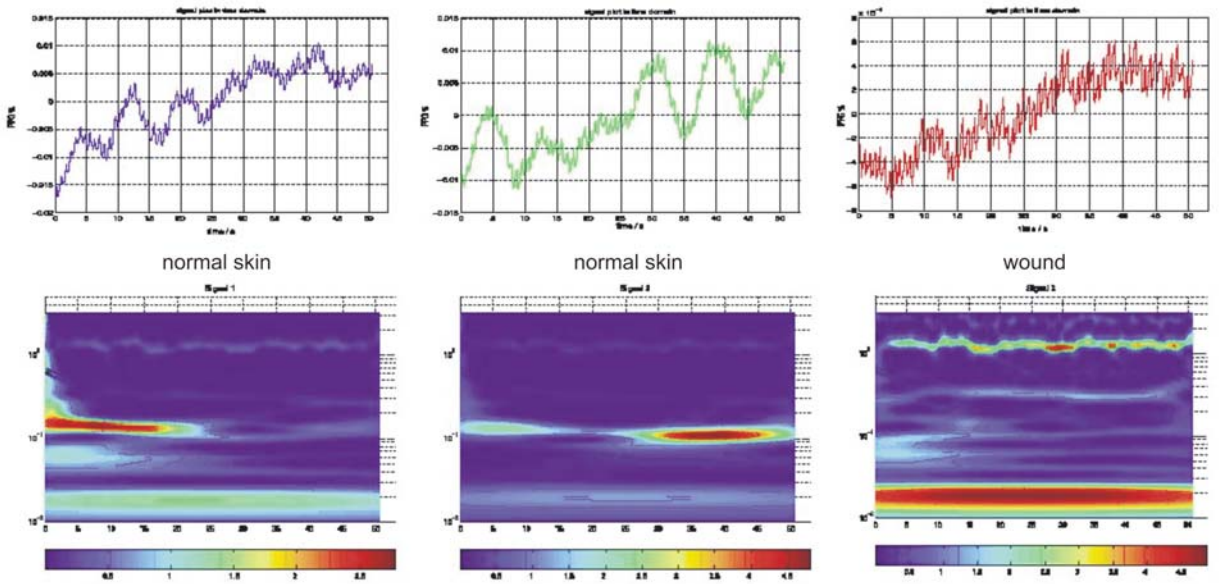

Fig. 7 Example of advanced analysis of transient signals: Wavelet transform of selected PPG signals from Fig. 6.

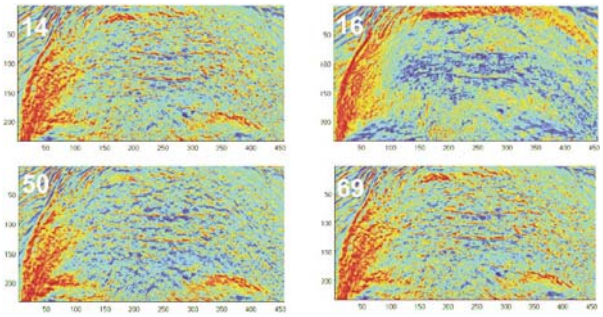

Fig. 8 Distributed "blood volume clouds" observed with PPGI on the forehead of a subject in sitting position and relaxed steady state, first observed in 2005. The post-processed and -colored pictures show perfusion coded images taken at 14, 16, 50 and 69 seconds of a PPGI video sequence.

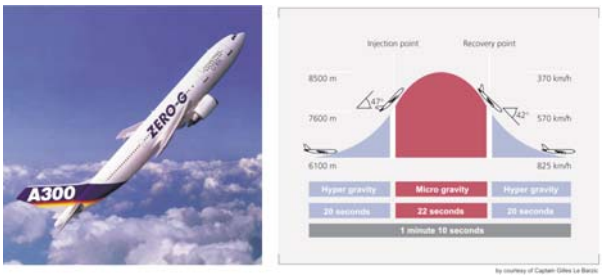

Fig. 9 Novespace Airbus A 300 Zero-G directly before initiation of the micro-gravity phase (left), flight phases of the parabolic maneuver (right).

micro gravity were measured in flight by a combination of PPG and PPGI optoelectronic sensor systems.

For the parabolic flight campaign, a specially prepared Airbus A300 is equipped with up to twelve separate experiments from different university research groups. The campaign consists of 4 to 5 flight days. In one flight, the aircraft accomplishes 31 parabola maneuvers. These flight maneuvers follow a special trajectory, resulting in up to 22 seconds of microgravity conditions inside of the aircraft (Fig. 9). The maneuver is divided into 3 phases. In phase one, the aircraft gradually pulls up its nose from a steady horizontal position and starts climbing at an angle of approximately 47 degrees. This "injection" phase takes about 20 seconds, during which the aircraft experiences an acceleration of around 1.8 times the gravity level at ground, i.e. 1.8 g. The engine thrust is then reduced to the minimum required to compensate for air drag, and the aircraft follows a free-fall ballistic trajectory – i.e. a parabola – lasting approximately 22 seconds, during which weightlessness is achieved. At the end of this period, the aircraft must pull out of the parabolic arc, a maneuver which gives rise to another 20-second period of 1.8 g inside the aircraft, after which it returns to normal-level flight altitude. Thus, the entire parabolic phase takes about 1 minute. These maneuvers are flown repeatedly, with a period of 3 minutes between the start of two consecutive parabolas, so that there is a 2 minute "rest" period at 1g. After parabolas 10 and 20 however, the resting interval is increased to 6 minutes.

Viewing the data from different subjects participating in the flights ascertained that fluid shifts occurred in all subjects. This proves that the small time span of about 20 seconds of a single parabola is already sufficient for a clear detection. Furthermore, and as predicted, a clear shift from the lower body parts to the head was verified.

Fig. 10 shows typical PPG measurements. These recordings were taken from one male and one female subject, using sensors with green and infrared light sources. They were placed on the subjects' foreheads. The detected light-intensity changes are displayed in curve 1 (green light) and 2 (infrared light). The lower black curve shows the development of g-forces during the parabola. As

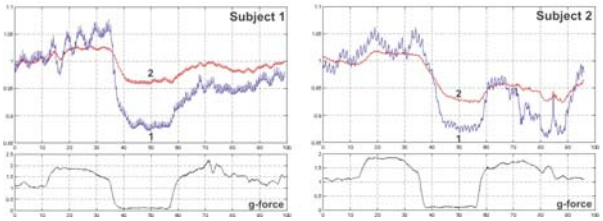

Fig. 10 Dynamics of blood volume shifts of two subjects during the parabolic flight maneuver. Measuring point on the forehead, using green (1) and infrared (2) light sources, normalized at start of measurement.

can clearly be seen, the detected backscattered light intensity is in rapid decline immediately after the implementation of zero-gravity. This corresponds to an increasing blood volume in the transilluminated skin beneath the sensor. Astonishingly, comparing the data of the different subjects reveals that all of them reacted very quickly to the altered gravitational force. The time span between a change of gravity and the minimum detected light intensity (or maximum if measured at the legs) was very short (only a few seconds) [12].

3. Modern technology and medicine in tandem: new diagnostic concepts and medical strategies pave the way into the future of Telemedicine, Homecare and Ambient-Assisted Living

Diagnostic measuring methods based on biomedical technology are in widespread use today, typically involving patients' visits to a doctor or a hospital, where measurements are then made. However, in certain circumstances patients are too far away from the required facilities – be it while traveling in remote regions, or even inside an orbiting spaceship. A range of telemedical sensor concepts, systems solutions and procedures – some already on the brink of clinical implementation – have been developed for such situations. These include:

- Intra-corporal telemetric diagnostic and monitoring systems for physical (e.g. bladder pressure) and chemical (e.g. intra-corporal laboratory) parameters,
- Mobile diagnostics using "labs-on-chips" (e.g. in aeronautical medicine),
- Autonomously active, telemetrically controlled implants (e.g. cardiac pacemakers, gastric pacers, nerve-stimulating devices, etc.),
- Implantable and extra-corporal modular micro-system platforms,
- Wearable smart medical devices and intelligent wearable devices,
- Extra-corporal telemetric diagnostic and monitoring systems for personal healthcare,
- Miniaturized sensor systems for 24/7 surveillance of high-risk cardiovascular patients.

Pioneering these developments in Germany is the "Micro-Medicine" initiative launched by the Germany Society for Biomedical Technology (DGBMT), part of the Association of Electrical Engineering (VDE) [13]. With help of substantial research funds, the initiative supports and accompanies the introduction of new micro-medical procedures and, co-jointly with renowned professionals from all parts of the healthcare system, has successfully established telemedicine/disease management, neuro-prosthetics and instrument/implant invasivity as key research areas.

The advantages of improved efficiency in medical care, including home care, due to these ongoing biomedical research and development projects are apparent. While patients and doctors mostly take a positive view of telemedical applications, the entire economic, technical and legal framework is still evolving. Propriety systems in hospitals and doctors' practices are one reason why companies and investors are still reluctant to market specialized solutions and products.

The following illustrations show two exemplary developments from our research group at RWTH Aachen, respectively concerned with micro-sensor systems for long-term applications and tele-self-monitoring.

A 24/7 monitoring system based on a micro-optic in-ear PPG sensor was developed for early diagnosis of irregularities in the human cardiovascular system [14] (Fig. 11). By means of a miniaturized electronic unit, the native plethysmogram can simultaneously be acquired for selected wavelengths and processed locally by a microcontroller. The resulting signal is then transferred wirelessly to a personal digital assistant (PDA) or PC, where heartbeat, heartbeat variability, oxygen saturation (SPO2), breathing and slower perfusion rhythms can be evaluated. The sensor geometry was optimized for the novel in-ear application scenario by means of Monte Carlo Simulations [11].

Tele-medical procedures have been used since approx. 30 years. For example, already in 1984, an on-board ECG was transmitted

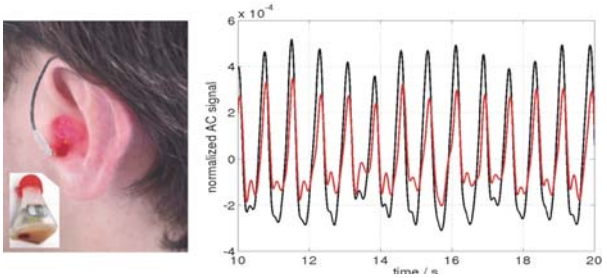

Fig. 11 Miniaturized optoelectronic sensor concept for in-ear pulse oximetry and typical photoplethysmograms obtained simultaneously for infrared and red illumination.

from a cargo ship around the entire globe. Telemedicine is useful for bridging large distances between doctors (with diagnostic systems) and patients, or between general and specialist doctors– notably during long-distance travel and expeditions, as well as in military or space missions [15]. Likewise, healthcare systems in countries with small and highly dispersed populations have long since taken an interest in such systems.

Nonetheless, a frequent disadvantage of telemedicine is the lack of bio-data sensor systems on site. Here, standard mobile telephones will soon offer a viable alternative (Fig. 12), since today's integrated video-camera technology is in principle already capable

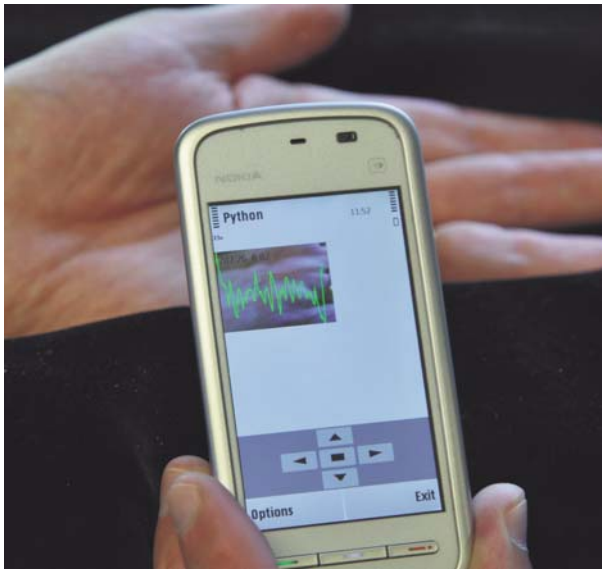

Fig. 12 Tele-monitoring of skin perfusion using a standard mobile phone. For online self-monitoring, data recorded by the camera is passed continuously to a tele-monitoring center. In case of (non-acute) retro-monitoring, data can be recorded first (and preprocessed at regular intervals), then forwarded on.

of recording and transmitting patients' vital parameters – such as local skin perfusion in the case of injured, inflamed or wounded skin – to 24h call-centers with qualified medical staff. If needed, a doctor can establish contact with patients to guide them through a 'cinematographic' recording of the relevant parameters, inform them about their condition, suggest appropriate measures, or dispatch on-site medical assistance, such as the well-known Flying Doctors in Australia.

4. Training and studying of biomedical technology

Present and future healthcare systems are becoming ever more technical. Making effective use of today's possibilities and know-how requires more than just engineers or doctors. More than ever before, what is needed now are competent experts with interdisciplinary working knowledge of the intersections between medicine, man and technology, and possessing the ability to think and communicate pluralistically – in accordance with the varied distribution of competencies across different disciplines.

University degree courses in Biomedical Engineering focusing precisely on these qualifications are on offer in virtually all European countries. The degrees are organized in consecutive parts, depending on the particular specializations and degree structures offered by different universities (vocational bachelor degrees or research-oriented master's degrees, with subsequent doctoral programs). Most degrees are still situated in the faculties of electrical engineering, since the theoretical foundations of electrical engineering and information technology form an important basis for medical technology. More and more combined medical-technology degrees are offered jointly by different universities, such as in Stuttgart (engineering sciences) and Tübingen (medicine) as of winter term 2010/11. International compatibility is also set to increase amongst partner universities and courses offered by various national bodies.

Graduates, in particular those with master's degrees, can find suitable employment in many areas:

- Research institutes and universities
- Hospitals and healthcare systems
- Companies in various areas of medicine and medical products
- Pharmaceutical industry
- Biotechnology companies
- National and international bodies
- Self-employment

Their qualifications equip them with a broad knowledge base in engineering sciences, are in highly demanded and honored accordingly by industry, and enable them to quickly and competently specialize in different areas. Thus all students of biomedical disciplines can look confidently towards the future – and be part of it.

5. Concluding remarks and outlook

In summary, one can say that if medical treatment today has become subject to evaluation as never before, this is in no small part due to biomedical technology. It provides us with impressive data on both the efficacy and costs of a treatment.

Needless to say, the applications of biomedical technology briefly outlined here represent only a very limited and subjective selection. Around the world, intensive research is underway in many other important areas, such as the quantification of pain sensations, e.g. in caring for mother and fetus (incl. prenatal and perinatal pain sensations), as well as in early- and new-born children. For a long time, babies and small children have been considered less pain-sensitive in relation to adults, and the reactions of early- and new-born children to pain were classified accordingly as subcortical (and thus unconscious) reflexes [16]. While pain was thus rightly viewed as a subjective experience, it was almost exclusively relegated into the domain of conscious, speakable and cognitively apprehended adult experience. This assessment is increasingly considered to be mistaken [17, 18].

Likewise, research and development of adapted Ambient Assisted Living (AAL) systems solutions and in particular of assistance systems for elderly and handicapped people is on the increase. While these and other modern sub-areas of biomedical technology are today still in their infancy, they are certain to become highly significant in future, not least due to demographic trends.

On the other side, achieving this requires policy-makers' clear commitment to research and financial support of the healthcare system. Yet the politicians who look to Lancet, Nature or Science as a basis for decision-making and allocation of public funds are few – if any [19].

Nonetheless, the future of biomedical technology is assured. We can all count on this technology, as well as standing to benefit from it personally – bearing in mind that excellence comes with responsibility.

Acknowledgements

The author would like to acknowledge the financial support of the German Research Foundation (DFG grant BL200/9-1 and BL200/9-2 "Beruhrungsloses, kamerabasiertes Meßsystem zur nichtinvasiven praventiven Erkennung lokaler Anderungen und Defekte der Hautdurchblutung mittels CCD-Videotechnik im Sichtbaren und nahen Infrarot"), the German Aerospace Center (DLR, contract No. PF#-7/5 "Visualizing and quantifying rapid fluid shifts along the body axis in humans during parabolic flights"), the German Federal Ministry of Education and Research (R&D grand 16SU2261 „INohr-implementiertes MONIToringsystem zur Praventiven Uberwachung der Herz-Kreislauf Funktion von Risikopatienten IN-MONIT" in the MicroSystems Technology Framework Program) and of the Czech Republic Ministry of Education, Youth and Sports (MSM grant 6840770012 "Trans-disciplinary research in the area of Biomedical Engineering II") for his research work presented in this paper.

References

[1] LUSCHER, T. F.: Gibt es kosteneffiziente Fortschritte in der Medizin? *Kardiovaskulare Medizin,* No. 8, 2005, pp. 39–40
[2] HUTTEN, H.: Quo vadis BMT? *Biomedizinische Technik / Biomedical Engineering,* No. 43/S1, (1998), pp. 4–7
[3] Source: DSO, Eurotransplant, 20100823-DE01
[4] GEREON, A.: Science and Technology in Medicine, An Illustrated Account Based on Ninety-Nine Landmark Publications from Five Centuries, *Springer Science+Busines Media,* New York, 2006, ISBN: 978-0387-30171-6
[5] MATTHES, K.: Untersuchungen uber die Sauerstoffsättigung des menschlichen Arterien blutes. *Arch. Exp. Path. Pharmacol.*, 179 (1935), pp. 698–711
[6] HERTZMAN, A. B.: The Blood Supply of Various Skin Areas as Estimated by the Photoelectric Plethysmograph. *Amer. J. Physiol.,* No. 124, 1938, pp. 329–340
[7] HERTZMAN, A. B., DILLON, J. B.: Applications of Photoelectric Plethysmography in Peripheral Vascular Diseases. *Amer. Heart J.,* No. 20, 1940, pp. 750–761
[8] BLAZEK, V., SCHULTZ-EHRENBURG, U.: Quantitative Photoplethysmography. Basic Facts and Examination Tests for Evaluating Peripheral Vascular Functions. *VDI Verlag Dusseldorf,* (1996), ISBN 3183192209
[9] SCHULTZ-EHRENBURG, U., BLAZEK, V.: Value of Quantitative Photoplethysmography for Functional Vascular Diagnostics. *Skin Pharmacol Appl. Skin Physiol,* No. 14, 2010, pp. 316–323
[10] HULSBUSCH, M., BLAZEK, V.: Rhythmical Phenomena in Dermal Perfusion – Proved Assessment Strategies and New Discoveries. *Advances in Electrical and Electronic Engineering,* No. 3, Vol. 4, 2005, pp.112–117
[11] HULSBUSCH, M.: *A Functional Imaging Technique for Optoelectronic Assessment of Skin Perfusion.* PhD thesis, 2008, RWTH Aachen University
[12] BLANIK, N., HULSBUSCH, M., HERZOG, M., BLAZEK, CLAUDIA, R.: *Assessment of Human Hemodynamics under Hyper- and Micro Gravity: Results of two Aachen University parabolic flight experiments. Acta Polytechnica,* 47, 4–5, 2007, 29–32
[13] www.vde.de/de/fg/dgbmt/arbeitsgebiete/mikromedizin/seiten/imm-homepage.aspx
[14] VOGEL, S., HULSBUSCH, M., HENNING, T., BLAZEK, V., LEONHARDT, S.: In-Ear Vital Sings Monitoring Using a Novel Micro-Optic Reflective Sensor. *IEEE Transactions on Information Technology in Biomedicine,* Vol. 13, No. 6, 2009, pp. 882–889
[15] JACKL, A. (Hrsg): Telemedizinfuhrer Deutschland, *Jahrbuch der Telemedizin,* Bad Neuheim, 2007, ISBN 978-3-937948-06-5.
[16] MERSKEY, H.: On the Development of Pain. *Headache,* No. 10, 1970, pp. 116–123
[17] ANAND, K.J.S., HICKEY, P.R.: Pain and its Effects in the Human Neonate and Fetus. *N. Engl. J. Med.,* No. 317, 1987, pp. 1321–1329
[18] RUTTER, N., DOYAL, L.: Neonatal Care and Management of Pain Historical and Ethical Notes. *Semin Neonataln,* No. 3, 1998, pp. 297–302
[19] HELD, K.: Editorial, *Flug-Medizin,* 13. Jahrgang, 48, 2006, p. 3.

Ivo Cap – Jan Barabas *

LOW FREQUENCY ELECTROMAGNETIC FIELDS: FRIEND OR FOE?

The issue of electromagnetic fields and their effects on human health has long been discussed within the scientific community. The lack of undisputable evidence confirming the dangers of these fields leads to great uncertainty and public concerns. On the other hand, positive effects and possible therapeutic use of the mentioned fields has also been explored and currently hints at feasible application thereof in regenerative and therapeutic applications. The following article provides a balanced insight into the issue at hand and provides details of recently proposed mechanisms of actions.

Keywords: Electromagnetic field, Bio–electromagnetism, Electric properties of Cells, Electromagnetic Smog, Electromagnetic Therapy.

1. Introduction

Electricity in every conceivable form has become an integral part of our everyday lives. Many daily tasks that we perform depend on it and there is no sign that the *current* progress will slow down any time soon. However, because living organisms evolved over billions of years in a world with a reasonably weak magnetic field and with few electromagnetic (EM) energy sources, they interacted with and adapted to this specific range of EM fields (EMF). Thus, due to the widespread presence of new EMF sources, health issues have been brought up because we still lack a thorough understanding of the fundamental properties of these fields.

Since the first observations of health disturbances related to long-term exposure to electric power line configurations were reported 20 years ago, there has been a goodly amount of scientific discussion about the bioeffects of extremely low frequency magnetic fields (ELF-MF). While the basics of electromagnetic interaction with materials were elucidated over a century ago and stated as the well-known Maxwell's equations, the application of these basics to biological systems is very difficult because of the extreme complexity and multi-level organization in living organisms. This difficulty has slowed the progress of understanding the EM bioeffects and phenomena that might directly influence our health. Nevertheless, it is clear that any explanation is beyond the scope of conventional physics and that we must concentrate our efforts at the cellular and subcellular level, where the smallest of changes could trigger the greatest of damage, Jakusova [1].

The purpose of this article is to attempt to give a balanced overview of the issue at hand, including review of select health studies in this field, proposal of therapeutic applications and elucidation of novel mechanisms of action based on the modulation of membrane voltage, paving the road to forthcoming venues for guiding morphogenesis both in tissue engineering and in regenerative medicine.

2. Health issues and considerations

Health concerns are especially associated with carcinogenic or co-carcinogenic effects of electromagnetic fields. Herein reviewed studies indicate no clear link between low frequency EMF (LF–EMF) and increased cancer risk, although childhood leukemia increase has been documented in several epidemiological and toxicological studies.

Karipidis et al. [2] examined low and high grade glioma risk in various patients. A group of 414 histologically confirmed glioma cases and a group of 421 controls from Melbourne, Australia were matched by age, sex and postcode of residence. Results indicate increased glioma and HGG (high–grade glioma) cases in expert hygienist methodologies, though not of statistical significance.

Incidence of kinase 4 inhibitor gene ($p18^{INK4C}$) deletion and/or mutation in electric energy workers was explored by Erdal et al. [3]. A choice of 31 male electric workers and 30 healthy males between 30 – 40 years of age and in the same geographical area and with similar lifestyles was selected. While exon 1 band migration was indifferent in all participants, exon 2 of two electric workers was slow in migration with respect to the controls. However, the limited results do not suggest any significant risk of cancer increase.

Both Johansen and Olsen [4] and [5] conducted a study among male and female electric utility workers in Denmark. The total number of subjects was 32 006, and while increased cancer

* **Ivo Cap, Jan Barabas**
Faculty of Electrical Engineering, University of Zilina, Slovakia, E-mail: ivo.cap@fel.uniza.sk

was predicted, only slightly higher rates of occurrence were reported and no excess of brain cancer, leukemia or breast cancer were reported.

Cumulative effects of both electric and magnetic fields were investigated by Miller et al. [6]. In their report the authors observed an increase in leukemia, especially due to mutual electric and magnetic field exposure. However, in another study involving 764 adults, Willett et al. [7] found little evidence between occupational EM exposure and acute leukemia.

Childhood leukemia accounts for approximately one third of all child cancers. A summary of select childhood leukemia studies is presented in Table 1:

Childhood leukemia studies Table 1

Study conductor	Number of subjects	Results
Verkasalo et al.[8]	35 cases, <17 years old	General increase of leukemia risk; brain tumor (only boys)
McBride et al.[9]	596 cases, <15 years old	Elevated risk in all subjects
Savitz et al.[10]	448 cases, <15 years old	Elevated risk in all subjects
Linen et al.[11]	1026 cases, <19 years old	No correlated risk increase
Schuz et al.[12]	489 cases, N/A years old	Moderate increase in childhood leukemia, though not statistically significant

The exact mechanism of action is unknown, although a melatonin-based hypothesis was proposed by Henshaw and Reiter [13], in which magnetic fields from power lines suppress the nocturnal melatonin production of the pineal gland. Moreover, mutual gene-environment interactions need also be considered.

Cellular and animal studies, on the other hand, provide no evidence of direct DNA damage or tumor growth. Another reason to consider is the abstractness when comparing in-vitro and in-vivo setups, whereby the former lack natural reparatory and regulatory mechanisms present in their natural environments. Other physiological effects, such as heart rate variability, melatonin suppression, sleep disturbances or anomalous EEG activity, while reported, do lack any consistent results and raise questions whether these are solely tied to electromagnetic exposure or rather represent a risk cofactor.

3. Emerging regenerative and therapeutic methods

Over the past years, numerous studies have observed positive effects of controlled low frequency electromagnetic field exposure. The following studies highlight two most prominent regenerative applications – soft tissue and bone repair although they have not explained or quantified the observed effects in a satisfactory fashion. However they incited further research in this area and possible mechanisms of actions are discussed in detail further down this article.

The viability of ELF EMFs in soft tissue regeneration after injury was investigated by Vianale et al. [14]. In their study they applied ELF magnetic fields (1 mT intensity, 50 Hz frequency) to human keratinocyte cell line (HaCaT) and evaluated keratinocyte proliferation and production of various proinflammatory chemokines. Accelerated growth was observed after 48 hours of exposure when compared to the control group, but no difference in cell viability was detected. Proinflammatory chemokine production was reduced significantly after 72 hours of exposure. Especially sensitive to the applied field was the NF-κB signaling pathway which decreased to almost non-detectable levels after just one hour of exposure, inversely correlated with cell density. These findings indicate the possible favorable role of ELF electromagnetic fields in wound healing through keratinocyte growth stimulation and reduction of chemokines.

Effectiveness of ELF electromagnetic fields in modifying specific biochemical properties of human skin keratynocytes (HaCaT) was also evaluated by Lisi et al. [15]. In their ventures, the authors applied 7 Hz ELF electromagnetic fields with intensities of 100 μT for one hour, twice daily, which resulted in both shape and morphological changes, which are attributed to different actin distribution. The authors, based on evidence of increased expression of both differentiation and adhesion markers (involucrin, β-catenin) further conclude that higher level keratinocyte expression was achieved.

Lisi et al. [15] reported similar observations as those by Cricenti et al. [16]. Infrared wavelength-selective scanning near-field optical microscopy was again used to examine HaCaT cells post 24 hour exposure to alternating magnetic fields (sinusoidal shape, 1 mT intensity, 50 Hz frequency). Reflectivity studies at both wavelengths ($\lambda_1 = 6.45$ μm and $\lambda_2 = 3.04$ μm) univocally reveal an increase of newly synthesized protein and different phospholipids distribution. This finding coincides with a previous study conducted by the same authors and confirms increased segregation in the cell membrane of the sulfur rich protein marker B4 integrin. Additional structural and morphological changes were also detected which lead to increase in adhesion area between individual cells.

Potential therapeutic application of pulsed electromagnetic fields in rheumatoid arthritis (RA) was evaluated by Selvam et al. [17]. RA was induced in rats using heat-killed *Mycobacterium tuberculosis*. Observed were increased levels of lipid peroxides and depletion of antioxidant enzymes, however more interesting is the decrease of plasma membrane Ca^{2+} ATPase (PMCA) activity and elevated levels of intracellular Ca^{2+} and prostaglandin E2 levels. The affected limb was then exposed to 5 Hz, 4 μT PEMF for 90 minutes, which resulted in restoration of the altered parameters and a pronounced antiexudative effect. The reasoning behind this is through the stabilizing effect of pulsed electromagnetic fields on cellular membranes as experienced via PMCA and Ca^{2+} level

restoration leading to inhibition of prostaglandin E_2 levels, indicating a possible use in supportive treatment of human rheumatoid arthritis.

Adenosine receptor affinity and density in view of PEMFs was explored by Varani et al. [18]. The authors discovered that the 75 Hz, 1mT generated field mediated an upregulation of certain adenosine receptors and leads to a functional increase thereof in bovine chondrocytes and fibroblast-like synoviocytes, without altering adenosine affinity and drug-receptor interactions. These finding suggest that PEMFs could positively influence inflammatory joint diseases.

Possible use of various ELF-EMF types in bone fracture therapy was explored by Zhang et al. [19]. Four electromagnetic field types were investigated: rectangular (REMF), triangular (TEMF), sinusoidal (SEMF) and pulsed (PEMF), all of which showed different effects (proliferation, differentiation, mineralization) on osteoblast cells obtained from rat calvaria bones.

Wei et al. [20] applied PEMFs with a frequency of 48 Hz and intensity of 1.55 mT to both rat-derived osteoblast cells and MC3T3-E1 cells. Based on their experiments, the authors noted that the used PEMFs "did not affect proliferation and differentiation of the osteoblast-like MC3T3-E1 cells, however promoted proliferation, decreased differentiation at proliferation stage and promoted differentiation at differentiation stage of primary osteoblast cells".

4. A behind the scenes look

There are numerous cell types in living organisms, some terminally differentiated (e.g. neurons), while others maintain their proliferative status throughout the whole life cycle of the organism. In case of wound or bone fracture healing, initial rapid proliferation is necessary in order to restore the functional integrity of the organism. During this period, however, the disruption of the cell cycle at specific checkpoints may lead to uncontrolled division of cells. On the other hand, a unique opportunity also arises that allows us to bioelectrically (in addition to already present endogenous bioelectric signals) control the mitotic activity via targeted transmembrane voltage variations. This approach presents a plausible explanation of findings in the previously mentioned studies and a tractable technique for functional experiments.

Membrane potential (V_{mem}) changes vary with cell type, ranging from millisecond timeframes seen in neurons and muscle cells, to possibly minutes and even days in diurnal cycles, in which case we speak of steady-state membrane potentials. The actual transmembrane voltage is the result of numerous channels and pumps, which segregate ions across the cell surface and are governed by the concentration gradient and charge distribution. To be able to control the cellular Vmem one must first fully understand the endogenous mechanisms responsible for modulating specific ion channels and transporters and subsequently appropriately, and in a controlled fashion, alter the course of such actions in a favorable way.

Numerous studies suggest that membrane potential is a key regulator of proliferation in a number of cell types. Furthermore, specific modulation of V_{mem} is required for both G1/S[1)] phase and G2/M[2)] phase transitions. In this context, inhibition of G1/S progression can be achieved in specific cell types, such as lymphocytes, astrocytes, fibroblasts and Schwann cells via membrane depolarization. The ensuing S phase initiation relies on hyper-polarization and omission thereof results in a so-called reversible cell cycle arrest, which has been documented in B cell lymphocytes, amongst others. Expression of various proteins was also effected, including IL-1/2 and transferring, both of which are implicated in cell cycle control.

On the other hand, the G2/M transition relies on the depolarization of the plasma membrane. In view of our current understanding, the proposed models outline a rhythmic oscillation of membrane potential throughout the cell cycle, with a spike in hyperpolarization occurring before DNA synthesis followed by a prolonged period of depolarization necessary for mitosis. The exact threshold of V_{mem} necessary to drive cells though proliferative stages is not known, and is likely to vary between cell type and differentiation stage [21].

This lack of practical knowledge could be one of the reasons behind the many inconsistencies encountered in currently available studies, and places emphasis on future research in this area. However, one should note that our current understanding of this issue is still rudimentary and far from complete.

The transmembrane voltage is indeed only one variable in the whole process of cell division. Additionally, temporal variations must be added to existing models of signaling systems due to V_{mem} oscillations occurring during the cell cycle. Also of notable importance is the assumption, or rather oversimplification that V_{mem} is indicative of the whole cell – whereas in reality, distinct domains of membrane voltage around the cell periphery exist in forms of micro-domains, presumably established by distinct population of channel/pump proteins. Finally, while the transmembrane voltage is the best-known and most tractable of the cellular bioelectric parameters, sub-cellular organelles such as mitochondria or nuclei all possess a transmembrane voltage of their own. Future efforts must concentrate on subcellularly-targeted voltage reporter proteins, functionally altering the bioelectric signaling in distinct intracellular locales [21].

[1)] The G1/S transition is a stage in the cell cycle at the boundary between the G1 phase and the S phase. It is a "point of no return" beyond which the cell is committed to dividing; in yeast this is called START and in multicellular eukaryotes it is termed the restriction point.

[2)] The G2/M cell stage checkpoint prevents cells from entering mitosis when DNA is damaged; thereby producing an opportunity for DNA repair and stopping the proliferation of damaged cells.

5. Membrane potential in cancer therapy and emerging microtubule-related treatments.

Neoplasia is characterized by abnormal proliferation of cells and is closely tied to alterations in membrane potential and unique bioelectrical properties of tumor tissue. Two distinct ionic pathways of action have been documented in currently available literature:

Potassium channels,

Proton, chloride and sodium flux.

Although documented, the resulting physiological role of V_{mem} due to alterations of the above pathways is still not well understood. However, when compared to healthy tissue types, cancer cells exhibit overall depolarization. Thus, hyperpolarization therapy might be a feasible therapeutic method in the future.

Another possible pathway for controlling and/or arresting (cancer) cell proliferation stems from the idea of a *microtubule*[3] related mechanism, pictured in Fig.1.

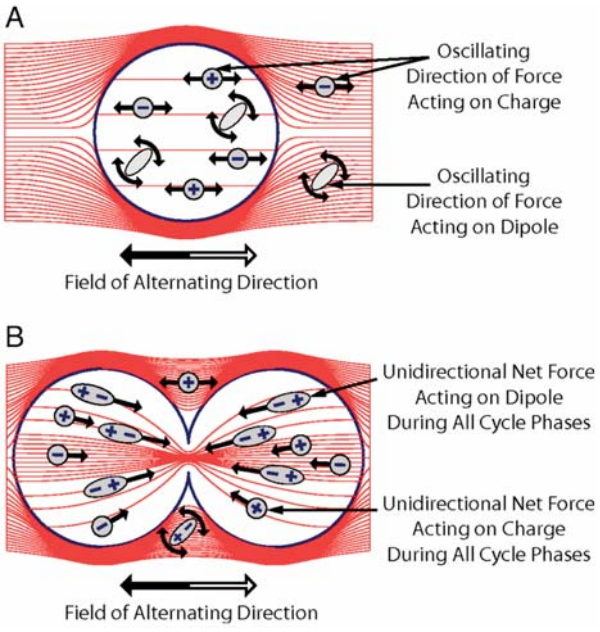

Fig. 1. Idea behind the anti-microtubule mechanism [22]

Two distinct cell phases are shown – quiescent, Fig.1A, wherein the AC field is uniform within the cell and during cellular division, Fig.1B wherein the non-uniform AC field induces forces that result in the "propulsion" of dipoles towards the furrow. Optimal orientation of the applied field (i.e. parallel) is crucial in this case, however also relatively difficult to achieve due to the randomness of the division axes in multiple cells and the relatively long application time of over 16 hours.

The above proposed mechanism of action was evaluated in numerous trials conducted by Kirson et al. [22] by means of external insulated electrodes. The said trials included treatment of various cancer cell lines, including human breast carcinoma and human non-small-cell lung carcinoma amongst others and favorable results prompted a clinical trial on 10 patients with recurrent glioblastoma. Results indicate that the disease progression and overall survival rate more than doubled with no serious, device-related adverse events reported. However, two possible disadvantages were highlighted – undesirable excitation of muscular tissue (i.e. cardiac) and, more seriously, a possible damage of rapidly diving normal cells, such as those of bone marrow, but these have yet to be evidenced in real-life applications.

6. Conclusion

The issue of electromagnetic fields of arbitrary frequencies and biological systems is complex and implications are far reaching. To date, numerous studies have reported mixed results in this area, and the influx of new studies only continues to underline this uncertainty.

However, since the times of first macroscopic observations, focus has slowly progressed onto cellular or sub-cellular space, offering a wealth of options to explore and document. One of these options is the modification of the transmembrane voltage via induced currents (eddy currents) in emerging cancer treatments. Physiological parameters, such as membrane voltage and specific ion content, may also be used as in vivo markers to identify special subpopulations of cell types, including various tumor types.

The other possibility consists of manipulating highly polarized structures such as microtubules found within the cell via electric and/or magnetic fields. Positive observations in this area indicate a viable method for controlling undesirable cell proliferation, including numerous tumor types, though the efficacy and means of application has to be further studied and significantly improved to warrant clinical use thereof.

The detailed understanding of the contribution of transmembrane voltage and microtubule manipulation associated with the cell cycle, and especially the integration of this knowledge into biochemical and genetic mechanisms occurring during complex morphogenesis, will reveal fascinating aspects of interdisciplinary biophysics and will offer significant opportunities for the biomedicine of cell engineering, cancer and regenerative medicine.

[3] Microtubules are part of the cytoskeleton and serve as structural components within cells. They are involved in many cellular processes including mitosis, cytokinesis, and vesicular transport. Their structure is predominantly similar to that of proteins and they are highly polarized.

To conclude, the current state of research discussed in this article still does not offer enough evidence to warrant a unanimous answer on whether *possible* negative effects of electromagnetic fields outweigh the *early-reported* positive effects of targeted electromagnetic field exposure or vice-versa. However, with every new study published and further elucidation of mechanisms of action, we might find out sooner than later a satisfactory answer to the question posed in the title of this paper.

References

[1] JAKUSOVA, V.: *UV Radiation and Mobile Communication - Physical Properties, Biological Effecte and Health Protection (in Slovak),* Vysoka skola zdravotnictva a socialnej prace Sv. Alzbety, Bratislava, ISBN 978-80-89464-00-5, 2009.

[2] KARIPIDIS, K., GILES, G. et al.: Occupational Exposure to Low Frequency Magnetic Fields and the Risk of Low Grade and High Grade Glioma, *Cancer Causes Control* 18(3): 305-13, 2007.

[3] ERDAL, N., ERDAL, M.E. et al.:.Lack of Effect of Extremely Low Frequency Electromagnetic Fields on Cyclin-dependent Kinase 4 inhibitor Gene p18(INK4C) in Electric Energy Workers, *Arch Med Res* 36(2): 120–123.

[4] JOHANSEN, C., OLSEN, J.H.: Mortality from Amyotrophic Lateral Sclerosis, other Chronic Disorders, and Electric Shocks among Utility Workers, *Am J. Epidemiol* 148(4): 362–368, 1998.

[5] JOHNSEN, C., OLSEN, J.H.: Risk of Cancer among Danish Utility Workers-A Nationwide Cohort Study. *Am. J. Epidemiol.* 147(6): 548–555.

[6] MILLER, A.B., TO, T. et al.: Leukemia following Occupational Exposure to 60-Hz Electric and Magnetic Fields among Ontario Electric Utility Workers. *Am. J. Epidemiol.* 144(2): 150–160, 1996.

[7] WILLET, E., ROMAN, E. et al.:.Occupational Exposure to Electromagnetic Fields and Acute Leukaemia: Analysis of a Case-control Study. *Occup Environ Med* 2003; 60:577–583.

[8] VERKASALO, P. K., PUKKALA, E. et al.: Risk of Cancer in Finnish Children Living Close to Power Lines. *BMJ* 307(6909): 895–899, 1993.

[9] MCBRIDE, M.L., GALLAGHER, R.P. et al.: Power-frequency Electric and Magnetic Fields and Risk of Childhood Leukemia in Canada. *Am J Epidemiol* 149(9): 831–842, 1999.

[10] SAVITZ, D.A., WACHTEL, H. et al.: Case-control Study of Childhood Cancer and Exposure to 60-Hz Magnetic Fields. *Am J. Epidemiol* 128(1): 21–38, 1988.

[11] LINET, M.S., HATCH, E.E. et al.: Residential Exposure to Magnetic Fields and Acute Lymphoblasticleukemia in Children. *N Engl J. Med* 337(1): 1–7, 1997.

[12] SCHUZ, J., GRIGAT, J.P. et al.: Childhood Acute Leukaemia and Residential 16.7 Hz Magnetic Fields in Germany. *Br J. Cancer* 84(5): 697–699, 2001.

[13] HENSHAW, D. L., REITER, R.J.: Do Magnetic Fields Cause Increased Risk of Childhood Leukemia via Melatonin Disruption?, *Bioelectromagnetics Suppl* 7: S86–97, 2005.

[14] VIANALE, G., REALE, M. et al.: Extremely Low Frequency Electromagnetic Field Enhances Human Keratinocyte Cell Growth and Decreases Proinflammatory Chemokine Production, *Br J. Dermatol* 158(6): 1189–1196, 2008.

[15] LISI, A., FOLETTI, A. et al.: Extremely Low Frequency 7 Hz 100 microT Electromagnetic Radiation Promotes Differentiation in the Human Epithelial Cell Line HaCaT. *Electromagn Biol Med* 25(4): 269–280, 2006.

[16] CRICENTI, A., GENEROSI, R. et al.: Low-frequency Electromagnetic Field Effects on Functional Groups in Hhuman Skin Keratinocytes Cells Revealed by IR-SNOM. *J. Microsc* 229 (Pt 3): 551–554, 2008.

[17] SELVAM, R., GANESAN, K. et al.: LF and Low Intensity Pulsed EM Field Exerts its Antiinflammatory Effect through Restoration of Plasma Membrane Calcium ATPase Activity. *Life Sci* 80(26): 2403–2410, 2007.

[18] VARANI, K., DE MATTEI, M. et al.: Characterization of Adenosine Receptors in Bovine Chondrocytes and Fibroblast-like Synoviocytes Exposed to Low Frequency Low Energy Pulsed Electromagnetic Fields. *Osteoarthritis Cartilage* 16(3): 292–304, 2008.

[19] ZHANG, X., ZHANG, J. et al.: Effects of Different Extremely Low-frequency Electromagnetic Fields on Osteoblasts. *Electromagn Biol Med* 26(3): 167–177, 2007.

[20] WEI, Y., XIAOLIN, H. et al.: Effects of Extremely Low-frequency-pulsed Electromagnetic Field on Different-Derived Osteoblast-like Cells. *Electromagn Biol Med* 27(3): 298–311, 2008.

[21] BLACKISTON, D., MCLAUGHLIN, K. et al.: Bioelectric Controls of Cell Proliferation. *Cell cycle* 8(21): 3527–3536, 2009.

[22] KIRSON, E., DBALY, V. et al.: Alternating Electric Fields Arrest Cell Proliferation in Animaltumor Models and Human brain tumors." PNAS 104 (24):10152–10157, 2007.

R. Radil – J. Barabas *

SIMULATION OF LOW FREQUENCY ELECTROMAGNETIC FIELD EFFECT ON CELL MEMBRANE CHANNELS MODEL

According to many current investigations, which approve the direct impact of potassium or sodium channels to the cell dividing processes, the presented article outlines an attempt to simulate influence of low frequency electromagnetic field to the cell membrane channels. Activation or inhibition of ion channels could be achieved by various mechanisms e.g. most common is chemical way. In contrast with this fact, the article describes simulations of external low frequency electromagnetic field application on the cell model, which should provide results comparable to the conventional methods.

Keywords: Low frequency electromagnetic field, eddy currents, potassium channels, sodium channels, cancer therapy

1. Introduction

From the most recent studies of human cells it is clear that bioelectrical properties of this nonlinear structure depend on many parameters complementing each other. Nowadays, most of studies are focused on transmembrane voltage and its impact on the cell cycle processes. About 40 years ago Cone et al. in their work [1] started with theories about transmembrane potential and its role in the cell dividing processes. Other studies [2, 3] approved that changes in transmembrane voltage could slow down or even stop processes of cell differentiation and thus should have impact in cancer therapy.

The transmembrane voltage is influenced by concentrations of ions in extracellular and intracellular environment which depend on activation of ion channels. That means that transmembrane voltage is a complex variable which depends on various processes outside or inside the cell. Probably the most important part of this problem is activation/inhibition of ion channels, which directly influences the concentration of extra/intra cellular ions and thus has impact to the cell proliferation and differentiation.

As a proposal for solution of the said problem an attempt to simulate effect of homogenous low frequency electromagnetic field (LF EMF) exposure to the cell model extended by ion channels is presented.

2. Hodgkin-Huxley electric cell model

Electromagnetic field and interaction thereof with cells is best explained at the microscopic level. Each cell in a living organism is composed of two parts – the inner cytoplasm (along with the nucleus and other organelles) and the outer membrane. Conductivity-wise, the outer membrane can be considered an insulator, and as such all current seems to flow in the extracellular fluid-filled space. However, the total cell resistance is analogous to that of a simple electronic R-C circuit as can be seen in Fig. 1 – the insulating membrane being the capacitance and cytoplasm the resistance. The lipid bilayer is represented as a capacitance (C_m). Voltage-gated and leak ion channels which represent the natural permeability of the membrane to ions are denoted by nonlinear (g_n) and linear (g_L) conductances, respectively. The electrochemical gradients driving the flow of ions are represented by nonlinear (E_n), and linear (E_L) voltage sources, ion pumps and exchangers are represented by current sources (I_p). The resulting transmembrane voltage (V_m) is equal to the difference between inner and external media electric potentials (φ_i and φ_e, respectively) [4]

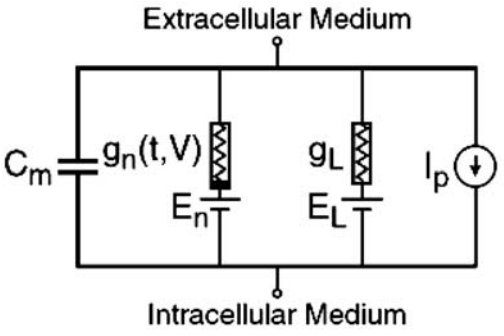

Fig. 1 Hodgkin-Huxley electric model of a biological cell [4]

The membrane current (I_m) is comprised of two components:
- resistive (conductive) current,
- capacitive (displacement) current,

* **R. Radil, J. Barabas**
Department of Electromagnetic and Biomedical Engineering, Faculty of Electrical Engineering, University of Zilina, Slovakia,
E-mail: radil@fel.uniza.,sk

both of which depend on the transmembrane voltage (V_m). Thus, the membrane current can also be rewritten as a function of V_m:

$$I_m \equiv I_m(V_m) = C_m \times \frac{\partial V_m}{\partial t} + I_p(V_m, q) \quad (1)$$

where the variable q represents certain state variables (such as the ionic concentrations), represented by a system of differential equations. It is clear that by modifying the transmembrane voltage via application of exogenous electromagnetic fields one can directly influence cellular dynamics.

According to this template an electromagnetic model of the cell has been created as a spherical capacitor, which is shown in Fig. 2. As it is shown in the picture, this model is placed into the homogenous LF EMF generated by Helmholtz coils.

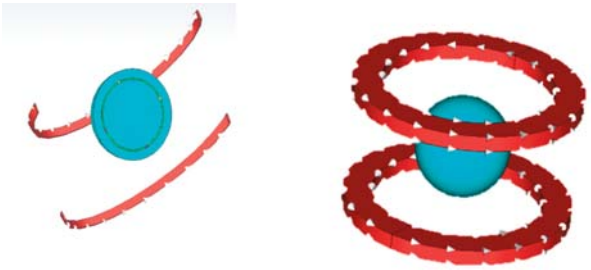

a) *b)*

Fig. 2 Cell model as a spherical capacitor: a) cross-section; b) whole model

It consists of three different layers, each of which is defined by values from Tab. 1.

Values of material conductivities and permittivities [5] Table 1

	Conductivities	Relative Permittivities
External	σ_e = 0.12 S/m	r_e = 80
Membrane	σ_m = 1 μS/m	r_m = 9.04
Internal	σ_i = 0.53 S/m	r_i = 50

3. Modeling of low frequency electromagnetic field influence on ion channels

In addition to the Hodgkin-Huxley model, the Goldman-Hodgkin-Katz (GHK) equation from [5] is used as a basis for modeling of ion channels. Practical application of the GHK is in cell membrane physiology to determine the equilibrium potential across a cell's membrane taking into account all of the ions that are permeant through that membrane. This is necessary because perfect ion channel selectivity is not possible in living systems. The following GHK equation considers a case of various conductivities (specifically Na^+, K^+ and Cl^-) and is expressed as:

$$V_m \beta \frac{RT}{F} \ln \frac{P_k[K^+]_{out} + P_{Na}[Na^+]_{out} + P_{Cl}[Cl^-]_{out}}{P_k[K^+]_m + P_{Na}[Na^+]_m + P_{Cl}[Cl^-]_m} \quad (2)$$

wherein:

V_m ... is the transmembrane voltage [mV]
R ... is the ideal gas constant [8.314472 $J.K^{-1}.mol^{-1}$]
T ... is the temperature [K]
F ... is the Faraday's constant [96485.3399 $C.mol^{-1}$]
P_x ... is the concentration of a specific ions [$x = K^+; Na^+; Cl^-$]

As it is clear from the equation and the Hodgkin-Huxley model, the ion channels represent a conductive way through the cell membrane. From this point of view the channels were modeled as a conductive tube through the membrane as it is shown in Fig. 3. Each of the channels is placed along the axes x and y. Material properties are defined for sodium and potassium channels according to [6] and are summarized in Table 2.

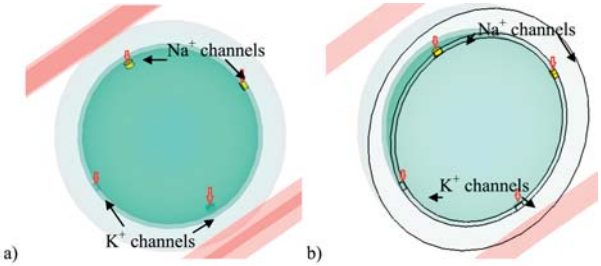

Fig. 3: Modeling of ion channels: a) localization of ion channels in the membrane; b) cross-section

Material properties of ion channels[1)] Table 2

	Sodium	Potassium
Electric conductivity	σ_{eNa} = 2100 S/m	σ_{eK} = 1640 S/m
Thermal conductivity	σ_{TNa} = 142 W/(Km)	σ_{TK} = 102.5 W/(m)
Material density	ρ_{Na} = 971 kg/m^3	ρ_K = 862 kg/m^3

After finishing the proposal of ion channels, the properties of used LF EMF were set up. The homogeneous electromagnetic field is generated by Helmholtz coils with a 1A current, frequency of 50 Hz and default sinusoidal excitation signal. This external field was then applied on the cell model. The results are compared with the simulations from [2], what can be seen in Figs. 4 and 5.

[1)] source: Chemicool – sodium, potassium, [online]: http://www.chemicool.com/elements

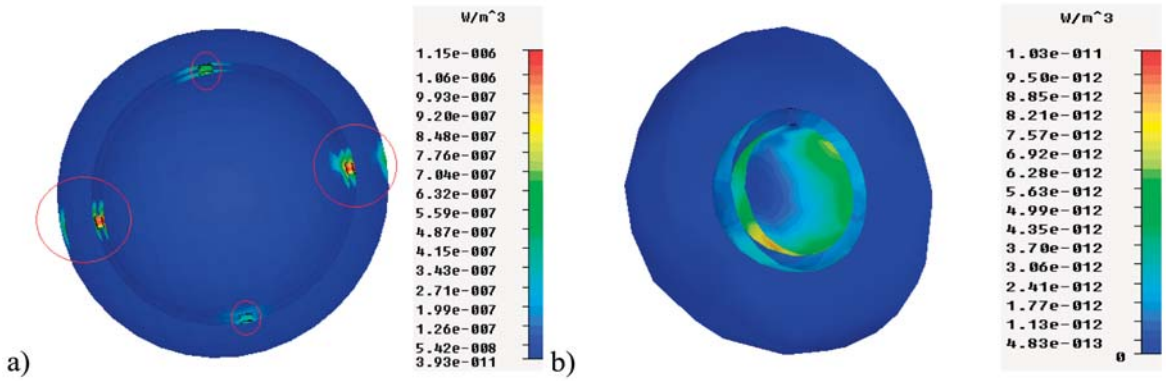

Fig. 4: Simulation results: a) Cross-section of El. Loss. Density around the ion channels in the cell membrane; b) Cross-section of El. Loss. Density without the channels in the membrane

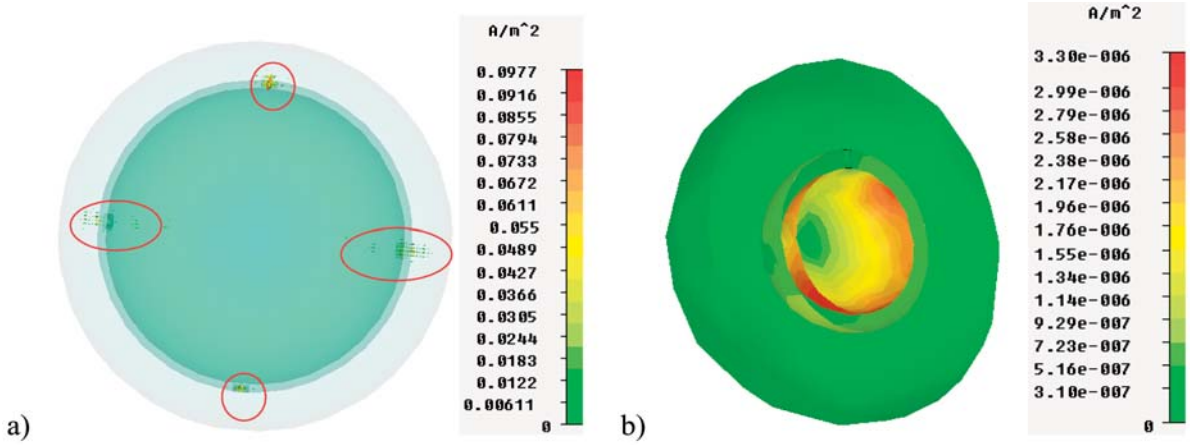

Fig. 5: Simulation results: a) Eddy current distribution through the ion channels; b) Eddy current distribution without the ion channels presence in the membrane

The differences between electric loss density of ion channels and the cell without ion channels exceed one order of magnitude. Similar situation is with eddy current distribution through the ion channels and without the ion channels. From the presented results it is our assumption that ion channels are probably the most influenced structures of the cell exposed to the external electromagnetic field and thus the changes on the ion channels level should have impact to the cell dividing processes as it is described in [7, 8].

The simulations further approve that not only electromagnetic properties, but also position (in this case rotation) of the cell in the electromagnetic field is important for evaluation of the effect on ion channels. As it is shown in Figs.4 and 5 the channels near the horizontal axis where is the highest concentration of eddy currents are more influenced than the channels around the vertical axis.

4. Conclusion

It is well known that electromagnetic field could influence a living organism. Specific effects of electromagnetic field are quite well described and a lot of studies approved e.g. thermal impact of mobile phones to humans head structures [10]. In this article an attempt to describe some nonspecific effects of low frequency electromagnetic field was made.

For this purpose two main types of ion channels – Na^+ and K^+ channels were simulated (their importance is described in [7, 8]). Based on our simulations it is probable that application of external low frequency electromagnetic field could influence the activation/inhibition of ion channels and thus could have impact on the transmembrane voltage and, finally, on cell proliferation.

It should be remembered that ion channels designed in this case represented only linear part of the whole problematic due to the simulations limitations which do not allow solution of such a complicated nonlinear problem as the case of biological cell is. To achieve the best simulation result as possible it is necessary to find solution in simulation of the nonlinear and linear structures together, which is currently a challenging task for future research.

References

[1] CONE Jr., C.D.: Unified Theory on the Basic Mechanism of Normal Mitotic Control and Oncogenesis. .*J. of Theoretical Biology*, Vol. 30, 1971, pp. 151–181

[2] BARABAS, J., RADIL, R.: Investigation of Cellular Transmembrane Potential Variations via Exogenous Low Frequency Electromagnetic Fields. *Clinician and Technology J.*, Vol. 40, 2010, pp. 41–45

[3] BINGGELI, R., WEINSTEIN, R. C.: Membrane Potentials and Sodium Channels: Hypotheses for Ggrowth Regulation and Cancer Formation Based on Changes in Sodium Channels Gap Junctions. *J. of Theoretical Biology.* Vol. 123, 1986, pp. 377–401

[4] SIMURDA, J.: *Bioelectrical Phenomena I*, CERM Brno, 1995

[5] GIMSA, J., WACHNER, D. A.: Unified Resistor-capacitor Model for Impedance, Dielectrophoresis, Electrorotation, and Induced Transmembrane Potential. *Biophysical J.*, 1998, vol. 75, No. 1, pp. 1107–1116.

[6] KUNZELMANN, K.: Ion channels and cancer. *The J. of Membrane Biology,* Vol. 205, 2005, pp. 159–173

[7] ROGER, S., POTIER, M., VANDIER, CH., BESSON, P., LE GUENNEC, J-Y.: Voltage-Gated Sodium Channels: New Targets in Cancer Therapy? *Current Pharmaceutical Design,* 12, 2006, pp. 3681–3695

[8] PSENAKOVA, Z., BENOVA, M.: Measurement evaluation of EMF effect by mobile phone on human head phantom. *Advances in Electrical and Electronic Engineering,* Vol. 7, 2008, pp. 346–349.

Barbora Czippelova – Daniela Gombarska *

MODELLING OF ARTERIAL BIFURCATION BY MEANS OF ELECTROMECHANICAL MODEL WITH DISTRIBUTED PARAMETERS

The present paper deals with the computer-aided modelling of blood vessels bifurcations using the electro-mechanical analogy with the electric transmission lines. The present model allows assessing the Murray's cubic law and its comparison with the real state of large and small arteries branching in the human body.

1. Introduction

Knowledge of detailed mechanisms of blood circulation in a human body is important in many diseases diagnoses. Very effective way to obtain useful information is provided by computer–aided modelling of cardiovascular system. Many models are based on the electromechanical analogy. The recent models using analogy of the blood vessel with an electrical transmission line with distributed parameters are connected with modern powerful computers, which are able to perform extremely demanding mathematical calculation. On the basis of theoretical analysis [1] we have developed model of the human arterial system in the MATLAB environment [2]. This model allows to simulate different phenomena taking place in the arterial system and to search for proper medical diagnostic methods, e.g. [3]. We have found direct connection between the blood pressure wave velocity and the properties of the blood vessel [4]. In the present paper modeling of arterial bifurcation and its influence on the blood flow is demonstrated.

2. Theory

The theoretical model resulting from the electro–mechanical analogy describes the flow of blood in a vessel taken as an elastic tube. The blood flow is taken as the laminar flow of a viscous liquid. The tube with liquid is modelled by an electrical transmission line [1], [2], the elementary segment of which can be substituted by the longitudinal impedance Z_L and transverse admittance Y_T given by

$$Z_L = -\frac{j\omega\rho J_0(a\, r_0)}{\pi r_0^2 J_2(a\, r_0)} \quad \text{and} \quad Y_T = j\omega\frac{2\pi r_0}{k_w(E_w + j\omega\eta_w)}, \quad (1)$$

where $a = \sqrt{-\frac{j\omega\rho}{\eta}}$ is the blood parameter, ρ the blood density, η the blood viscosity, ω the angular frequency of the transmitted wave, r_0 the tube internal radius, E_w and η_w the tube wall elastic modulus and tissue viscosity and k_w the dimension factor. J_0 and J_2 are the Bessel functions of the 0–th and 2–nd orders. According to the transmission line theory, the quantities (1) allow to express the complex propagation constant k and the complex wave impedance Z_0

$$k = \sqrt{Z_L\, Y_T} \quad \text{and} \quad Z_0 = \sqrt{\frac{Z_L}{Y_T}} \quad (2)$$

The secondary parameters $\boldsymbol{k}$ and $\boldsymbol{Z}_0$ are important for the investigation of propagation of the blood pressure and blood flow waves in the vascular system.

3. Investigation on the arterial bifurcation

Cardiovascular system is very complex and widely bifurcated system, the primary function of which is to supplement oxygen and nutrients to every cell of the human body. From the heart to the distal parts the arteries bifurcate and build more complex system. Each arterial embranchment, Fig. 1, influences the blood pressure and blood flow waveforms and causes their changes in various parts of the circulatory system. In the electromechanical analogy model of arterial bifurcation the branching part represents the impedance mismatch which causes the blood pressure and blood flow wave reflections. Thus the final shape of the blood pressure and blood flow waveforms in each vessel are the result of the summation of the primary wave and reflected waves. In general, the waves up to order 20-th harmonic (reflected from the bifurcations and also

* **Barbora Czippelova, Daniela Gombarska**
Faculty of Electrical Engineering, University of Zilina, Slovakia, E-mail: gombarska@fel.uniza.sk

from the source of the signal) contribute to the final shape of the waveform [5].

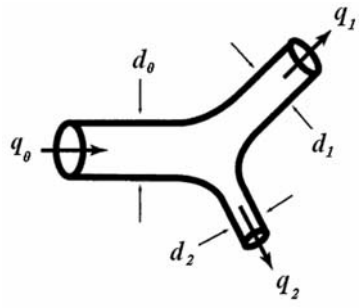

Fig. 1. Blood vessel branching

Basically two elementary conditions are valid for the arterial branching:

- The law of mass conservation – the blood flow in the mother vessel is equal to the sum of blood flows in daughter vessels

$$q_0 = q_1 + q_2 \tag{3}$$

- In laminar blood flow case (turbulent flow on the bifurcation does not arise), the blood pressure is equal in all vessels in the place of branching

$$p_0 = p_1 = p_2 \tag{4}$$

In order to investigate the influence of the branching vessels geometrical properties on the blood pressure and blood flow waveforms a simple arterial bifurcation is modelled by means of electromechanical model. The main interest is in the effect of the branching on the blood pressure and blood flow waveforms. Therefore all the reflection phenomena are located to the arterial branching which is achieved through used terminal segments; both daughter vessels are terminated with their characteristic impedance (for the 1st harmonic component).

The conditions (3) and (4) listed above imply that the combination of the daughter vessels is parallel and the impedance $\boldsymbol{Z}_{0T}$, which represents the output impedance of the mother vessel, is given as parallel combination of the characteristic impedances of branching daughter vessels $\boldsymbol{Z}_{01}$ and $\boldsymbol{Z}_{02}$ as

$$\frac{1}{Z_{0T}} = \frac{1}{Z_{01}} + \frac{1}{Z_{02}}. \tag{5}$$

The reflection coefficients $\boldsymbol{R}_U$ for blood pressure (equivalent to voltage) and $\boldsymbol{R}_I$ for the blood flow (equivalent to current) of basic vascular branching can be defined as

$$R_U = \frac{Z_{0T} - Z_{0m}}{Z_{0T} + Z_{0m}} \tag{6}$$

$$\boldsymbol{R}_I = \frac{Z_{0T} - Z_{0m}}{Z_{0T} + Z_{0m}} = -\dot{\boldsymbol{R}}_U, \tag{7}$$

where $\boldsymbol{Z}_{0m}$ is the mother vessels' characteristic impedance.

Transmission of the energy through the arterial branching is the most effective if the absolute value of the reflection coefficient is minimal. Simple condition, which defines the vessel radii of the arterial branching for the most effective transmission of energy through the arterial bifurcation is given by the Murray's cubic law, e.g. [6] and [7]

$$r_0^3 = r_1^3 + r_2^3. \tag{8}$$

The influence of the arterial branching on the haemodynamical quantities (blood pressure, blood flow) is investigated using the model in Fig. 2. The mother vessel is divided into 20 segments and both daughter vessels into 10 segments. Red arrows point to "measurement" sites.

The influence of the daughter vessels' radii on the blood pressure and blood flow waveforms is studied. All used geometrical and mechanical parameters of the vessels and of the blood are summarized in Tab. 1.

Table 1

Diameter of mother vessel	0.5 cm
Length of the mother vessel	30 cm
Length of the daughter vessels	15 cm
Arterial wall thickness of the mother vessel	0.67 mm
Arterial wall thickness of the daughter vessels	0.44 mm
Terminal resistance	1.44×10^{10} Pa·s/m^3
Modulus of elasticity	0.4 MPa
Blood density	1.06×10^3 kg·m^{-3}
Blood viscosity	3.25×10^{-3} Pa·s

Optimum radii of the daughter vessels appointed on the base of cubic law is $r^* = 0.397$ cm. In order to investigate the influence of the daughter vessel radii on the blood flow dynamics daughter, the radius values were chosen as $r = 0.357$ cm; 0.318 cm; 0.278 cm; 0.238 cm and 0.437 cm; 0.476 cm (it means 90%, 80% 70%, 60% and 110%, 120% of r^*, respectively). Absolute values and the phases of the reflection coefficient for all values of the radius and for the 1st harmonic component are shown in Fig. 3.

The reflection coefficient achieves the minimum absolute value $|\boldsymbol{R}_U| = 0.041$ in the case of the daughter vessels having the optimum radius r*. In this case the phase achieves the value $\psi_U = -153°$, which is in the transient area, where the phase changes from 0° for radii less than r^* down to the −180° for the radii greater than r^*. The absolute values of the reflection coefficient $|\boldsymbol{R}_U|$ for all other daughter vessel radii are greater than those for the optimum radius. For smaller diameters the reflected wave is in phase with the progressive pressure wave and the resultant blood pressure in the mother vessel increases. For greater radii the blood pressure wave reflects with opposite phase and the reflected

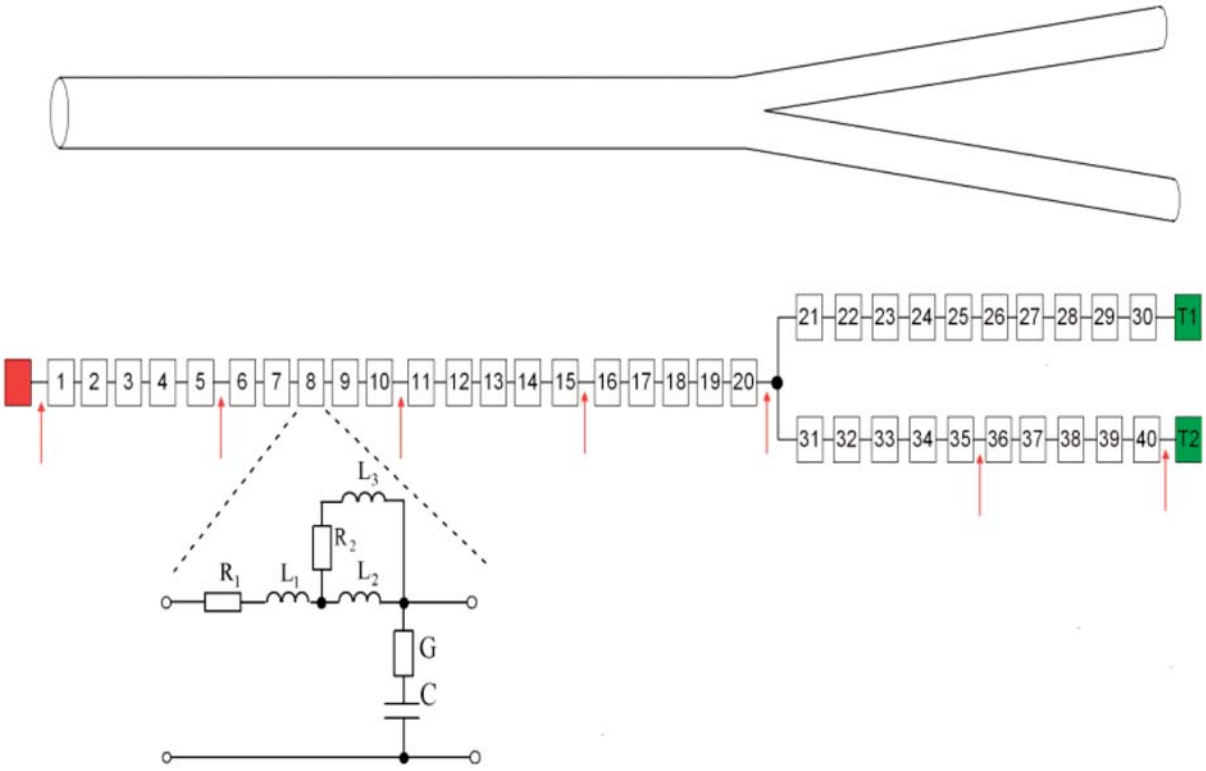

Fig. 2. Simulation of the vessel branching

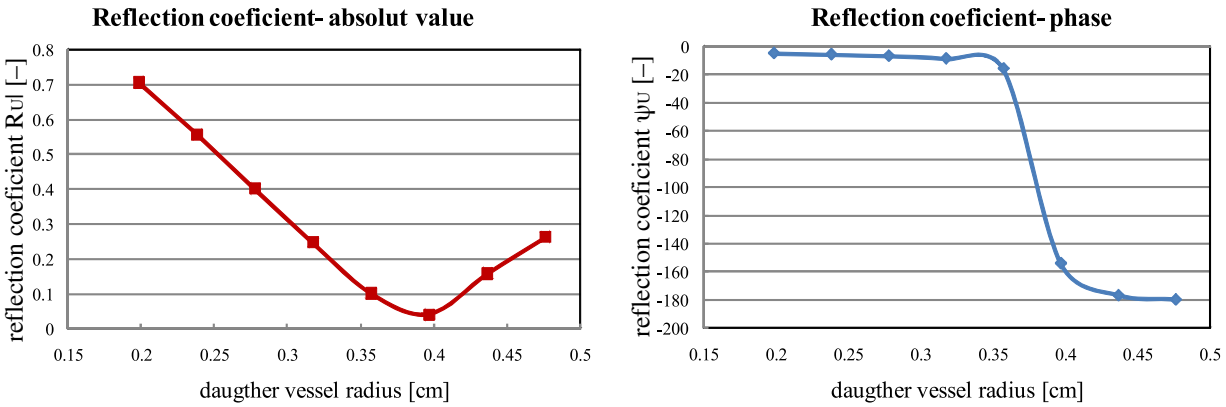

Fig. 3. Reflection coefficient of the blood pressure wave

wave suppresses the resultant blood pressure wave in the mother vessel. According to the (7): $\boldsymbol{R}_I = -\boldsymbol{R}_U$, therefore the resultant blood flow increases for greater daughter vessel radii and decreases for radii smaller than r^*. These facts proof the cube law.

All the facts listed above are depicted in detail in the figures 4 to 7. The blood pressure magnitude for the biggest investigated daughter vessel radius $r = 0.476$ cm measured before branching reaches the value 113 mmHg and the magnitude of blood flow is 4.17×10^{-7} m^3/s. In case of the smallest investigated radius $r = 0.238$ cm the magnitude of blood pressure is 133.9 mmHg and magnitude of blood flow 1.52×10^{-7} m^3/s, Fig. 4. Besides changes in magnitude, the decrease in vessel radius implies also changes of blood pressure waveform, where the pulse profile can include up to three maxima for $r = 0.238$ cm due to the wave reflections. The results of blood flow and blood pressure time-dependence denote the significant influence of outgoing vessel diameter on the blood flow dynamics.

Figs. 5, 6 and 7 show the propagation of blood pressure and blood flow waves along mother vessel for three different radii. In Fig. 5 there are depicted pressure and flow waveforms for the radius calculated from the cubic law. It is evident that for this case the energy transmission is optimal. Fig. 6 shows the propagation of

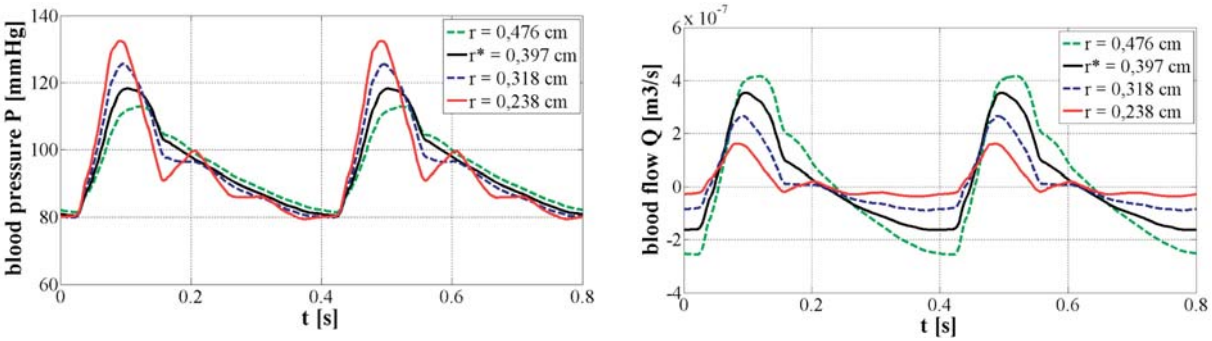

Fig. 4 Blood pressure and blood flow before branching for four different vessel radii

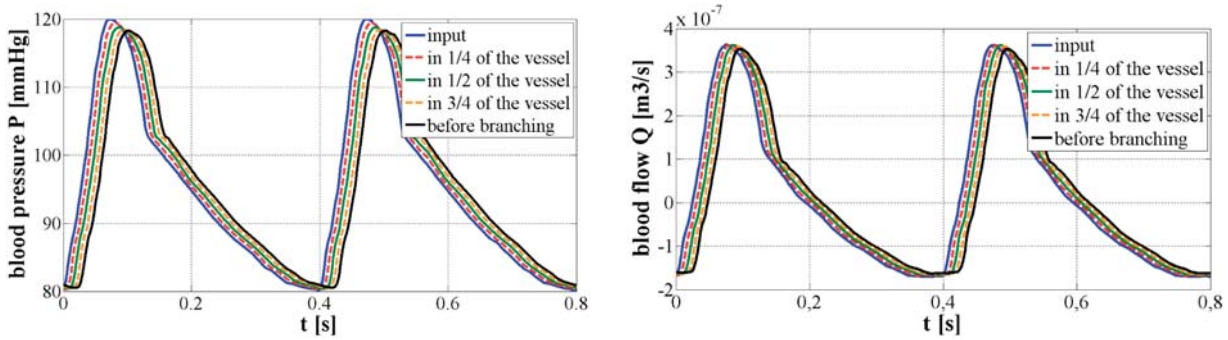

Fig. 5 Blood pressure and blood flow for r = 0.3 cm*

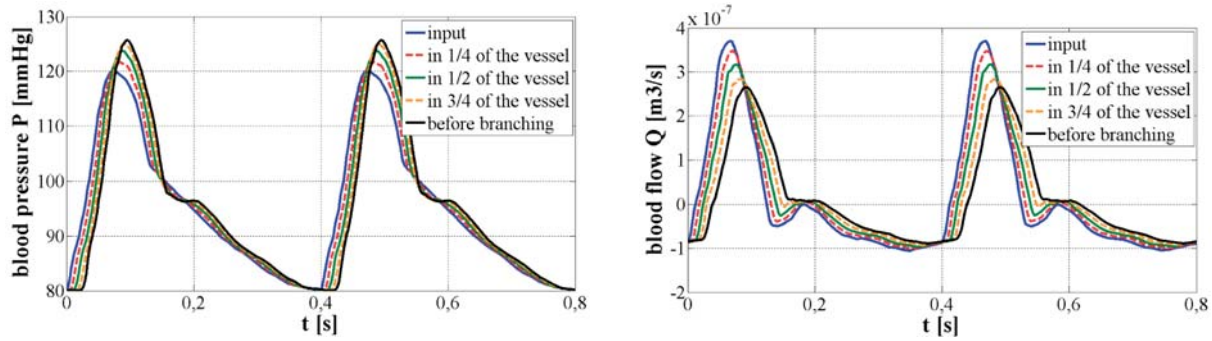

Fig. 6 Blood pressure and blood flow for r = 0.318 cm

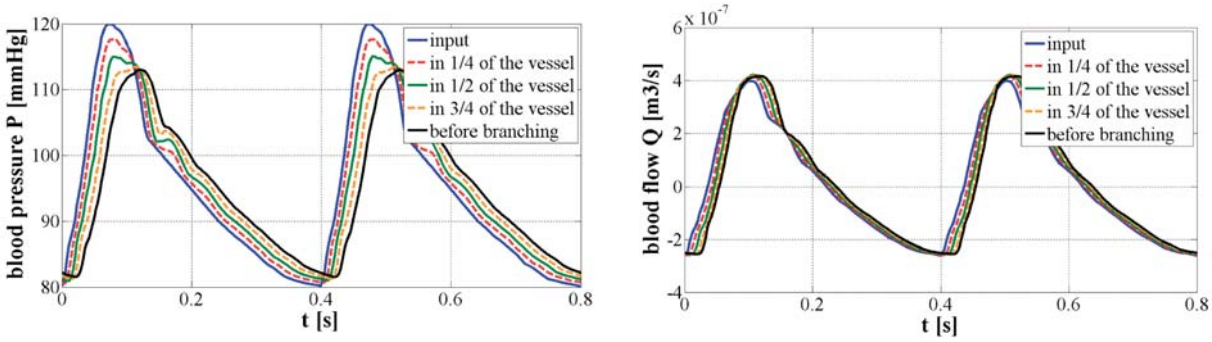

Fig. 7 Blood pressure and blood flow for r = 0.476 cm

heamodynamic waves for daughter vessel diameter $r = 0.318$ cm. Blood pressure increases along the artery and blood flow decreases due to reflections and also the second maximum appears in the waveforms. On the other side for the daughter vessel diameter bigger than r^* ($r = 0.476$ cm) blood pressure wave decreases as it travels along the mother vessel whereas blood flow increases very slightly, Fig. 7.

In the cardiovascular system of the human body all three cases of bifurcation occur. Bigger arteries bifurcate in the way of $r_0^3 < r_1^3 + r_2^3$ (e.g. aorta $r = 0.57$ cm) branches into two common iliac arteries ($r = 0.52$ cm)), whereas peripheral arteries bifurcate in the way of $r_0^3 > < r_1^3 + r_2^3$ (e.g. brachial artery ($r = 0.24$ cm) branches into ulnar artery ($r = 0.21$ cm) and radial artery ($r = 0.16$ cm)). Occasionally the branching with minimal reflection coefficient can be found (e. g. popliteal artery ($r = 0.2$ cm) divides into anterior tibial artery ($r = 0.13$ cm) and posterior tibial artery ($r = 0.18$ cm)). As there is great amount of peripheral bifurcations in the cardiovascular system the influence of these branching points is dominant. It results in increasing the blood pressure towards the periphery and also in appearance of the second maximum in the blood pressure waveform in the more peripheral measured signals.

4. Conclusion

The present study describes the partial phenomenon of the vessels bifurcation, which is important for understanding reflections of blood pressure waves and their influence on the blood pressure pulse profile. The computer-aided model has approved the Murray's cubic law and it has described the deviations from this law in large and small arteries bifurcations. Modeling of physiological processes with help of modern powerful computers gives an effective tool for the present medicine. Simulation of different parts of a human body allows developing non-invasive diagnostic and prognostic methods supporting the treatment of various diseases.

References

[1] CAPOVA, K., BLAZEK, V., CAP, I., BUCKULIAKOVA, L.: Physiological fluid systems modelling and visualisation. I*nternational J. of Applied Electromagnetics and Mechanics 14* (2001/2002), IOS Press, pp. 377–380, ISSN 1383-5416

[2] CAPOVA, K., CAP, I., BLAZEK, V.: Brain Haemodynamics Modelling Using Electromagnetic Systems Characteristics. *International J. of Applied Electromagnetics and Mechanics 19* (2004), No. 1-4, IOS Press, pp. 457–462. ISSN 1383-5416

[3] CAPOVA K., BLAZEK V., CAP I.: Investigation of Brain Arterial Circle Malformations Using Electrical Modelling and Simulation. *Advances in Electrical and Electronic Engineering,* Vol. 5 (2006), No. 1-2, pp. 212–217. ISSN 1336-1376

[4] CZIPPELOVA B., CAP I.: Pulse Wave Velocity Calculation by Means of Electromechanical Model of Blood Vessel, *TRENDY V BMI 2009* – Bratislava, pp. 149–152, ISBN 978-80-227-3105-8

[5] CZIPPELOVA B., GOMBARSKA D.: *Investigation of Blood Pressure and Blood Flow Wave Propagation on Arterial Bifurcation,* Proc. of the IEEE 2009 – Králíky, pp. 44–47, ISBN 978-80-214-3938-2

[6] SHERMAN T. F.: On Connecting Large Vessels to Small – the Meaning of Murray's law. *J. Gen. Physiology*, Vol. 78 (1981), pp. 431–453.

[7] REVELLIN R. et al.: Extension of Murray's law using a non-Newtonian model of blood flow. *Theoretical Biology and Medical Modelling,* 2009, 6:7 Open Access: http://www.tbiomed.com/ content/pdf/1742-4682-6-7.pdf .

Vitaly Levashenko – Sergey I. Karas – Miroslav Rusin – Evgeny E. Sizov *

SOME METHODS FOR DEVELOPMENT OF ANALYTICAL MODULE IN TELEMEDICINE SYSTEM FOR A CHILD MONITORING

Telemedicine system is system that provides distance medical help and wide application of these systems is started. In the paper two telemedicine systems for pediatrics and specifications of their development are considered. This system will be used for decision different aspects in pediatrics, but both of these systems have similar structure and include special analytical module. The analytical module is used for estimation of initial data and forming of preliminary decision about patient state. Two methods for development of the module are proposed. One of them is based on fuzzy decision trees and second is logistic regression for prediction. These methods are alternative and amplify with one another.

1. Introduction

Like most activities in society today, medical practice as well as research is intimately dependent on Information Technology (IT). One of tendencies of IT application in medicine is development of system to render medical help in distance [1]. There are many rural or sparsely inhabited areas, where access to specialized healthcare is limited or none, e.g. mountains, tundra, under-developed countries. There is a lack of experts, often only nurses in small medical centres, and patients must travel to larger cities, which often may take a lot of time that could prove fatal. For these regions, telemedicine projects could be a solution as they overwhelm distances and provide immediate responses. Another case is an area hit by a disaster, where electricity, network or traffic infrastructure can be damaged [2]. In this situation conditions are even worse than in cases above, making patient treatment a lot harder. Telemedicine applications will play an increasingly important role in health care and provide tools that are indispensable for home health care, remote patient monitoring, and disease management that encompasses not only rural health and battlefield care, but nursing home, assisted living facilities, and maritime and aviation applications.

Most of telemedicine systems include special modules for analysis of obtained data and information. Principal goal of these modules is useful for physicians in assessment of patient state and diagnostics. These modules allow: selecting the most important prognostic factors and their combinations for diagnostic tasks and for prediction of therapy outcome; extraction of knowledge from medical database in the form of interpretable linguistic classification rules with interval values of prognostic factors, etc. In particular, the fuzzy logic, neural networks, genetic algorithms, decisions trees and other methods provide the necessary support for developing highly efficient automated diagnostic system for more accurate diagnosis. These methods have different characteristics, properties, and utilities that are dependent on decided problem. But it is very important to use correct methods for decision of specific problem of a telemedicine system. In this paper we consider development of two telemedicine systems that have special analytical modules for assessment of patient state. These systems are intended for application in paediatrics for children monitoring and are designed by the Siberian State Medical University (Tomsk, Russia) [3] and the University of Zilina (Zilina, Slovakia) [4].

2. Telemedicine systems in Paediatrics

Telemedicine systems are systems that provide distance medical help. Depending on a specific application, this service can be information spreading, examination result transfer, sharing medical records, audio/video consultations, surgeries etc. but usually more of them cooperating [5].

Application area of a telemedicine system has an important impact on the process of design and elaboration. Telemedicine systems from different medical domains are distinguished by structure too [2, 6]. Some general recommendations for elaboration of paediatric telemedicine system have been presented in [7]. In particular, next modules can be included in system:

* **Vitaly Levashenko[1], Sergey I. Karas[2], Miroslav Rusin[3], Evgeny E. Sizov[4]**
[1] Department of Informatics, University of Zilina, Slovakia, E-mail: Vitaly.Levashenko@fri.uniza.sk
[2] Medical and Biological Cybernetics Chair, Siberian State Medical University, Tomsk, Russia
[3] Department of Informatics, University of Zilina, Slovakia
[4] Siberian State Medical University, Tomsk, Russia

- *Growth Record:* Some diseases influence the child's height, therefore, it is important to keep track of it. Later, graphs can be generated from these data.
- *Development Milestones:* Some diseases can also influence the child's development, so proper records should be kept.
- *Immunization:* Immunization is one of priorities in paediatric HIV. The records should be stored to provide recommendations later or alert doctors.
- *Social History:* Information about child's life, e.g. people he/she lives with, socio-economic background, education information, details about previous care providers are gathered here.
- *Counselling information:* Evidence-based counselling using patient's socio-economic data and adherence relative information helps in providing healthcare.

Both doctors and patients benefit from telemedicine systems. They represent cost-effective, time-saving and quality enhancing way for providing health care. They may help avoid unscheduled visits or prevent frequent patient transportation. Let us consider some examples of paediatric telemedicine systems that demonstrate advantages of utilising ICT in medicine [8–12]. In paper [8], it is shown that by using telemedicine application real-time diagnosis can be brought to neonatal facilities without in-house paediatric cardiologists. Instead of using courier to deliver videotape, which is time-consuming, videoconferencing is preferred. Furthermore, improved education and monitoring of children with asthma have been shown to be highly effective in controlling symptoms and preventing failure of outpatient therapy. Using Internet-based applications this can be achieved.

The paediatric monitoring systems are used in different aspects of health care. It can be a simple consultation system for parents in the form of website. However, some complex systems allow obtaining a child diagnosis from distance. Systems usually specialize in helping with diagnosing a specific disease. They may be also used to educate both children and parents.

System for blood glucose measurement, developed by Gammon et al. [9], relies on mobile and wireless technologies. A designed device is used to automatically transfer readings from child's blood glucose monitor into his/her parent's mobile phone. This results in reassurance on parents' side and works as an aid in families' self-management of diabetes.

Chan et al. [10] created an Internet-based application for asthmatic children that provide therapeutic and diagnostic monitoring. It includes an asthma symptom diary and video transfer based on store-and-forward technology. Videos capture patients using their controller medication inhaler or peak flow meter use.

Telemonitoring has proved useful in improving care for high-risk infants. Program Baby CareLink was designed to provide enhanced medical, informational, and emotional support to families of very low birth weight infants during and after their neonatal intensive care unit (NICU) stay [11]. Parents have access to virtual visits during an infant's hospitalization or remote monitoring after discharge.

A telemedicine system for HD teleconferences has been used in Chillicothe, Ohio (USA). It allows real-time consultation with neonatologist or paediatric cardiologist resulting in more precise and quicker diagnoses. The project enables specialists in Columbus, Ohio, to view distressed newborns with exceptional clarity, examine detailed x-rays, view lab results and consult with attending physicians in Chillicothe in real-time [12]. The system includes typical workplace of doctor for distant consultation (Fig.1).

Fig. 1 Doctor using teleconsultation, the upper display showing his motions, the lower specialists [12]

3. Development of telemedicine systems for child monitoring

Let us consider another system for child monitoring elaborated for the Neonatal Department of Zilina clinic (Fakultna nemocnica s poliklinikou Zilina) by a team from the University of Zilina. This system is designed to act as an information system concerning newborn healthcare. Healthcare is also about prevention, therefore, systematic education is needed. The main aim was to develop a consulting system with a doctor, by which the patient could get information about health care without need to personally visit a specialist. By using it, it is possible to educate as well as interactively solve the newborn care issues raised.

The basic prototype of the system consists of tree parts:

a) *article section* where a user can obtain information in a passive way in the form of articles published by the administrators
b) *discussion section* where a user can actively join on-line discussion and get the answers for specific questions from a specialist or other patients
c) *administration section* where access is limited only to the persons assigned with administration task

The *Articles section* of this system provides a convenient interface for reading, searching filtering and articles. The user has access

to the latest report of published articles, but also to the archive. To facilitate the search a collection of the most frequently entered phrases and a list of the most read posts are available. Group of the chosen articles will still be on hand as reference

The *Discussion section* was added to the system to provide a place for the laymen or the specialists to exchange their knowledge. It was intentionally divided into these groups as there are topics dedicated to either group. If a topic is dedicated to the specialists, this topic is read-only for laymen. The distinction between these types of users is made during a registration process.

The *Administration section* was developed to allow assigned persons to add new content to the system. The interface for creating, editing and deleting articles was provided. Articles can contain images to graphically support the text. In this system part it is also possible to manage the administrators' accounts but only for a super administrator.

This system is currently in the development phase. It was launched temporarily to gather information from the Neonatal Department, e.g. user-friendliness, website design etc, as the system is being developed for it. The foundations for an information system have been laid, which in future may be extended to support other forms of consultation (video/audio), storing health records, etc. in order to increase the quality of healthcare. Another extension will be elaboration and design of the analytical module for child health examination. The basic conceptions and principal methods for this module development were presented in [4, 13]. The *Analytical section* will be elaborated in the system for this module. The principal goal of this section is preliminary examination of child health before visit to clinic.

4. System for monitoring and Assistant for paediatrician (ASSPED)

The system ASSPED is a complex paediatric decision support system that is developed and used in Tomsk region (Russia) [3]. This region covers an area over 300 000 km^2, with the most of it inaccessible due to taiga and swamps. The combination of these factors opens an opportunity for the use of telemedicine. A lot of the residences possess only small medical centres. For more difficult cases an advice or intervention from a specialist is needed. Transportation is a burden; both financial and physical, therefore, if possible it should be avoided. The system mentioned above could be a solution as its main function will be to assess the seriousness of a case. Therefore, the monitoring telemedicine system is the principal component of the ASSPED. This component is meant for the monitoring of children health for early detection of disease and include a special analytical module for definition of a patient state. Results of preliminary medical checkup are used for analysis. Temperature, pulse, coverlet and similar data form initial information for analysis. X – ray investigation, blood test and urine analysis are included in preliminary examination too if these results were implemented as a preliminary. Based on the analysis of initial information the analytical module detects the state of a child health by four levels:

Normal (green): The patient can receive health care in a basic medical centre or does not need medical help.
Intermediate (yellow): The patient needs some medical observation and this patient state requires control in a basic medical centre or by telemedicine centre in some time.
Monitoring (blue): The patient needs a treatment and will be monitored by the telemedicine system continually.
Hospitalisation (red): The patient needs hospitalisation immediately.

This information is obtained and analysed by a physician-analyst that has possibility to confirm or to change a derived patient state. After this control the decision about the child's health is sent to the basic medical centre.

Therefore, the analytical module for detection of the patient's health state is important for correct functioning of the ASSPED system.

5. Methods for development of analytical module of the telemedicine system

Two principal methods were used in the development of analytical modules in the ASSPED system and in the developed telemedicine system presented above in section 2. The first of these methods is a logistic regression [3]. The second method is Fuzzy decision tree (FDT) [14]. The decision about a patient's health state is implemented by these methods independently (Fig. 2). But results of both methods are analyzed and definitive decision is determined by the special weight algorithm that will be elaborated in step of the module testing.

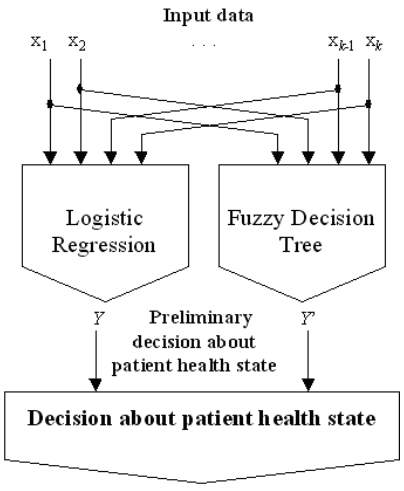

Fig. 2 Structure of the analytical module of the telemedicine system

Logistic regression is a mathematical technique used to make prediction. It is used in medical and social sciences, but also in marketing applications. The main principle of logistic regression is a logistic function. The input, z, of the logistic function is a set of independent variables. There is a coefficient associated with each independent variable that expresses contribution of this factor to the overall result, called *regression coefficient*. The output, Y, of the logistic function is a binary variable expressed by probability, meaning an interval $\langle 0, 1 \rangle$.

$$Y = \frac{1}{1 + e^{-z}}, \tag{1}$$

where $z = \beta_0 + \beta_1 x_1 + \beta_2 x_2 \ldots + \beta_k x_k$; k is the number of input variables; β_0 is a value of z when all independent variables are zero.

Variables x for the developed modules were indicated as results of a preliminary medical check-up and their values were defined along with doctors. The Y is the level of a patient's health state and has four values.

The application of the logistic regression in the ASSPED system allows improving the detection of a patient's health state in comparison to the heuristic methods [3]. But the next step of this module development can be the combination of two methods for decision support. The FDT can be used as additional approach for this module. The FDT was used as a basic method in the development of nomogram for prostate cancer detection [4, 14] and now is used for analytical decision in the produced telemedicine system (section 3).

Induction of FDT is a useful technique to find patterns in data in the presence of imprecision, either because data are fuzzy in nature or because we must improve their semantics. We proposed the algorithm to induction of new types of FDT: unordered, ordered or stable FDT [15]. The use of our cumulative information estimations allows to precisely estimate mutual influence of attributes [14, 15]. We introduced also the cost of diagnostics into classification algorithms. Our algorithm has a minimum cost of decision process based on different criteria of optimality.

In the FDT, each non-leaf node is associated with an initial attribute A_i. When A_i is associated with a non-leaf node, the node has m_i outgoing branches (m_i is number of possible values of attribute A_i). The j-th branch of the node is associated with value $A_{i,j}$. The class attribute B has mb possible values $B_1, \ldots, B_{jb}, \ldots, B_{mb}$. Let the FDT have R leaves $L = \{l_1, \ldots, l_r, \ldots, l_R\}$. There is also a vector of values $F_r = [F_1^r; \ldots, F_{jb}^r; \ldots, F_{mb}^r]$ for each r-th leaf l and each j_b-th class B_{jb}. Each value F_{jb}^r means the certainty degree of the class B_{jb} attached to the leaf node l_r.

In fuzzy cases, a new instance e may be classified into different classes with different degrees. Then, each leaf $l_r \in L$ corresponds to one (r-th) classification rule. The condition part of the classification rule is a group of conditions presented in the form "attribute is attribute's value" and those conditions are connected with an operator.

These attributes are associated with the nodes in the path from the root to the leaf l_r. The attribute's values are the values associated with the respective outgoing branches of the nodes in the path. The conclusions of the r-th rule are the values of the class attribute B with their truthfulness vector $\boldsymbol{F}_r$ values.

For example, the path $Pr(e) = \{[A_{i_1 j_1}(\mathrm{e})]r, \ldots, [A_{i_s j_s}(e)]r, \ldots, [A_{i_S j_S}(e)]r\}$ from the root to the r-th leaf. This path $P_r(e)$ consists of S nodes which are associated with attributes $A_{i_1}, \ldots, A_{i_s}, \ldots, A_{i_S}$ and respectively their S outgoing branches associated with the values $A_{i_1 j_1}, \ldots, A_{i_s j_s}, \ldots, A_{i_S j_S}$. Then the r-th rule has the following form:

IF (A_{i_1} is $A_{i_1 j_1}$) & ... & (A_{i_s} is $A_{i_s j_s}$) THEN B (with truthfulness $\boldsymbol{F}^r$).

Our approach uses several classification rules for classification of a new instance e. That's why there may be several paths whose all outgoing node's branches are associated with values $A_{i_S j_S}(e)$ greater than 0. Each path $P_r(e)$ brings about leaf node l_r and corresponds to one r-th classification rule. In this case each r-th classification rule should be included in the final classification with a certain weight $W_r(e)$. The weight is for instance e and the r-th rule is given by the rule $W_r(e) = \prod_{s=1}^{S} [A_{i_s j_s}(e)]^r$, where $[A_{i_s j_s}(e)]^r$ is the value of the attribute A_{i_s}, for the new instance e. The weight $W_r(e)$ is equal 0 if there is an attribute's value $A_{i_s j_s}$ whose membership function equals 0. Values of class attribute B for the new instance e are: $\mu_B(e) = \prod_{r=1}^{R} W_r(e) \times \boldsymbol{F}^r$, where F^r is the truthfulness of the r-th rule.

Therefore, two methods for elaboration of analytical module for telemedicine system are considered in this paper and will be used in real application. The output of these methods will determine if a patient should be treated locally, be monitored or immediate transportation is required. Using this information, medical staff can decide on the next stage of treatment more responsibly and greater attention can be paid to a patient's health.

6. Conclusion

We induced telemedicine and telemedicine systems as a possible tool for remote diagnosis and rendering a medical help on distance. We presented a web-based paediatric telemedicine system that allows consultation as well as educates. Web-based applications are widely spread therefore they can be reached by majority of population and this approach can contribute to higher quality of health.

The system ASSPED is a complex system that offers recommendation about child's health. This information about patient's state is based on analysis of results of a preliminary medical check up. A physician can confirm or change a derived patient state and this decision is stored at the basic medical centre.

An analytical module for child monitoring was proposed that utilises two methods: logistic regression and Fuzzy decision tree. Logistic regression is a technique used for prediction. Fuzzy decision trees are able to deal with imprecise real life data and are based on fuzzy classification rules. These methods work independently. However, their results are analyzed together and the final decision is made.

References

[1] ACKERMAN M. J., BURGESS L. P. et al. *Developing next generation telehealth tools and technologies: Patients, systems, and data perspectives. Telemedicine and e-Health,* 16(1), 2010, pp. 93–95

[2] BASHSHUR R.L., SHANNON G.W. *History of Telemedicine.* Evolution, Context, and Transformation. 2009, 466p.

[3] KOLOMEJCOV A.O., SIZOV E.E. *Implementation of logistic regression statistical method for definition of children groups with high risk of disease. In Proc. of the 16th Int. Conf. on Modern Technique and Technologies,* Vol. 2, pp. 40–42 (in Russian).

[4] ZAITSEVA E., MATIASKO K., DOBROTA D., *A Decision Support System for Early Diagnostics in Oncology. In Proc. of the 2nd Int. Conf. on Advanced Information and Telemedicine Technologies for Health (AITTH-2008)*, 1–3 October, Minsk, Belarus, 2008, pp.117–121.

[5] GRASCHEW G., ROELOFS T.A., et.al. *2020 - New Technologies for the workplace of the physician of the future. In Proc. of the 5th Int. workshop on Digital Technologies,* 20–21 November, Zilina, Slovakia. 2008.

[6] TULU B., et al. *A Taxonomy of Telemedicine Efforts with respect to Applications, Infrastructure, Delivery Tools, Type of Setting and Purpose. In: Proc. of the 38th Hawaii International Conference on System Sciences,* 2005

[7] PAUL, S.; BHATTACHARYA, S.D et al. *A web-based electronic health care system for the treatment of paediatric HIV. In Proc. of the 11th International Conference on e-Health Networking, Applications and Services,* 16–18 Dec., 2009, pp.175–180.

[8] SABLE C., CUMMINGS S., et al. *Impact of Telemedicine on the Practice of Paediatric Cardiology in Community Hospitals, Paediatrics, Vol. 109, No. 1*, 2002, pp.e3.

[9] GAMMON D., ÅRSAND E., et al. *Parent-Child Interaction Using a Mobile and Wireless System for Blood Glucose Monitoring, Journal of Medical Internet Research, Vol. 7, No 5,* 2005, pp. e57.

[10] CHAN D., CALLAHAN C., et al. *An Internet-Based Store-and-Forward Video Home Telehealth System for Improving Asthma Outcomes in Children.* American Journal of Health-System Pharmacy, Vol. 60, No. 19, 2003, pp. 1976–1981.

[11] GRAY J., SAFRAN C., et al. *Baby CareLink: Using the Internet and Telemedicine to Improve Care for High-Risk Infants.* Paediatrics, Vol. 106, No. 6, 2000, pp. 1318–1324.

[12] BARBER P., DOVYAK J., MANTEY S. *HD videoconferencing links critical care newborns from rural hospitals to tertiary care facilities, specialists,* 2008. Available on internet <http://www.telehealthvrc.org/news/2008/telemedicine.shtml>

[13] LEVASHENKO V., ZAITSEVA E., et al. *Nomogram for assistance in treatment of prostate cancer. In 5th International workshop on Digital Technologies (DT 2008),* 20–21 November, Zilina, Slovakia, 2008.

[14] LEVASHENKO V., ZAITSEVA E., *Usage of New Information Estimations for Induction of Fuzzy Decision Trees.* In Proc. of the 3rd IEEE Int. Conf. on Intelligent Data Engineering and Automated Learning, Kluwer Publisher, pp. 493–499, 2002.

[15] LEVASHENKO V., ZAITSEVA E., PUURONEN S. *Fuzzy Classified Based on Fuzzy Decision Tree. In Proc. of the IEEE International Conference on Computer as a Tool,* pp. 823–827.

Tatiana Strapacova – Klara Capova – Milan Smetana *

BIOMATERIALS INHOMOGENEITIES DETECTION BY ELECTROMAGNETIC METHODS

The paper deals with the biomaterials nondestructive testing using electromagnetic methods. The eddy current testing and electromagnetic - acoustic transducer methods are analyzed and applied for evaluation of conductive prosthetic materials. The defects detection results achieved by simulations and measurements using both methods are compared and discussed.

1. Introduction

Biomaterials are the materials used to manufacture prostheses, implants, and surgical instruments. They have to be completely compatible with the human body and designed not to provoke rejection by our bodies (skin, blood, bone, etc.). The biomaterials which are used in medical praxis are natural (collagen, cellulose – called biological biomaterials) or synthetic (metallic, ceramic and glass, polymeric biomaterials). The fails that usually affect the prosthetic replacement result from combination of circumstances including fatigue and stress corrosion. Periodic evaluation of the state of the devices is the significant interest particularly in the case of prosthetics whose failure can be fatal. An example of such a device is the artificial heart valve or total hip replacement. This article presents rather new techniques that have been developed for the detection of defect that occurs in the prosthetic replacements. The main condition for evaluation using electromagnetic methods is that the biomaterials are conductive.

The metallic biomaterials represent the group of materials which could be evaluated using electromagnetic methods. Metals have been used almost exclusively for load-bearing implants, such as hip and knee prostheses (hard tissue replacement). Metals have also been used as parts of artificial heart valves, as vascular stents, and as pacemaker lead (soft tissue replacement). The metallic biomaterials which are currently used in trauma and orthopedic surgery are Ti and its alloys, CoCr alloys, Stainless steels, dental metals, others.

Special type of soft tissue replacement is an artificial heart valve. Prosthetic heart valves which are used in medical praxis create two main groups. The first are bioprosthetic valves (fabricated from animal or homografts) and the others are the mechanical heart valves. These valves can be constructed using various material combinations such as metal and polymers or plastics, [2].

One special type of mechanical heart valve prostheses is the Bjork-Shiley Convexo Concave (BSCC) heart valve. BSCC heart valve has been used to replace the aortic or mitral valves. Fig. 1 shows typical design of the valve. This type of heart valve is made from metal. Occasionally the weld at one of the ends of the outlet strut develops a fracture and fails due to various reasons including mechanical fatigue and stress corrosion cracking. Although the valve in this condition performs normally, this may be a precursor to a fracture and eventual failure of the other leg of the outer strut, which leads to fatality. Hence, there is a considerable interest in detecting fractures of outlet strut in BSCC heart valves, [1].

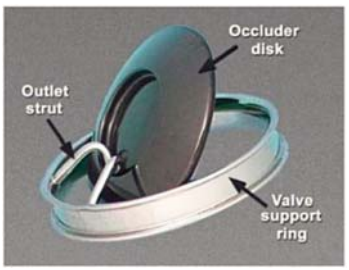

Fig. 1 Typical design of the BSCC heart valve

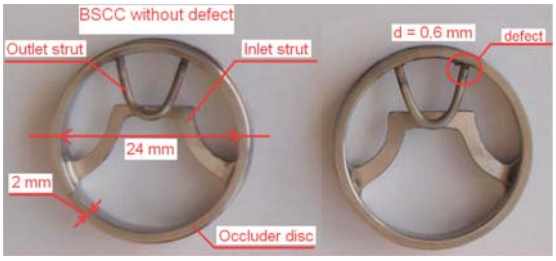

Fig. 2 Prototype of the BSCC heart valve with defect

* **Tatiana Strapacova, Klara Capova, Milan Smetana**
Department of Electromagnetic and Biomedical Engineering, Faculty of Electrical Engineering, University of Zilina, Slovakia,
E- mail: strapacova@fel.uniza.sk

CoCr alloy – Hayness 25 and Stainless steel 316L were used in experimental part. Two possible approaches to establish the biomaterials inhomogeneities are presented in this report. The present paper deals with non-destructive testing using electromagnetic methods for this purpose.

2. Eddy Current Texting – ECT

One of the widely utilized electromagnetic methods is the eddy current testing. In this method, the coil is excited by alternating current and eddy currents are induced in conductive object placed in vicinity of the conductive material. It changes the magnetic field around conductive objects where cracks and defects prevent the flow of the eddy currents, and thus leading to changes of the impedance of the pick-up coil. The method is especially suitable for detection of surface and near surface defects. The main advantage of ECT is its high sensitivity to small and shallow defects that occur in prosthetic replacement, [3].

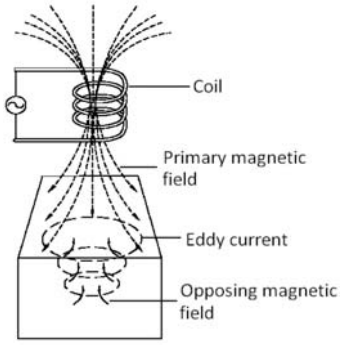

Fig. 3 Fundamental principle of the ECT method

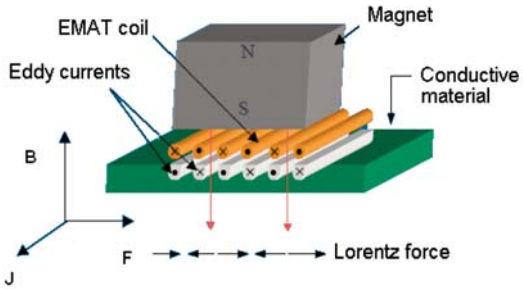

Fig. 4 Ultrasonic waves generation using EMAT

3. Electromagnetic – Acoustic Transducer Testing – EMAT

The second approach uses the Electromagnetic – acoustic transducer testing. This transducer converts electromagnetic energy to acoustic energy. When a coil of wire placed near the surface of an electrically conducting object is driven by an alternating current at the desired ultrasonic frequency, it produces a time varying magnetic field which in turn induces eddy currents in the material under test, Fig. 4. If an external static magnetic field is present, the interaction of these eddy currents with the static magnetic field results in a magnetic volume force. This force results in the generation of a wave that propagates through the specimen. When the wave passes the region of the receiving EMAT, local eddy currents are induced in the conductive material, thus resulting in a time varying magnetic field which induces voltage in the coil. EMATs are one of the several types of noncontact ultrasonic transducers. EMATs have been successfully used for applications ranging from flaw detection to thickness gauging and stress measurement, [4].

4. Numerical Evaluation and Experimental Measurement– EMAT Method

The commercially available software OPERA-3D based on the Finite Element Method (FEM) is utilized for the purpose. Spatial configuration of the EMAT inspection is shown in Fig. 5. The problem deals with EMAT probe, placed above a material under investigation. The probe coil with dimensions is shown in Fig. 5. It is supplied with current density $J = 1\text{A/mm}^2$ and frequency of the signal was $f = 50$ kHz. The second part of the EMAT probe is magnet with magnetic field which is orientedperpendicular to the surface. This configuration of the EMAT probe provides generation of a shear wave. The same configuration of the probe was used for experimental measurement,

too.

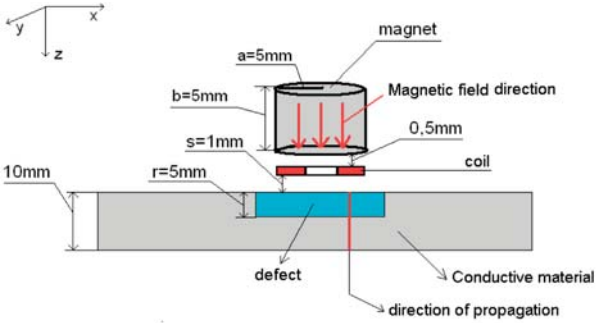

Fig. 5 Spatial configuration of the EMAT evaluation

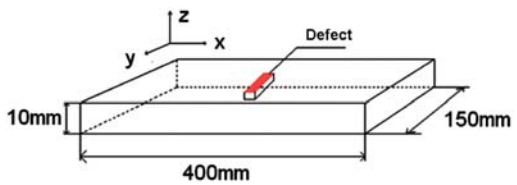

Fig. 6 Dimensions of the inspected material

Properties of the investigated material, dimensions and electromagnetic parameters of the material were set according to the real dimensions and electromagnetic parameters of the specimen, Fig. 6. The specimen was made of biomaterial SS 316 and has a conductivity of $\sigma = 1.35.106$ S/m and relative permeability of

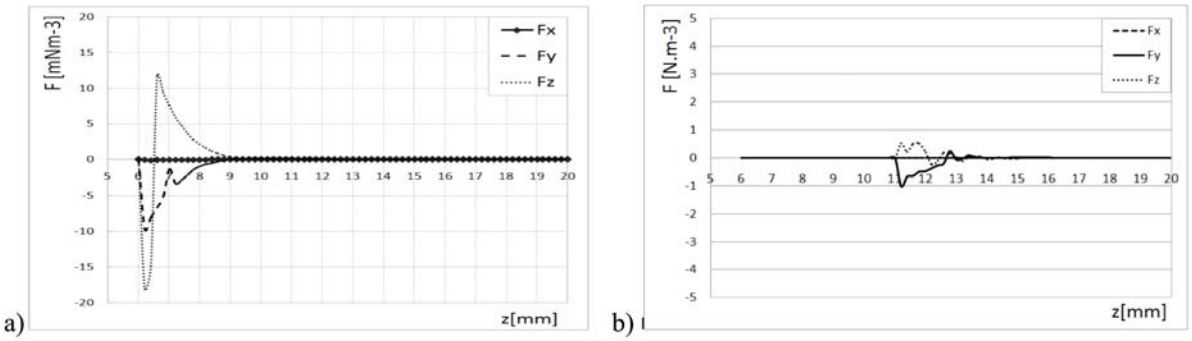

Fig. 7 Waveform of the Lorentz force components in direction to the material a) without defect, b) with defect

μr = 1. The defect was localized in the middle of the samplel. The result of the numerical simulations shows the waveform of the Lorentz force for material with defect and without defect.

Based on the simulation results we can detect the defect in a material specimen. The z – component of the Lorentz force has the highest value and it represents shear waves, as it was mentioned in configuration EMAT probe.

The experimental measurements were realized using EMAT device and EMAT probe. During the inspection the probe was positioned on the specimen without defect and with defect. The defect in the specimen can be characterized as a volume defect. The reflected ultrasonic waves – echoes from the defect were detected.

Fig. 8a shows the transmitting signal which was sent into the inspected material without defect. The Fig.8b shows the echo re-

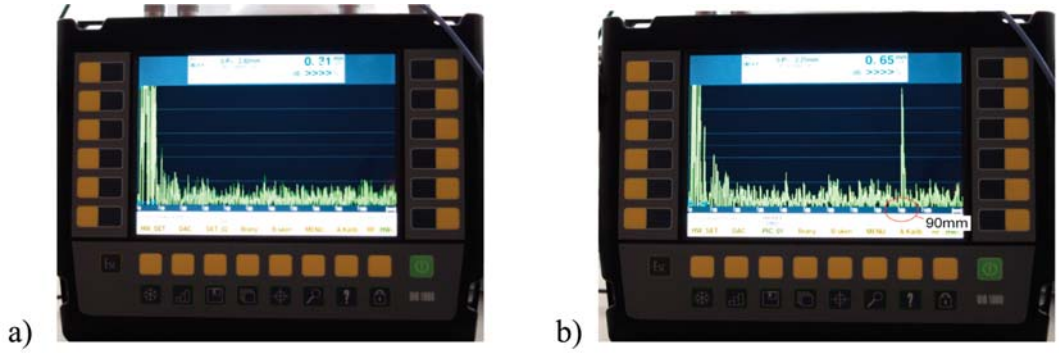

Fig.8 Signal detected from inspected material a) without defect, b) with defect

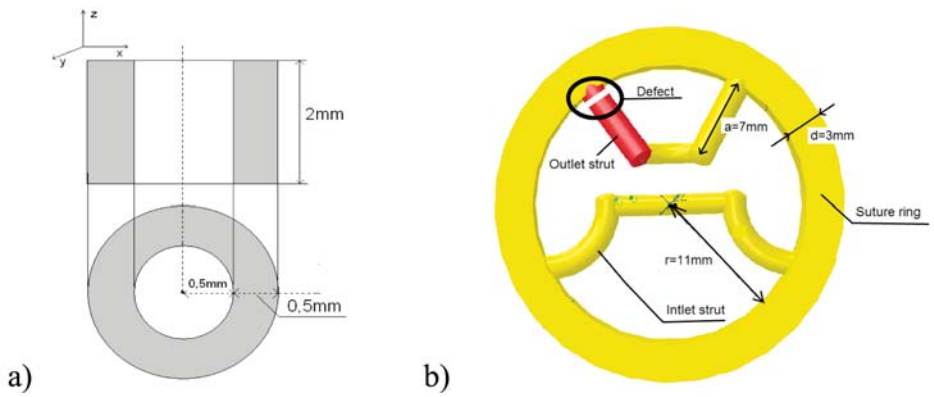

Fig. 9 a) Dimension of the coil, b) Dimension of the BSCC heart valve

flected from the defect which was localized at the depth of x = = 90mm under the surface of the inspected material sample.

5. Numerical Evaluation and Experimental Measurement – ECT Method

Complicated design of the BSCC heart valve does not allow the scanning of the material the possibilities of sweep frequency eddy current inspection of BSCC are investigated in the paper using numerical means. Standard self-inductance pancake probe, shown in Fig. 9a, is used for the inspection. Dimensions of the probe are set up according to the dimensions of the heart valve. Dimensions of the catheter which would be used for encapsulations of the coil are considered as well. The probe is positioned 1 mm above the weld of the outer strut where a crack is considered to appear. The current density of the exciting signal is kept constant during the inspection at a value of $J = 1$ A/mm^2, while its frequency is changed in a wide range starting from 10 kHz up to 500 kHz.

A complex model of the BSCC is developed. The dimensions and electromagnetic properties of the model are adjusted according to real dimensions and material properties of the BSCC heart valve. The dimensions of the heart valve are shown in Fig. 9b. The developed model considers the electromagnetic parameters of the Co-Cr alloy (Hayness 25), the conductivity is adjusted to $\sigma = 1.14 \cdot 10^6$ S/m and the relative permeability to $\mu_r = 1$.

The considered defect is localized at one end of the outlet strut, Fig. 9b. The defect is non-conductive, i.e. fatigue crack, and it represents single leg fracture (SLF) of the BSCC. Dimensions, orientation and depth of the defect are adjusted according to the real conditions that may appear in the outlet strut of BSCC heart valve. The width of the modeled defect is set to $w = 0.1$ mm and its depth d is varied from 0.1 up to 1.9 mm with a step of 0.2 mm. The simulations are run for the intact outlet strut (IOS) as well as for SLF for comparison. Numerical simulations using the developed model are carried out to calculate the probe response signal.

The results of the numerical simulations of the model introduced above are presented in this section. Fig. 10 shows amplitude frequency spectrum of the probe response signal in absolute values for four cases. The curve denoted as IOS represents the sweep frequency response signal dependence for the intact outlet strut. The

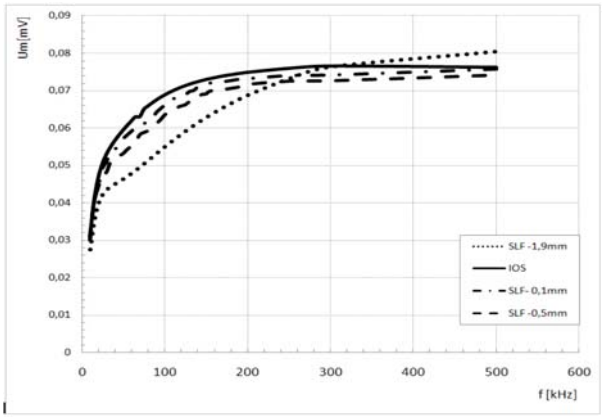

Fig. 10 Amplitude frequency spectrum of the probe response signal in absolute values

other three dependences are for the single leg fracture (SLF) with different depth of the defect, i.e. 0.1 mm, 0.5 mm and 1.9 mm. The inductive component is dominant in the probe response signal and thus the phase frequency spectrum does not show almost any difference between the IOS and the SLF.

It is evident from the presented results that there is a clear difference in the amplitude frequency spectrum between the IOS and SLF mainly for the 1.9mm which is significant within the frequency range 70 kHz up to 150 kHz.

There was used the prototype of the BSCC heart valve in experimental part. The prototype was made from CoCr alloy type Hayness 25, Fig. 2. One prototype of the valve was without defect (intact outlet strut – IOS) and other prototype of the valve contained the defect on the one end of the outlet strut, Fig. 2. The depth of the defect was $d = 0.6$mm.

The eddy current testing probe with coil parameters $L = 0.35$ μH and $N = 600$ turns was used for the measurement The probe was positioned above the outlet strut with defect, in proximity of $s = 1$ mm, Fig. 11a. The reference signal represents the signal from BSCC without defect.

Fig. 11b. shows a block diagram of the measurement, where are SG – signal generator, PA – power amplifier, P – probe, $R = 0.5\Omega$, HV – prototype of the heart valve, LIA – Lock- in amplifier with

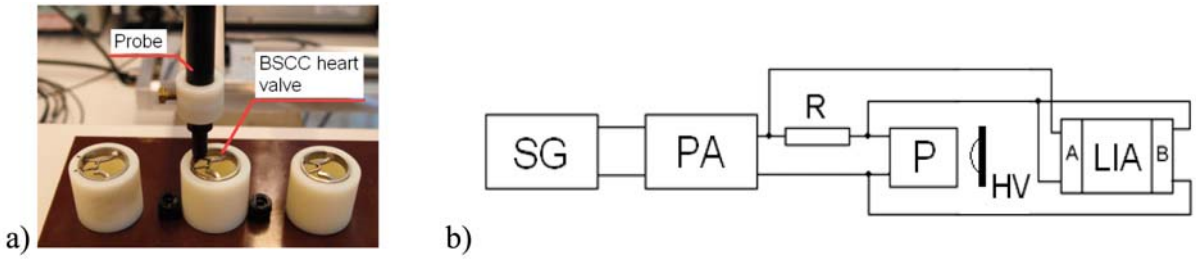

Fig. 11: a) Orientation of the probe and prototype of the valve, b) The system block diagram of the measurement

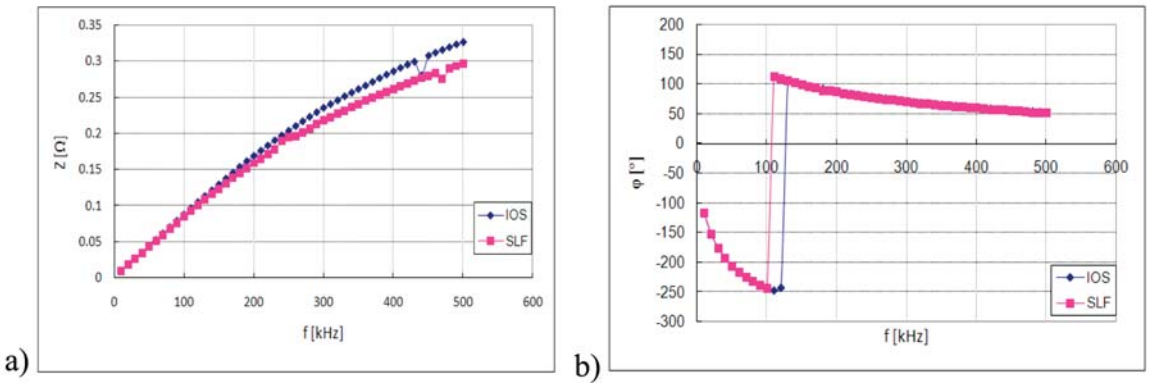

Fig. 12: a) Dependence of impedance amplitude on frequency, b) Dependence of impedance phase on frequency

two channels A and B. The signal generator produces the excitation waveform which is amplified to drive the excitation coil. The probe generates a magnetic field around the heart valve during the test.

The results show that the detected signal is different for the IOS and SLF valves, because of different eddy current flows. This demonstrates that a SLF can be detected by measuring detected signal variation in dependence on frequency. It can be concluded that the sweep frequency technique proposed for the eddy current inspection of BSCC outer strut is very promising. It helps to overcome one problem connected with eddy current inspection of the material objects where the scanning over an inspected surface is not needed.

6. Conclusion

The paper introduced new approaches for defect detection in a biomaterial for prosthetic replacement with focus on artificial heart valve use. Both models of the biomaterial specimens and the artificial heart valve were developed and proposed methods were verified using numerical simulations and experimental measurements. The presented results of the numerical simulations and experiments clearly showed that the EMAT method is convenient for detection of volume cracks which could affect the biomaterials of prosthetic replacements. From the achieved results of the evaluation of BSCC heart valve using ECT method the differences in the amplitude frequency spectrum of the intact outlet strut and the strut mainly with deeper defect are evident.

Acknowledgement

This work was supported by the Slovak Research and Development Agency under the contract No. APVV-0194-07.

This work was supported by grant of the Slovak Grant Agency VEGA, project No. 1/0308/08.

The authors express their thanks to Prof. R. Grimberg for lending the valve prototypes.

References

[1] VAN NEER, P.: *The Bjork- Shiley valve: Detecting Broken Strut Using Standards Diagnostic Ultrasound Instruments,* MSc Thesis,2005

[2] BORRERO, J. R., CURE, J., FABRE, N. J., ROSADO, E.: *Mechanics of Prosthetic Heart Valves.* Applications of Engineering Mechanics in Medicine, GED University of Puerto Rico, Mayaguez, 1993, http://academic.uprm.edu/~mgoyal/materialsdec2003/j03prostheticheartvalve.pdf

[3] JANOUSEK, L., MAREK, T., GOMBARSKA, D.: *Eddy Current Non-destructive Testing of Conductive Materials,* Communications – Scientific Letters of the University of Zilina, No. 8, 2006, pp. 29–33, ISSN 1335-4205

[4] MAXFIELD, B.: *Electromagnetic Acoustic Transducer,* Ultrasonic Nondestructive Evaluation, Engineering and Biological Material Characterization, Chapter 8, CRC Press LLC 2004.

Katarina Istenikova *

THE INFLUENCE OF INHOMOGENEITY PRESENT IN LAYERED BIOLOGICAL STRUCTURE ON ELECTROMAGNETIC FIELD DISTRIBUTION

The knowledge of electrical properties of biological materials and their interaction with electromagnetic waves is necessary for suitable determining the effect of electromagnetic field on biological systems and, sequentially, prevention of undesirable consequences on human organism. Because of complex heterogeneous structure of human body the electromagnetic field distribution in biological systems is very complicated and depends, among others, on the type of tissue and on the presence of complicated layered structures and interfaces. With the knowledge of these electrical properties the absorption of energy and the field distribution which are the results of the solution to a boundary value problem can be obtained. This paper is focused on description of influence of inhomogeneity occurring in the human structure on electromagnetic field propagation. The inhomogeneity is represented by silicon brick and brain tumor placed into the model.

1. Introduction

Biological tissue is a complex and highly heterogeneous material. The dielectric properties of biological tissues have been of interest for over a century because they determine the pathways of current flow through the body and, thus, are very important in the analysis of wide range biomedical applications. The results from simple models phantoms of biological tissue for microwave hyperthermia at cancer therapy are not representative of the reality of different tissues, their associated shapes and boundaries, which will result in the electromagnetic (EM) propagation and power deposition rate. The reflected energy will be influenced not only by the wave impedance of each layer, but by the layer thickness as well. In a finite layered dielectric, multiple reflections and transmissions of electromagnetic wave occur at each boundary. Boundaries between tissues with divergent dielectric properties may produce localized hot spots and cannot be ignored. Analytical solution of a layered planar structure is given in this paper. The main concern of this paper is in influence of the inhomogeneity presence in layered structure on resulting signal.

The dielectric permittivity (ε) is a parameter which characterizes the interaction between the electric field and the bound charges in the material. Due to bound charges for lossy materials the permittivity is complex variable with both real (ε′) and imaginary (ε″) components. The interaction between the electric field and the bound charges in the tissue results in an oscillatory motion of the bound charges. The part of the motion that is 90° out of phase with the electric field is characterized by the real part of the permittivity (ε″) and is described as a lossless interaction. But as the bound charges oscillate, they also heat up due to friction-like forces within the molecule and from molecules nearby. This motion component is in phase with the electric field and is represented by the imaginary part of the permittivity (ε″). From the electrical engineering point of view, studying the bulk dielectric properties, mainly permittivity and conductivity, remains the most direct way of characterizing any substance [1], [2].

2. Wave propagation in biological materials

If material conductivity does not equal zero value a material is lossy. Biological tissues are lossy materials and this loss changes the way the wave interacts with the material and its propagation behavior. Power will be distributed in the lossy material as wave passes through it, thus causing loss to the propagating wave. If EM energy is cumulated in the material, the material will heat up.

To better understand how EM power is deposited in a lossy material, considering theory of waves, Ampere's law can be written in a form

$$\nabla \times \overline{\boldsymbol{H}} = (\sigma + \omega\varepsilon'')\overline{\boldsymbol{E}} + j\omega\varepsilon'\overline{\boldsymbol{E}} \qquad (1)$$

where $\bar{\boldsymbol{H}}$ represents magnetic field intensity (A/m), $\bar{\boldsymbol{E}}$ represents electric field intensity (V/m), σ is conductivity of the material and ω is an angular frequency (rad/s). The first term on the right-hand side of this equation represents the current that produces a loss (heat) in the material through movement of free charges and bound charges. The last term in (1) is the displacement current which represents the lossless portion of the oscillation of the bound charges [3].

* **Katarina Istenikova**
Department of Measurement and Applied Electrical Engineering, Faculty of Electrical Engineering, University of Zilina, Slovakia,
E-mail: istenikova@fel.uniza.sk

The loss properties of material are usually expressed as a loss tangent

$$tg\,\delta = \frac{\varepsilon''}{\varepsilon'} = \frac{\sigma}{\omega\varepsilon'_r\varepsilon_0} \tag{2}$$

where σ is the electrical conductivity (S/m), ε'_r is the relative dielectric constant, $\varepsilon_0 = 8.854191 \times 10^{-12}$ (F/m) is the permittivity of free-space and ω is angular frequency of applied electromagnetic field.

2.2. Relaxation processes in biological tissues

The response of biological tissues at microwave EM field is determined by the electro-chemical characteristics of cells, cellular structure and the intra-cellular fluid too. The permittivity of biological tissues is determined by several important dispersion phenomena whose contributions are normally restricted to specific band.

The dielectric spectrum of biological tissue is characterized by three main relaxation regions α, β, and γ at low, medium and high frequencies (more than 100MHz) and other minor dispersions between β and γ are reported as δ-dispersion, connected with proteins bound water [4]. The low frequency α-dispersion is associated with ionic diffusion processes at the site of the cellular membrane. The β-dispersion, in the hundreds of kilohertz region, is mainly caused by the polarization of cellular membrane, and finally the γ-dispersion, in the gigahertz region, is caused due to the polarization of the water molecules.

In general, dispersion characteristics of a large class of biological materials can be represented by Cole-Cole equation

$$\dot{\varepsilon} = \varepsilon_\infty + \frac{\varepsilon_s - \varepsilon_\infty}{1 + (j\omega\tau)^{1-p}}, \tag{3}$$

where ε_∞ and ε_s are the relative permittivities of material at infinite and zero frequencies respectively. The $(1-p)$ parameter represents distribution of relaxation in investigated material where p is a distribution parameter in the interval $0 \leq p < 1$ [4].

The classical representation of frequency dependence of complex permittivity real and imaginary parts respectively to the diagram is in plotting the normalized real and imaginary part of the complex permittivity as functions of normalized frequency $f_n = \omega\tau$. A dependence of normalized relative permittivity and imaginary part of complex permittivity on normalized frequency calculated for pure water (a fundamental component occurred in biological tissues) is in Fig. 1. The main impact on the dielectric processes in investigated materials have frequencies in the region of dielectric dispersion where the relative permittivity decreases.

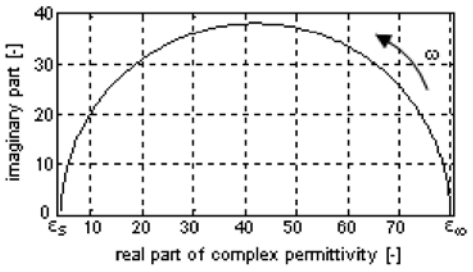

Fig. 1 Diagram for Cole-Cole equation in complex plane

One of the most commonly used models represents the parts of complex permittivity plotted as functions of $\log_{10}\omega\tau$. In this case, these two parameters are presented independently of each other, Fig. 2.

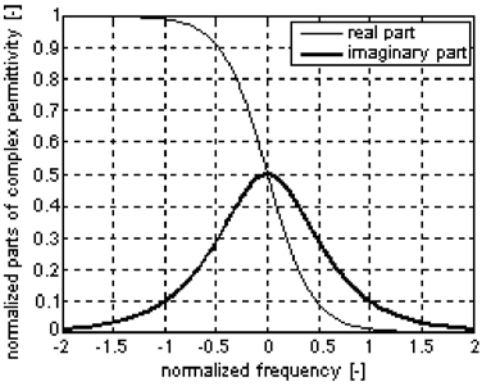

Fig. 2 Diagram for Cole-Cole equation, permittivity is a function of $\log_{10}\omega\tau$

Each biological material has its typical Cole-Cole diagram, which characterizes relaxation processes in chosen frequency region. Knowing the frequency dependence of real and imaginary part of complex permittivity enables the calculation of energy distribution in investigated biological tissue and optimization at hyperthermia planning at cancer treatment.

2.1. Boundary conditions for biological materials

Boundary conditions are very useful in interpreting and explaining characteristic behaviors of EM field interactions with biological systems. Because $\bar{E}$ is a vector, it can be resolved into two components, one tangential to the boundary and one normal to the boundary. Maxwell's equations require that the normal components of the $\bar{E}$ field at a charge-free boundary of two biological structures comply (4)

$$\varepsilon_1 E_{n1} = \varepsilon_2 E_{n2}, \tag{4}$$

where E_{n1} is the normal component of the $\bar{E}$ field in structure 1 at the boundary, E_{n2} is the normal component of the $\bar{E}$ field in structure 2 at the boundary, ε_1 is the permittivity of structure 1 and ε_2 is the permittivity of structure 2.

The boundary condition for the tangential components of the field at the boundary of two structures is

$$E_{t1} = E_{t2}, \tag{5}$$

where E_{t1} and E_{t2} are the tangential components of $\bar{E}$ field at the boundary in structures 1 and 2, respectively [5].

Boundary conditions can give us a rough understanding of processes in every layers of biological sample. Fig. 3 shows that the tangential component of $\bar{E}$ field will pass through all layers of tissue without changing, as is indicated in (4). On the other hand, Fig. 4 shows that normal component of $\bar{E}$ field changed by the layers of tissue, as is given in (5). The field would be attenuated by the lossy tissues and reflections would occur within the layers.

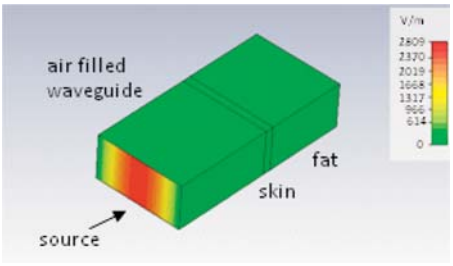

*Fig. 3 The propagation of tangential component of the **E** field in skin - fat layered structure for mode TE_{10}*

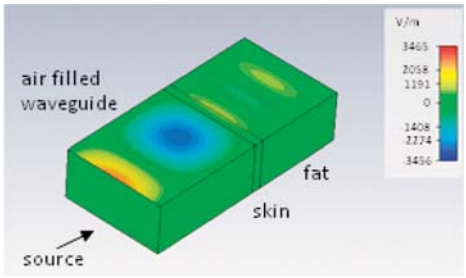

*Fig. 4 The propagation of normal component of the **E** field in skin - fat layered structure for mode TE_{10}*

2.3. Reflection and transmission characteristics in layered structures

When there are several layers of different tissues, the reflection and transmission characteristics become more complicated. Multiple reflections occur between tissue boundaries, with a resulting modification of the reflection and transmission coefficients, Fig. 5. The transmitted wave perpendicular to the boundary interacts with the reflected wave and both form standing waves in each layer. This phenomenon becomes especially pronounced if the thickness of each layer is less than the penetration depth for that tissue.

The un-dashed coefficients represent incident signal arriving from the left and the dashed ones represent incident signal arriving from the right. Then we can determine reflection and transmission coefficients

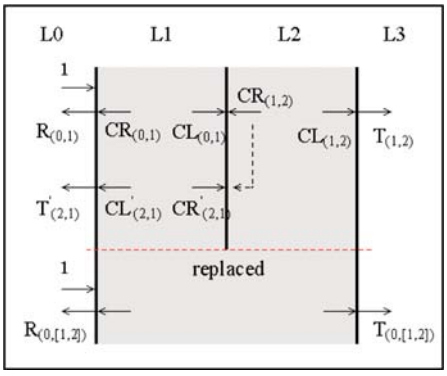

Fig. 5 Two-layered model with corresponding coefficients. CR and CL represent total sum of multiple reflections within sample

$$R_{(0,[1.2])} = R_{(0,1)} + \frac{CL_{(0,1)}CR_{(1,2)}T_{(2,1)}}{1 - CR'_{(2,1)}CR_{(2,1)}}, \tag{6}$$

$$T_{(0,[1.2])} = \frac{CL_{(0,1)}T_{(1,2)}}{1 - CR_{(1,2)}CR'_{(2,1)}}. \tag{7}$$

This procedure can be then applied for *n*-layered structure [6].

3. Numerical results

To depict the behavior of the EM field within a layered biological sample without inhomogeneity, the model of two homogenous tissue layers was processed in the software environment CST Microwave Studio for electromagnetic simulation of high frequency components. For simulations the frequency 9.295GHz which comes under the X-band frequency range was used. The dielectric parameters used for different layers of biological sample were chosen according to our previous measurement results using Hippel's method [7]. These data are presented in Tab. 1.

Dielectric parameters of biological layers — Table 1

	Frequency f (GHz)	Permittivity ε' (-)	Conductivity σ (S/m)
skin	9.295	41	0.15
fat	9.295	5	0.04
water	9.295	81	0.01

Numerical results were performed for layered structure created from the skin layer with constant thickness $d_1 = 2$mm and the fat layer with thickness $d_2 = 15$mm. Simulated layered structure was inserted into the waveguide with dimensions corresponding to the frequencies from X band.

In this case, the reflection coefficient of EM wave is influenced by energy storage in investigated biological material. The

influence of the discontinuity presence on power loss density is in Fig. 6.

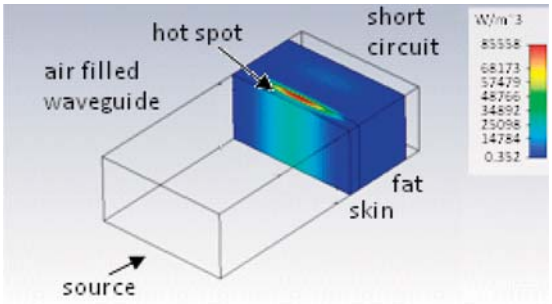

Fig. 6 The distribution of power loss density in skin - fat layered structure (short circuited wavegude)

A standing wave can be set up in the fat layer, which can create the raise of the energy storage. The EM fields with high density of electric field in the fat can create very painful subdermal hot spots, Fig. 6, that are difficult to treat, and must be avoided. A common way of mitigating this effect is to place a layer of water between the electromagnetic source and the body, Fig. 7. By propagating the field into the water first, the concentration of power at the surface of the body can be minimized and more uniform field distributions result. The water can be cooled to reduce the heat at and near the body surface.

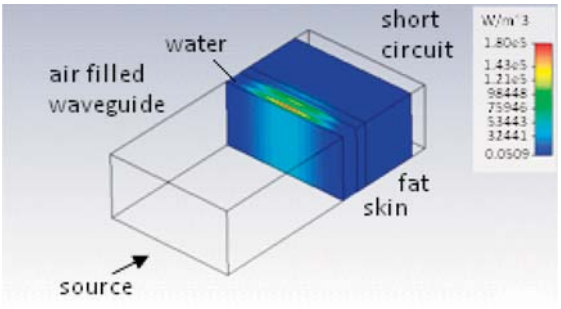

Fig. 7 The distribution of power loss density in skin - fat layered structure after placing the water layer between EM source and the body

To find out the influence of inhomogeneity presence in the volume of fat layer on electric energy field density distribution in layered structure was the main idea of this paper. The inhomogeneity - silicon brick - with dimensions 5×2×3 mm, with relative permittivity $\varepsilon' = 11.9$ and the loss tangent $tg\delta = 0.004$ was inserted into the fat volume directly under the skin layer. The electric energy density in layered structure distribution with silicon is shown in Fig. 8.

From Fig. 8 it can be seen the strong influence of inhomogeneity presence in the volume of fat layer on EM field distribution in investigated biological layered structure. Fig. 8 allows us to determine location of areas in the volume of fat layer with the

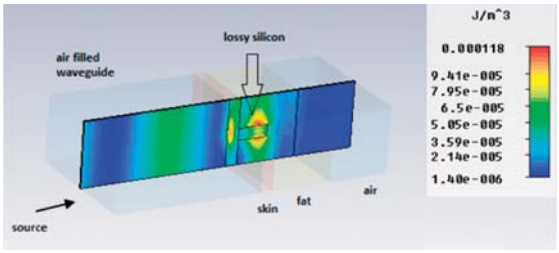

Fig. 8 The distribution of electric energy density in skin - fat layered structure (open waveguide) with silicon inhomogeneity.

spots characterised by higher electric field density. The temperature of biological material irradiated with high frequency EM field may arise in these areas.

The idea of next simulation was to find out the influence of tumor characterized with higher water content [2] presence on electric field energy density distribution and power loss distribution in layered biological structure. For this simulation a four-layered human head model consisting of skin, fat, bone and brain layer was created. The distance between the source and the media was choosen 4.5 mm. Dielectric properties of each layer are presented in Tab. 2.

Dielectric properties of head tissues [5] Table 2

	Thickness d (mm)	Permittivity ε' (-)	Conductivity σ (S/m)
skin	1.5	41	0.7
fat	1	5	0.04
bone	3	12	0.95

The inhomogeneity - spherical tumor - with diameter of 3 mm and with relative permittivity $\varepsilon' = 38$ and conductivity $\sigma = 11\ Sm^{-1}$ was inserted into the brain layer under the bone layer. This inhomogeneity is different in size and shapes in comparison with surrounding tissues. The electric energy density and power loss density in layered structure distribution with tumor is shown in Figs. 9 and 10.

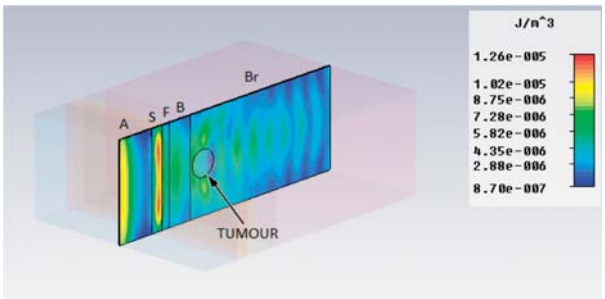

Fig. 9 The distribution of electric energy density in the multilayered human head model with presence of brain tumor, A - air, S - skin, F - fat, B - bone, Br - brain

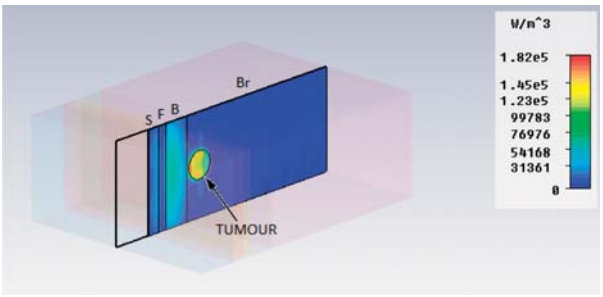

Fig. 10. The distribution of power loss density in the multilayered human head model with presence of brain tumor, A – air, S – skin, F – fat, B – bone, Br – brain

In the figures it is shown that the presence of tumor in the brain has a high influence on EM field distribution with result of having more field concentration than the surrounding brain layer.

4. Conclusion

Because of huge introduction of equipment which emit EM fields of various frequency ranges and intensities the scientists in electrical engineering are focused to study the way of EM field interaction with biological tissues. The experimental and numerical results connected with the study of dielectric properties of biological materials and their properties in the electromagnetic field and, on the other hand, the influence of dielectric properties of biological material on EM wave propagation gives us the information useful in medical diagnostics and therapy using microwaves. The microwave dielectric method has been one of the most reliable techniques for investigation of the dynamic structure of macromolecules and dielectric relaxation measurements have been applied to the investigation of dielectric properties of various biological tissues. This and other similar information inspired us to pay attention to observation of some materials behavior in biological tissues, particularly in tumors and layered structures.

The presented numerical results are useful at the microwave generator parameters optimization used for microwave hyperthermia at malignant tumors treatment. The obtained numerical results can be also useful at design of chosen human body part phantoms. In the view of this analytical approach which allows us to evaluate coefficients characterizing propagation of EM wave in the layered structure, the next parameters of EM wave like SAR (specific absorption rate) or the presence of inhomogeneities with different dielectric characteristic in investigated structure can be calculated [8]. Further theoretical and experimental investigations will be carried out to temperature dependences of dielectric properties of biological tissues, because it is inevitable to investigate the penetration of microwaves through different layers in clinical practice using microwaves.

Acknowledgment

The work has been done in the framework of Grant VEGA 1/0761/08 „Design of Microwave Methods for Materials Nondestructive Testing“ of the Ministry of Education of the Slovak Republic and project APVV-0535-07.

References

[1] TOFIGHI, M.R., DARYOUSH, A.: *Measurement Techniques for the Electromagnetic Characterization of Biological Materials,* Handbook of Engineering Electromagnetics, CRC Press, 2004.
[2] PEYMAN. A.: *Dielectric Properties of Tissues, Variation with Structure and Composition,* Proc. Conference ICAA, 2004, 863–864.
[3] FURSE C., CHRISTENSEN D. A., DURNEY C. H.: *Electric and Magnetic Fields: Basic Concepts,* Basic Introduction to Bioelectromagnetics, CRC Press, 2009.
[4] CHRIST, A., KLINGENBOCK, A., SAMARAS, T., GOICEANU, C., KUSTER, N.: *The Dependence of Electromagnetic Far-field Absorption on Body Tissue Composition in the Frequency Range from 300 MHz to 6 GHz,* IEEE Transaction on Microwave Theory and Techniques, vol. 54, 2006, 2188–2195.
[5] AKRAM, G., JASMY, Y.: *LabVIEW-Based Planar Multilayered Model for Estimation of the Absorbed Energy Inside Biological Tissues,* IEEE Antennas and Propagation Magazine, vol. 50 (2), 2008, 152–158.
[6] ZRNIK, J.: *Numerical Modelling of Electromagnetic Wave Interaction with Heterogeneous Biological Structure,* Proceedings of AMTEE'09, 2009, VI-13 – VI-14.
[7] ISTENIKOVA, K., FAKTOROVA, D.: *Influence of Biological Materials Dielectric Parameters on Electromagnetic Wave Propagation,* Proceedings of Elektro'10, 2010, TA5_44 – TA5_48.
[8] ISTENIKOVA, K., FAKTOROVA, D.: *Modelling of Scattering Parameters in Biological Tissues,* Proceedings of CPEE'10, p. 2010.

Libor Hargas – Dusan Koniar – Stanislav Stofan – Miroslav Hrianka *

SOPHISTICATED METHODS FOR TISSUE PERFUSION EVALUATED

This paper focuses on image acquisition system designing for biomedical image enhancement. It introduces the possibilities of diagnostics and analysis of tissue via virtual instrumentation. The two dimensional images shot by the camera provide information about the surface properties and degradation of a real skin. The main idea is based on the human skin parameters measured for healthy and ill skin. The aforementioned access provides parameters evaluation by creating a structure model. The anomalies are recognized by this model.

1. Introduction

When the image is taken, the light conditions are very important. If the image was too dark or bright, the image details are not visible. An optimal light must be maintained from this reason.

Solid-state light dimmers work by varying the "duty cycle" (on/off time) of the full AC voltage that is applied to the lights being controlled. For example, if the voltage is applied for only half of each AC cycle, the light bulb will appear to be much less bright than when it gets the full AC voltage, because it gets less power to heat the filament. Solid-state dimmers use the brightness knob setting to determine at what point in each voltage cycle to switch the light on and off.

Image segmentation can use global grayscale thresholding, global color thresholding, local thresholding, and morphological segmentation. Image segmentation is the process of separating objects from the background and each other so that each object can be identified and characterized.

Thresholding segments an image into a particle region—which contains the objects under inspection—and a background region based on the pixel intensities within the image. The resulting image is a binary image.

Thresholding can be used to extract areas that correspond to significant structures in an image and to focus analysis on these areas.

Thresholding an image is often the first step in a variety of machine vision applications that perform image analysis on binary images, such as particle analysis, golden template comparison, and binary particle classification.

2. Design of light regulation

On the basis of simulations a wiring dimmer was designed. The power supply is made directly from the mains supply 230V via input transformer [1]. Dimming feature is provided through one PWM channel, which generates pulses at the gate on a switching transistor [2].

The measurement card is generating impulses to the circuit. The protection and electrical separation of the measurement card from the power circuit is guaranteed through the opto coupler and driver.

The dimmer control performance is realized through virtual instrumentation. The proposed virtual instrumentation included a connection of high speed video camera applications and light microscope regulatory loop. This regulation is implemented by setting the optimal switching pulse width (duty cycle). The standard frequency pulse from the measurement card is about 25 kHz to 50 kHz.

The optimal duty cycle choice is realized by the ongoing analysis of statistical parameters of the histogram of image acquisition [3], [4].

The mean position of the image histogram is an important indicator of proper lighting (Fig. 1). The optimal mean value is the case in the mid-range gray level (128 at 8 bpp).

The measured characteristic is the value of the high speed video camera frame 60 fps. Based on measured images histograms for used halogen lamp and fps, the optimal duty cycle range is approximately 20–30 % The histogram mean was about 124, in duty cycle 25% and a value close to the optimum value.

* **Libor Hargas, Dusan Koniar, Stanislav Stofan, Miroslav Hrianka**
Department of Mechatronics and Eletronics, Faculty of Electrical Engineering, University of Zilina, Slovakia, E-mail: libor.hargas@fel.uniza.sk

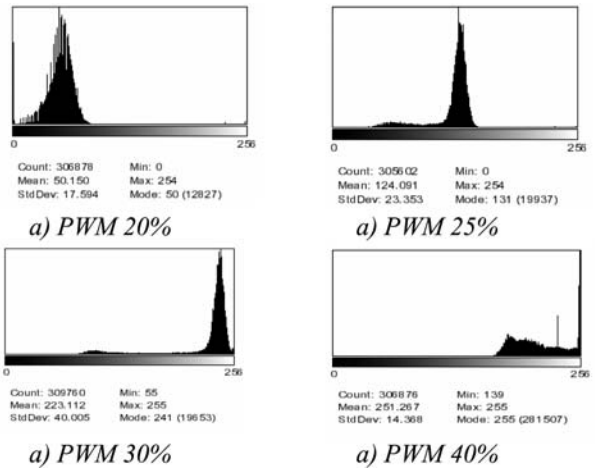

Fig. 1 PWM image histograms

Frequency increase caused a shifting of duty cycle towards higher values. The halogen lamp lighting regulation is realized on the basis of the measured characteristic. The approximation curve is in Fig. 2. The duty cycle is changed with 1% resolution and it tried to set up mean value near value 128. For different fps it is necessary to create different curves. The approximation for different fps is done by these curves.

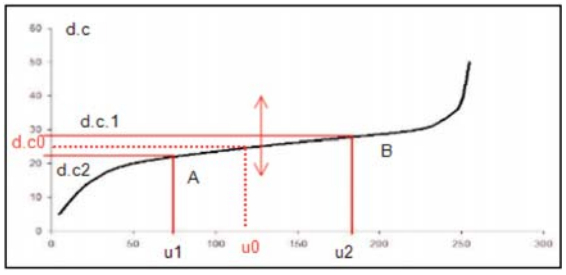

Fig. 2 Image histogram mean dependence on dimmer switching pulses duty cycle

We can approximate the curve between the points A and B (Fig. 2) as a linear line:

$$y = ax + b \tag{1}$$

$$A = \left[\mu_1, d \cdot c_1\right]; \quad B = \left[\mu_2, d \cdot c_2\right] \tag{2}$$

$$a = \frac{d \cdot c_2 - d \cdot c_1}{\mu_2 - \mu_1} \tag{3}$$

$$b = d \cdot c_1 - \frac{d \cdot c_2 - d \cdot c_1}{\mu_2 - \mu_1}\mu_1 \tag{4}$$

$$y = \frac{d \cdot c_2 - d \cdot c_1}{\mu_2 - \mu_1}x + d \cdot c_1 - \frac{d \cdot c_2 - d \cdot c_1}{\mu_2 - \mu_1}\mu_1 \tag{5}$$

$$\mu_i < \mu_0 \Rightarrow d \cdot c \uparrow \tag{6}$$

$$\mu_i > \mu_0 \Rightarrow d \cdot c \downarrow \tag{7}$$

$$d \cdot c_i - d \cdot c_0 = \pm \Delta d \cdot c \tag{8}$$

where $d \cdot c$ – duty cycle value
μ – gray level value

The dimmer control performance is realized through virtual instrumentation.

3. Image preprocessing

Global Grayscale Thresholding

Global grayscale thresholding includes manual thresholding and automatic thresholding techniques. Global thresholding works best when the inspection images exhibit a uniform lighting both within each image and across multiple images. Particles are characterized by an intensity range. They are composed of pixels with gray-level values belonging to a given threshold interval (overall luminosity or gray shade). All other pixels are considered to be part of the background. [5], [6]

Thresholding sets all pixels that belong to a range of pixel values, called the threshold interval, to 1 or a user-defined value, and it sets all other pixels in the image to 0.

Manual Threshold

The threshold interval in a manual threshold has two user-defined parameters: lower threshold and upper threshold. All pixels that have gray-level values equal to or greater than the lower threshold and equal to or smaller than the upper threshold are selected as pixels belonging to particles in the image. [7]

Automatic Threshold

Automatic thresholding techniques include:

- Clustering
- Entropy
- InterVariance
- Metric
- Moments

In contrast to manual thresholding, these techniques do not require to set up the lower and upper threshold values. These techniques are well suited for conditions in which the light intensity varies from image to image.

4. Threshold techniques

Clustering

Clustering is the most frequently used automatic thresholding method. It can be used when we need to threshold the image into more than two classes.

Clustering sorts the histogram of the image within a discrete number of classes corresponding to the number of phases perceived in an image. The gray values are determined, and a barycenter is determined for each class.

This process is repeated until it obtains a value that represents the center of mass for each phase or class.

The threshold value is the pixel value k for which the following condition is true:

$$\frac{\mu_1 + \mu_2}{2} = k\,, \tag{9}$$

where μ_1 is the mean of all pixel values that lie between 0 and k, and μ_2 is the mean of all the pixel values that lie between $k + 1$ and 255.

Entropy

Based on a classical image analysis technique, entropy is best for detecting particles that are present in minuscule proportions on the image. For example, this function would be suitable for fault detection.

In this method, the threshold value is obtained by applying information theory to the histogram data. In information theory, the entropy of the histogram signifies the amount of information associated with the histogram. The probability $p(i)$ of occurrence of the gray level i is represented:

$$p(i) = \frac{h(i)}{\sum_{i=0}^{N-1} h(i)}, \tag{10}$$

where $h(i)$ represents the number of pixels in the image at each gray level value

The entropy H of a histogram of an image with gray levels in the range $[0, N-1]$ is given by

$$H = \sum_{i=0}^{N-1} p(i)\log_2 p(i)\,, \tag{11}$$

If k is the value of the threshold, then the two entropies represent the measures of the entropy (information) associated with the black and white pixels in the image after thresholding.

Simplified, the threshold value is the pixel value k at which the following expression is maximized:

$$H = -\frac{1}{\sum_{i=0}^{k} h(i)} \sum_{i=0}^{k} h(i)\log_2 h(i) - \frac{1}{\sum_{i=k+1}^{N-1} h(i)} \sum_{i=k+1}^{N-1} h(i) \cdot \cdot \log_2 h(i) + \log_2\left(\sum_{i=0}^{k} h(i) \sum_{i=k+1}^{N-1} h(i)\right), \tag{12}$$

Interclass Variance

Interclass variance is based on discriminant analysis. An optimal threshold is determined by maximizing the between-class variation with respect to the threshold.

The threshold value is the pixel value k at which the following expression is maximized:

$$\sigma_B^2(k) = \frac{\left[\mu_T \omega(k) - \mu(k)\right]^2}{\omega(k)\left[1 - \omega(k)\right]}\,, \tag{13}$$

where

$$\mu(k) = \sum_{i=0}^{k} ip(i)\,, \tag{14}$$

$$\mu_T = \sum_{i=0}^{N-1} ip(i)\,, \tag{15}$$

$$\omega(k) = \sum_{i=0}^{k} p(i)\,, \tag{16}$$

Metric

For each threshold, a value determined by the surfaces representing the initial gray scale is calculated. The optimal threshold corresponds to the smallest value.

The threshold value is the pixel value k at which the following expression is minimized:

$$\sum_{i=0}^{k} h(i)\left|(i - \mu_1)\right| + \sum_{i=k+1}^{N-1} h(i)\left|(i - \mu_2)\right|, \tag{17}$$

where μ_1 is the mean of all pixel values in the image that lie between 0 and k, and μ_2 is the mean of all the pixel values in the image that lie between $k + 1$ and 255.

Moments

This technique is suited for images that have poor contrast. The moments method is based on the hypothesis that the observed image is a blurred version of the theoretically binary original. The blurring that is produced from the acquisition process, caused by electronic noise or slight defocalization, is treated as if the statistical moments of average and variance were the same for both the blurred image and the original image. This function recalculates a theoretical binary image.

In this method the threshold value is computed in such a way that the moments of the image to be thresholded are preserved in the binary output image.

The k-th moment m of an image is calculated as

$$m_k = \frac{1}{n} \sum_{i=0}^{N-1} i^k h(i) \tag{18}$$

where n is the total number of pixels in the image, N represents the total number of gray levels in the image (256 for an 8-bit image).

5. Human Tissue Measurement

Virtual instrument was built in collaboration with Jesenius Faculty of Medicine in Martin. Various tissue parameters can be measured for health skin or tissue. The parameters for unhealthy

skin or tissue can be measured too, with this developed virtual instrument (e.g. psoriasis vulgaris or lichen planus).

The good diagnostic index and parameter are used for derma blood supply evaluation. The derma blood supply is presented by vessels coverage. The goal of the developed virtual instrument is to find the vessels coverage of a searched tissue. The virtual instrument can find vessels coverage for healthy or pathological changed tissue. The region of interest (ROI) can be selected and processed statistically. The vessels coverage is a base for statistical analysis. The vessels are recognized and the ROIs percentage coverage is calculated.

The basic image analysis was performed in NI Vision Assistant. Then the script was converted to the LabVIEW [8]. The images of abdominal tissue were used as the base for statistical samples.

The script was preprocessed in NI Vision Assistant after the image analysis. Important color space was extracted and its thresholding was done in this step of processing. Then we created a binary mask together with morphological operators (dilatation, erosion, closing, opening). As these operations are basic for ROI creation we converted the script to LabVIEW. The results of images preprocessing are in Fig. 3.

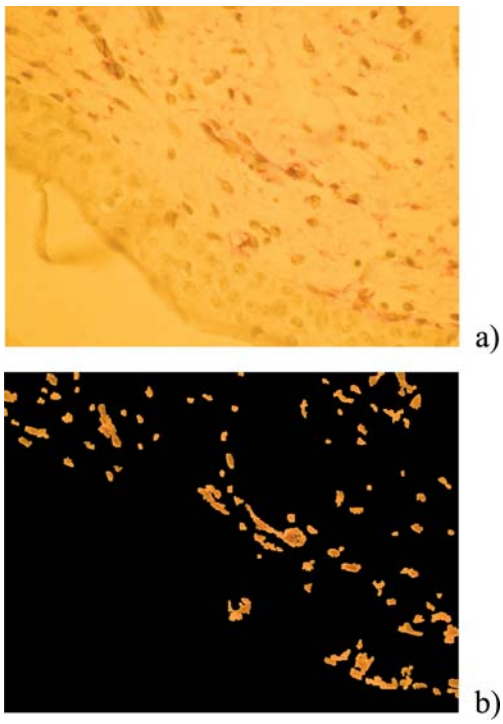

Fig. 3 a) Original image, b) result of preprocessing in NI Vision Assistant

If we want sharpen vessels in this tissue, we have to use a special colorized solution. We can perceive the sharpened vessels as dark red or rusty objects. The specimen background is created from epithelium cells, which are not relevant for our analysis. This fact is shown in Fig. 4.

The tissue samples are scanned as 24 bit RGB color images with JPEG compression. When the images are remapped to single color planes, the histogram can be done for each one of them. Following the histogram distribution and IMAQ tool measurement it can be determined that 8 bit color space Red and Green are approximately identical. The gray levels distribution is different for the color space Blue compared with the color spaces R and G. The differences are strong between the vessels and the background with cells in the color space B. Therefore the color space B is selected for a threshold. The gray levels values have a closed range, therefore the histogram stretching must be performed to improve gray levels distribution. The threshold is done on stretching image and in this way the threshold is refined.

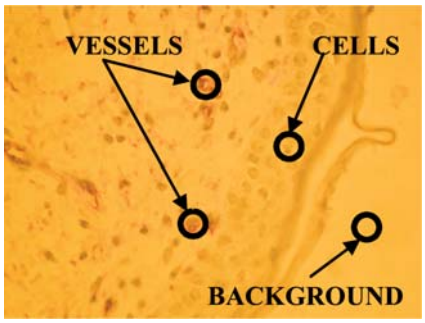

Fig. 4 Abdomen specimen

ROI can be selected manually or automatically. The image centroid is computed in an automatic mode and the ROI size is computed from the original image size (Fig. 5). The ROI centre and dimensions can be changed in manual mode by a user. The other parameters of selected ROI, e.g. threshold value, morphological operators and iterations counts, can be also changed in the manual mode.

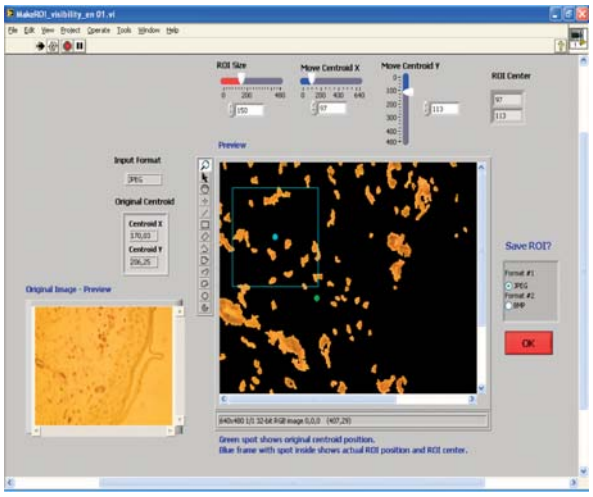

Fig. 5 Application front panel

6. Conclusion

The acquisition system for tissue samples contains intelligent illumination dimming hardware. The hardware automatically regulates halogen lamp lighting for a fast digital camera by means of a measurement card. Regulating parameter for dimmer (PWM duty cycle) is computed from the image features, the histogram distribution and the intensity relations. Dimming helps to preserve optimal light conditions for acquisition system. The optimal light conditions are important for accurate image processing. The dimmer eliminates abnormal heat generation in microscope condenser for the used high-power halogen lamp.

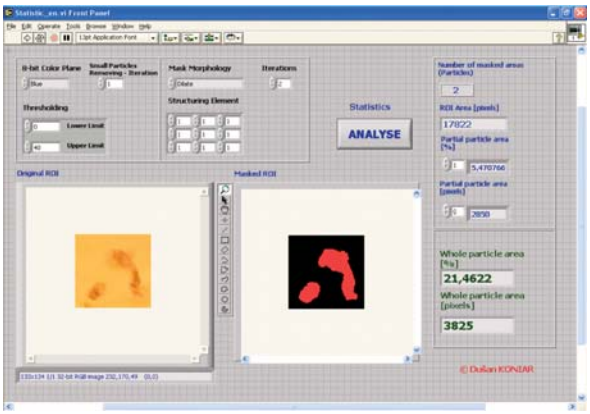

Fig. 6 Statistical analysis of human tissue

The derma blood supply is a good diagnostic parameter based on vessels coverage. The vessels coverage for healthy or pathologically changed tissue is searched by the virtual instrument. The consequential analysis can be a help for doctors to diagnose patients. The statistical analysis is realized for objective results comparison (Fig. 6). A ratio between vessels and other tissues (background and cells) can be measured and percentage of ROI vessels coverage can be enumerated. The virtual instrument can objectify tissue samples evaluation.

This virtual instrument can be the first segment in virtual instrumentation integration in medicine or imaging diagnostic methods.

Acknowledgements

This work has been supported by the grants No. 1/0704/08 and No.1/0087/09 of VEGA grant agency, the project "Centre of Experimental and Clinical Respirology", IMTS code: 26220120004, "Centre of Experimental and Clinical Respirology II", "Measurement of Respiratory Epithelium Cilium Kinematics" and R&D operational program „Centrum of excellence of power electronics systems and materials for their components", No.OPVaV-2008/2.1/01-SORO, ITMS26220120003 funded by the European Community.

References

[1] FRIVALDSKY, M., DRGONA, P., PRIKOPOVA, A.: *Design and Modeling of 200kHz 1,5kW LLC Power Semiconductor Rsonant Converter,* IEEE International conference on applied electronics, Pilsen, 2009.
[2] DRGONA, P., BOBEK, V., DOBRUCKY, B., FRIVALDSKY, M.: *Performance Analysis of Equation Computation for Real Time Model of PMSM for VHFIM Control of PMSM Position Drive,* EDPE 2009, Int. Conference on electrical drives and power electronics.
[3] DUCHON, F., STRENGER, M.: Microsoft Robotics Studio. In: *AT&P Journal Plus,* ISSN 1336-5010, No. 1, 2008, pp. 18–23.
[4] JURISICA, L., DUCHON, F.: Mapping in Mobile Robotics. In: *Acta Mechanica Slovaca*, ISSN 1335-2393, Vol. 12, No. 2-A, 2008, pp. 307–320.
[5] RUSS, J.C.: Image Processing Handbook, *CRC Press LLC*, 1999
[6] KLINGER, T.: *Image Processing with LabVIEW and IMAQ Vision*, Prentice Hall, 2003
[7] JURISICA, L., SUROVCIK, T.: Visual System as Evaluation Tool for Moving Mechatronics System (in Slovak). In: *Acta Mechanica Slovaca.* – ISSN 1335-2393. – Vol. 12, No. 3-B: Modelovanie mechanickych a mechatronickych sustav MMaMS 2008. Cerveny Klastor, 2008, pp. 375–380
[8] ZIDEK J.: *Graphical programming in development system LabVIEW(in Czech)*, Ostrava, 2002.

Európska únia
Európsky fond regionálneho rozvoja
Operačný program VÝSKUM a VÝVOJ
Agentúra Ministerstva školstva, vedy, výskumu a športu SR pre štrukturálne fondy EÚ

"Podporujeme vyskumne aktivity na Slovensku/Projekt je spolufinancovany zo zdrojov EU."

M. Gala – B. Babusiak – V. Novak *

AUTOMATIC CREATION OF HYPNOGRAM

Polysomnography is an important diagnostic method used in sleep monitoring of patients with various sleep disorders. The formulation of a precise diagnosis requires correct evaluation and interpretation of polysomnography EEG and this evaluation is provided by a doctor. In order to save time, various automatic evaluations methods have been developed. One of these methods is based on signal division into 30 second long sections which are subsequently analyzed and reduced using adaptive segmentation and parameters are computed from these segments. Cluster analysis is used to divide individual segments and the class with biggest quantity of segments is called "priority class". Definition of sleep states is then based on priority class. The end result is a hypnogram and the average success rate of the proposed method is about 68%.

1. Sleep

Sleep is a naturally occurring state of relatively suspended sensory and motor activity, characterized by total or partial unconsciousness and the inactivity of nearly all voluntary muscles. It is distinguished from quiet wakefulness by a decreased ability to react to stimuli. Various sleep stages are differentiated during sleep. Sleep architecture is made of sleep states.

The following sleep states exist:

- NREM – non-rapid eye movement sleep, there are three subtypes: NREM1, NREM2, NREM3-4,
- REM – rapid eye movement sleep.

Typical young human sleep is created by 4 or 6, alternating, 90 minute long NREM and REM sleep loops. The number of deep sleep and REM sleep stages decreases with age, by contrast increasing the number of short wakes. [1].

2. Diagnostics

Special laboratories for the study of sleep states exist. Various measurement methods are used in the process of sleep analysis. One such method is called polysomnography (PSG), which is an important diagnostic method for sleep monitoring of patients with sleep disorders or other psychical defects. The following biosignals and quantities are measured: EEG, EMG, ECG, EOG, respiration and blood oxygen saturation).

The resulting polysomnography record has a length of 8 hours and is subsequently divided into 30 second long sites which are then analyzed. However, the actual evaluation of sleep activity is very time-consuming and is provided by a doctor. In order to save time, various automatic evaluations methods are developed and one such method is detailed in the following paragraphs.

3. Implementation of the Automatic Sleep State Detection Algorithm

The proposed algorithm was tested on PSG records of children and consists of several steps. In our case we only used EEG and EOG records from all signals recorded in PSG. The total length of all records was approximately 70 hours and the target group consisted of children aged 6–15 years.

The main body of the algorithm is based on these basic steps:

- Creation of epochs
- Adaptive segmentation
- Cluster analysis
- Sleep state definition
- Hypnogram

Creation of epoch and adaptive segmentation

Several hours long EEG record (6–8 hours) is divided into 30 second long sites – epochs.

EEG signal is stochastic and non-stationary. Automatic analysis of EEG signal using computer equipment is primarily focused on the extraction of informative features with maximum possible discriminatory ability. By obtaining the spectral appearance of part of a signal with constant length one can also obtain signal deformation characteristics.

Adaptive segmentation is necessary because the EEG signal is non-stationary. Therefore, epochs are processed using adaptive seg-

* **M. Gala[1], B.Babusiak[1], V. Novak[2]**
[1] Department of Electromagnetic and Biomedical Engineering, Faculty of Electrical Engineering, University of Zilina, Slovakia,
E-mail: michal.gala@fel.uniza.sk
[2] Children's neurology clinic, University Hospital Ostrava, Ostrava-Poruba, Czech Republic

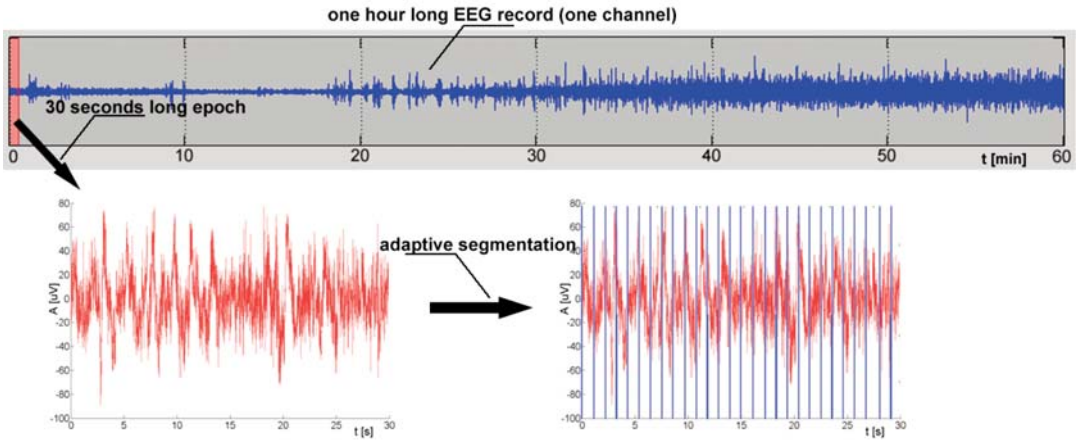

Fig. 1 Creation of 'epochs' and adaptive segmentation

mentation [4] and in our implementation a method based on signal standard deviation is applied.

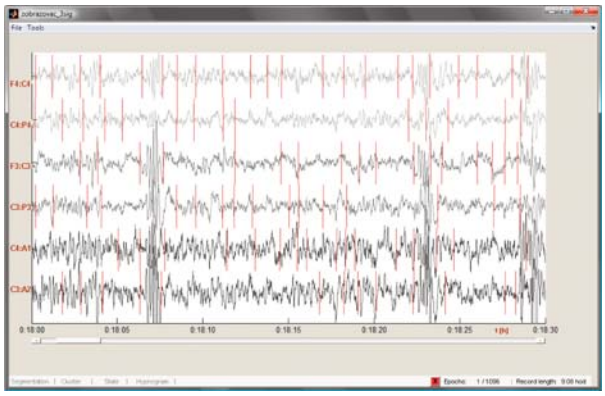

Fig. 2 Application of adaptive segmentation on EEG signal

Cluster analysis

In this step the generated segments are divided into classes using cluster analysis. Cluster analysis is the classification of objects into different groups, or more precisely, the partitioning of a data set into subsets (clusters), so that the data in each subset share some common traits – often proximity according to certain defined distance measure. Data clustering is a common technique for statistical data analysis, which is used in many applications (including data mining, pattern recognition, image analysis, bioinformatics and many more).

One of the simplest, non-hierarchical clustering methods is the K-means clustering method. The K-means algorithm assigns each point to the cluster whose center is the nearest. The center is the average of all the points in the cluster. Its coordinates are the arithmetic mean for each dimension separately over all the points in the cluster. The main advantages of this algorithm are its simplicity and speed which allows it to run on large datasets [5, 6]. In our case the cluster analysis splits segments into five different classes which were chosen empirically. Segments are then divided into classes based on specific parameters.

Parameter computation

Certain specific characteristics are required in order to best describe the electroencephalograph segments. Such characteristics include the time and frequency domain of EEG segments [4], amplitude variability, difference between maximum positive and minimum negative value of amplitude, 1st and 2nd derivation maximum value, average frequency and Hjorth parameters.

Sleep state definition and hypnogram

Segments are divided into classes for each of six channels independently. This means that, for example, class no. 1 can have different parameters in channel 1 compared to the same class in channel 2. In the next step the total number of segments in all classes is detected. If one of the classes has more than 66% of all segments (for one channel), this class is marked a priority class.

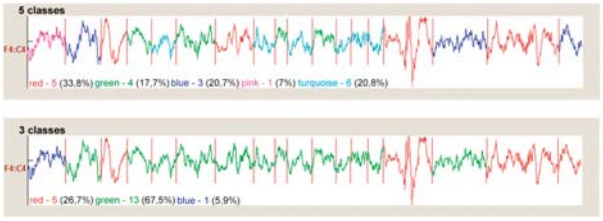

Fig. 3 Priority class definition

The actual sleep state is defined based on the priority class. If a priority class does not exist, cluster analysis with smaller number of classes is used. A simple neural network was used for the sleep state definition [2]. Six epochs of each sleep state (awake, REM, NREM1, NREM2, NREM3/4) were chosen for neural network training. All epochs (from channel F4:C4, C4:P4, F3:C3, C3:P3, C4:A1, C3:A2) were preprocessed by adaptive segmentation and all segments were described by Hjorth's parameters. These para-

meters were then used as a training set for the neural network [3]. The processing (adaptive segmentation, computing of parameters, cluster analysis) and the evaluation of the sleep record (using neural network) leads to the definition of a hypnogram.

4. Results

This method was tested on 8 sleep recordings (six children, two adults). The total time of all recordings was 70 hours. Success rate of this method is shown in Table 1.

Success rate of the proposed method Table 1

Age	ID	Sex	Record length [h:m:s]	Success [%]
6	3	F	10:06:30	72.38
8	5	F	09:08:30	55.20
8	6	F	07:03:30	57.85
9	4	M	08:57:00	72.25
11	1	F	07:44:00	73.92
15	2	M	09:42:30	67.53
47	7	M	08:10:00	35.41
47	8	M	08:14:00	25.10

The automatic sleep detection algorithm is primary intended for children's EEG records. We tested the method on adult's records too, but the success rate was minimal. The total success rate represents coincidence between two hypnograms. One hypnogram is created by a doctor and the second hypnogram is created using our algorithm. The success rate of sleep state detection is shown in Table 2.

The achieved success rate is a good starting point for further optimization of this method. More intensive cooperation with neurologists is needed to make the detection method more complete.

Success rate of the method based on sleep state detection Table 2

Success rate of sleep state detection [%]			
NREM3/4	NREM2	REM/NREM1	awake
78.00	81.39	55.21	56.04

Results of all patients are displayed in Figs. 4–9. The blue line represents the hypnogram created by the proposed sleep detection algorithm and the red line represents the doctor-created hypnogram.

5. Conclusion

This paper deals with one of the possible methods for automatic sleep state detection in children. Only basic steps of this method are described in this paper. Correct identification of sleep states is a complex problem. Cooperation with a neurologist is of utmost importance in order to make this method more complete. The current detection success rate of awake and REM/NREM1 states is about 50%, therefore in the first place a more complete detection of these states is necessary.

However, in view of the relatively high successful NREM3/4 state detection (78%), these methods can be used for sleepwalking detection. Coincidently, one of tested patients was a somnambulant. In the video record the patient was awake, but the doctor detected NREM3/4 state and the same state was detected by the algorithm. Thus, in conjunction with a video recording, the proposed algorithm can also be a good tool for nurses, potentially alerting the nurse or doctor of a somnambulant patient during the course of sleep recording.

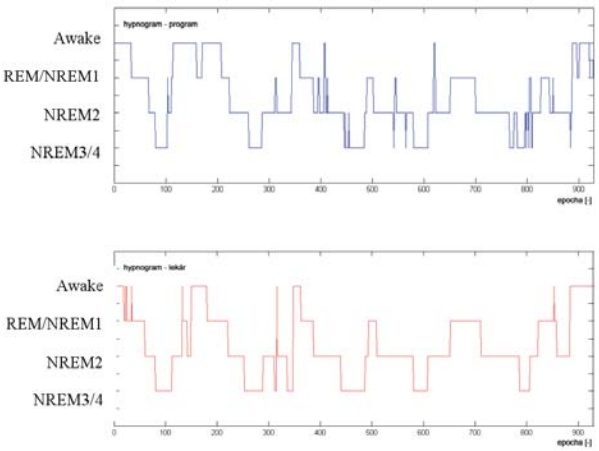

Fig. 4 Patient ID1

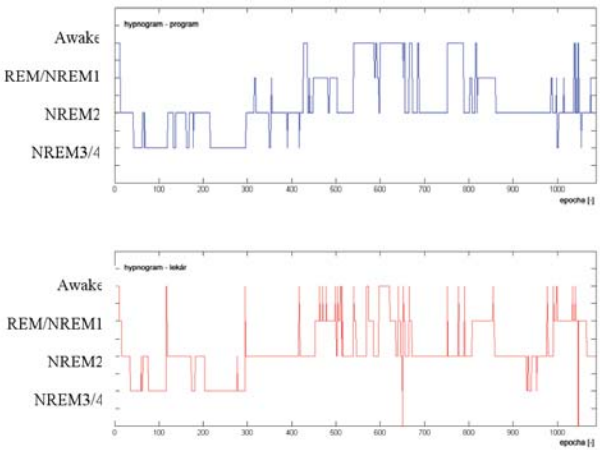

Fig. 5 Patient ID2

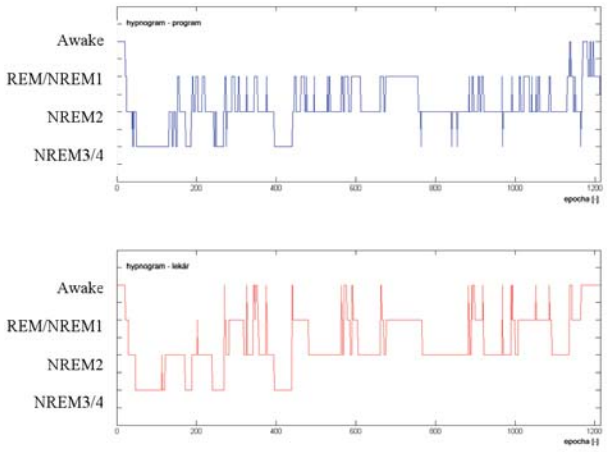

Fig. 6 Patient ID3

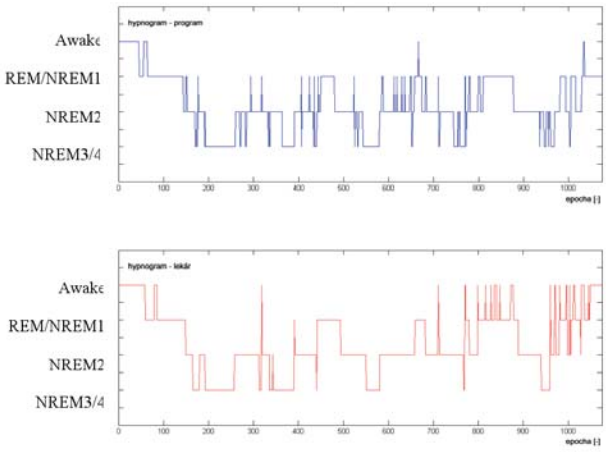

Fig. 7 Patient ID4

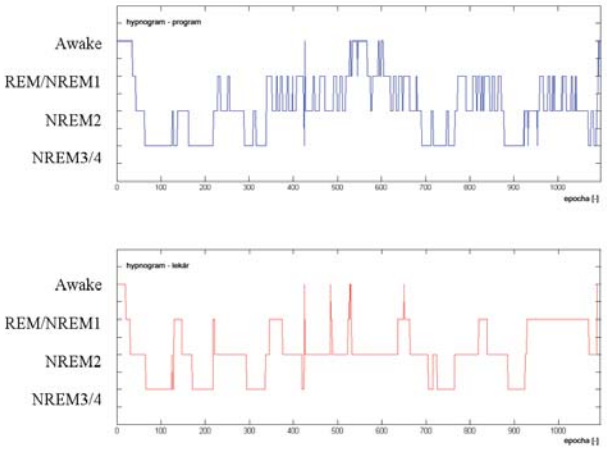

Fig. 8 Patient ID5

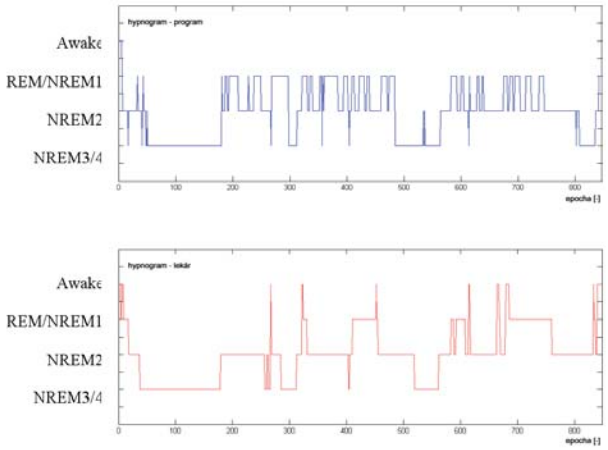

Fig. 9 Patient ID6

References

[1] IBER, C., ANCOLI, S., CHESSON, A: *The AASM Manual of the Scoring of Sleep and Associated Events,* American Academy of Sleep Medicine, Westchester, 2007.

[2] VONDRAK, I.: *Artificial Intelligence and Neural Networks*, FEI, VSB – TU : Ostrava, 2002.

[3] GALA M., MOHYLOVA, J.: *Detection of K-Complex in the EEG Signal,* www.springerlink.com:, Springer Berlin Heidelberg, 2010. Ed. O. Dossel, W C. Schlegel, Vol. 25, ISSN 1680-0737 (Print) 1433-9277 (Online); ISBN 978-3-642-03881-5 (Print) 978-3-642-03882-2 (Online)

[4] MOHYLOVA, J., KRAJCA, V. *Signal Processing in Medicine*, ISBN 80-8070-341-8, 2005.

[5] HARTIGAN, J. A., WONG, M. A. A.: *K-means Clustering Algorithm,* Applied Statistics 28, 1979, pp. 100–108.

[6] KARDI, T.: *K-mean Clustering Tutorials* [online]. [2007-11-12]. WWW: <http://people.revoledu.com/kardi/tutorial/kMean/index.html>

Marek Kukucka – Zuzana Krajcuskova *

AUTOMATIZED MULTI-ELECTRODE VOLTAGE MAP MEASUREMENT OF ACTIVE POINTS ON SKIN

Our contribution deals with the human skin voltage chart measurement. We have concentrated our effort on finding and following the measurement of active points on different parts of the skin's surface, to acknowledge their existence and position through a measuring process. The human skin has a certain impedance or resistance – it can be easily described and simulated using a substitute electric circuit. But the skin also contains parts with measurably lower impedance and different electric properties – we can show them clearly by measurement of voltage chart.

1. Introduction

The human skin has very interesting properties, especially from an electrical point of view. We can read about it in many literary sources. It has a certain impedance or resistance; it can be easily described and simulated using a substitute electric circuit. But the skin also contains parts with measurably lower impedance and different electric properties – we can see them clearly by a measurement of voltage map. These small parts on the skin's surface are called active points (acupuncture points) and they are known and have been used in acupuncture centuries ago. For many years a number of authors concentrated their efforts to measure them, to describe them and to learn about new properties of them. They are used in different new diagnostic and therapeutic medical devices nowadays. We would like to reveal exactly and with reproducibility through measurement some of those interesting properties of the human skin and the human body and bring something new into this area of our knowledge.

2. The electrical Model of Human Skin

The characteristic impedance of the skin and its capacity allows us to create an equivalent electric circuit of the human skin. But the skin also has other properties which we cannot easily include into that simple model. In 1988 Rosell found out that the skin, lightly impregnated with gel, has an impedance in the range approximately from 100 Ω to 1 MΩ in accordance with the frequency of input pulses [6]. In the lower area of the frequencies about 1 Hz, the impedance alternated from 10 kΩ to 1 MΩ and at higher frequencies from 100 kHz to 1 MHz impedance was in the range about 120 Ω to 220 Ω. Mechanical deformations also influence the skin impedance, except electrical parameters. The stretching of the skin's surface causes a drop of the skin's potential between the inner and the outer barrier of the layer from about 30 mV to 25 mV. It is approximately 50 kΩ impedance for 1 cm^2 barrier layer of the skin. The change of the skin's potential is a consequence of alternating the skin impedance considering the skin tension. The capacity of the skin alternates in borders from 0.02 to 0.06 μF/cm^2. A large part of this capacity is in the scleroderma. If this layer thins away, then the skin's capacity becomes smaller (as layers of skin fade away [8]). If this layer is completely eliminated, then the skin's capacity comes down almost to zero. The cell membranes as parts of the skin layers cause high skin capacity.

The equivalent model of human skin impedance cannot be expressed using a simple passive circuit only because the properties of the skin are nonlinear and alternating in time. The simplest model for the skin impedance interpretation is a parallel circuit containing a capacitor and a resistor and a serial resistor. This

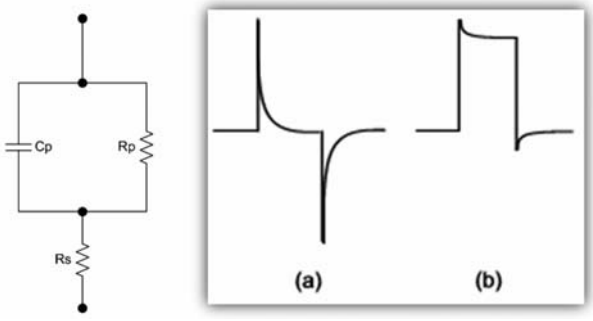

Fig. 1 The equivalent impedance model of the human skin; the response of the human skin to pulses of rectangular voltage connected to the skin's surface: a) skin with a scleroderma layer; b) skin without a scleroderma layer [8]

* **Marek Kukucka, Zuzana Krajcuskova**
Department of Radio and Electronics, Faculty of Electrical Engineering and Information Technology, Slovak University of Technology, Bratislava, Slovakia, E-mail: marek.kukucka@stuba.sk

model we can see on Fig.1. The parallel connection of the capacitor *Cp* and the resistor *Rp* in this model represents influence of the skin capacity and the serial resistor *Rs* represents the impedance of subcutaneous tissue [8]. Image on the Fig. 1 displays the reaction of the skin with rectangular voltage. It is plain to see from the reaction, that if the skin is without scleroderma then the electric current flowing trough is limited by the *Rs* resistance. Setting values for an equivalent model of human skin was difficult, because these values are closely dependent on the kind of skin and on the position of the measurement. For 0.8 cm^2 dry and clean skin, cleansed by ethanol and water values for the resistors and capacitor were established as follows: $Rs = 2$ kΩ to 200 kΩ, $Rp = 100$ kΩ to 500 kΩ and $Cp = 50$ pF to 1500 pF.

3. Electro-Acupuncture and Physical Structures Called Meridians

Physical structures meridians are objectively measurable, identifiable and describable specific paths in human body. They have special physical features and significance. They contain so called active points which are significant with: skin impedance between these points (100–200 kΩ) and surrounding skin (1 MΩ) is different, the electric capacity of these points is greater – within the limits 0.1 to 0.5 μF, in comparison with non active points where the capacity reaches only about 0.01 μF. Various authors in their works consider meridians as channels that lead electric charge in extracellular space [7]. The blockage of the flow of these currents leads to a higher concentration of positive or negative charge and a physical manifestation of that can be pain or some disease symptoms. Namely here are various qualitative indications on the skin's surface of significant meridian points, which are interesting from a technical point of view: high electric potential (to 300 mV), high electric capacity (0.1 to 0.5 μF), low electric resistance, higher skin respiration, higher local temperature, generation of infrasonic waves (from 2 to15 Hz). Some qualitative indications of deeper layer of the skin in significant meridian points: lower level of sensitivity for electric stimulation, higher electric capacity, higher conductivity of isotopic tracers. The measurement of electric parameters of the skin on meridians was described in various literal sources [5], [6]. Meridians have an important information, energetic and regulative function in the human organism and have been used since centuries in acupuncture prevention, diagnostics and therapy. Disorders in energy flow in the body then manifest in whole body form and state of the organism. They express in their primary energetically-information level and also in the psycho-regulation. The system of active points and meridians contains a multitude of information about the actual state of the organism. The problem is to find the appropriate key to evaluate this information. We have to respect the knowledge and laws of classic acupuncture when solving it.

In this paper we focus on physical verification or denying the existence of those points on the human body, using potential chart measurement on certain areas of the human body.

4. Structure chosen for measurement

Literature and various web sources describe in a wide range positions and properties of these physical body structures. Because of accessibility and position we have chosen the following one: *Large Intestine Meridian (Li)*. General distribution of Large Intestine Meridian [4] – it starts from the hand and goes to the head, along the anterior lateral side of the upper limb, then connects with the large intestine, lungs, teeth (especially the lower teeth), mouth, nose, and face. It meets the Lung Meridian of Hand Taiyin at the radial side of the tip of the index finger, the Stomach Meridian of Foot Yangming at the areas lateral to the wings of the nose, and the Du Meridian at DU14-Dazhui.

The main indications are:

disorders along its external course, including upper hemiplegia, tennis elbow, frozen shoulder, toothache; facial pain, spasm or paralysis; nasal discharge or obstruction, headache, pain conditions, either along its external course or on the other parts of the body, exterior patterns, both wind-cold and wind-heat.

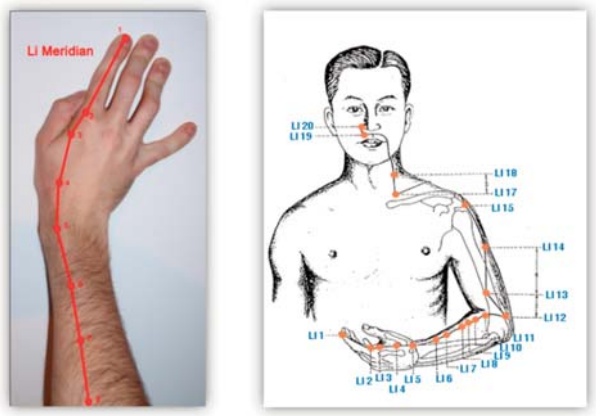

Fig. 2 Large intestine meridian path (Li Meridian)

5. Experimental Measuring Device

The basic construction element of the designed and realized measuring device is a processor from Atmel – ATmega16. The processor contains one serial port, eight 10-bit A/D converters and one SPI – Serial Peripheral Interface. For the controlled connection of measuring electrodes multiplexers DG406 were used. The device also contains a modified version of a peak detector. In addition, the device was extended by DDS – Direct Digital Synthesis generator from Analog Devices AD9833 which is controlled via a SPI bus by a microprocessor [2]. The communication with the PC covers the module DLP-USB232M which serves as a converter of the USB interface to UART – Universal Asynchronous Receiver/Transmitter. This module and the connected computer are separated from the measuring device by a two channel insulator ADUM1201 from Analog Devices, because of the safety of the patient. Supplying the device from accumulators is the way how

to protect the human operator or the measured object from potential electric injury.

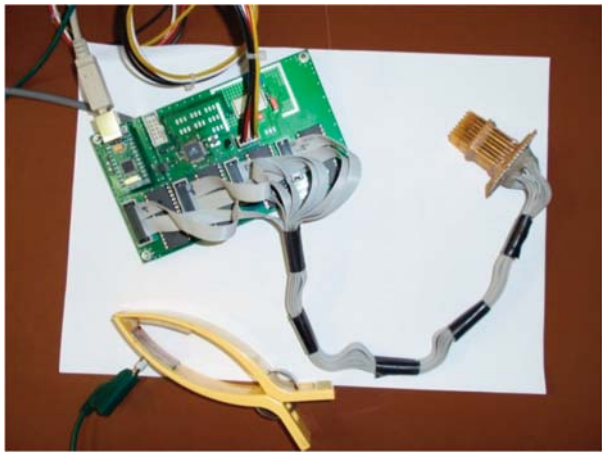

Fig. 3 Measuring device with connected electrodes

Our measurement was realized using needle electrodes [2], [3] (Fig.4.). There are 64 electrodes placed into a 8 × 8 matrix on an isolative holding construction. Each of the electrodes is created by a brass needle located in a cavity shell with a nib which allows fitting each of the electrodes to the surface of the human body and make the contact. All the electrodes measure the change of voltage with regard to a reference electrode placed on the chosen suitable position on the body. The distance of needle peaks is 2.5 mm.

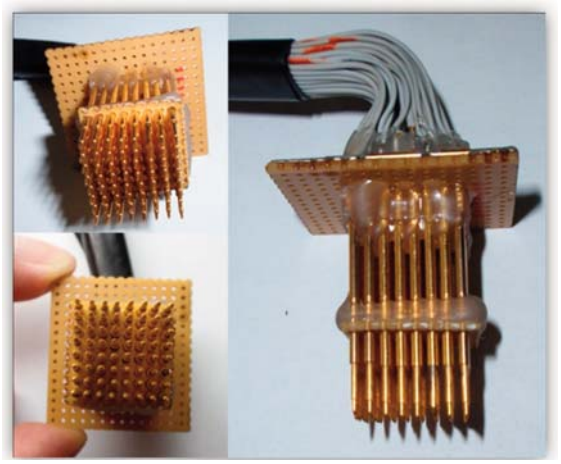

Fig. 4 Measuring 8 × 8 needle electrodes

6. Searching for Active Point Position

Before the measurement we had to choose a meridian appropriate to our technical abilities for measuring. We had two suitable options. One was to find an active point on the LU meridian of the lungs or the second one on the large intestine meridian – the LI meridian. We finally decided for the large intestine meridian because of its path by the outer side of the hand perfectly accessible for our needle sensor. We started to measure according to the marked positions for the measuring probe on Fig. 5.

Fig. 5 Searching for active point No.4 on Li meridian, experimentally chosen positions for measuring electrodes from 1 to 10, along the Li meridian

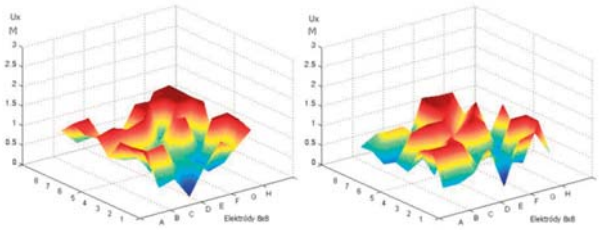

Fig. 6 A voltage chart measured on positions 1 and 2.

All ten points were measured a few times, an example of obtained voltage charts we can see visualized in 3D on the picture Fig. 6. During the measurement process on the large intestine meridian we found a point which showed a significant change in comparison with previous measurements. It was the active point No.4 on the large intestine LI meridian. This point was precisely analyzed many times. The measuring probe was positioned as we can see on Fig. 7. The point was measured repeatedly, each measurement was performed in a different time and all the measurements proved the existence of that active point.

From the measurement with electrodes placed on A position (Fig. 7.) the area of lower values of measured voltage Ux in lower left quadrant is visible (Fig. 8.).

After a change of electrode position to B position (Fig. 7.) it is clearly visible that the area of the lower measured voltage Ux moved into the center of chart (Fig. 9.).

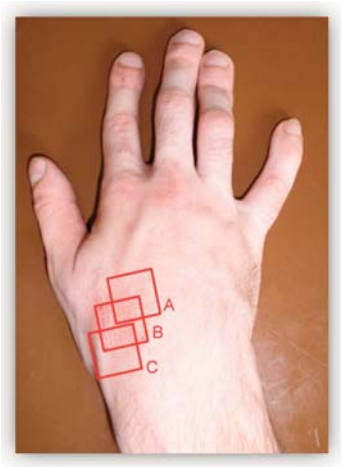

Fig. 7 Localization of active point No.4 on Li meridian, in B position

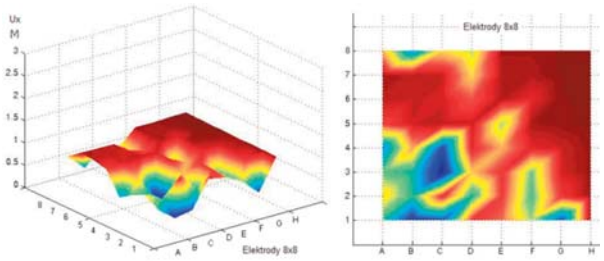

Fig. 8 Measuring voltage chart on A position in 3D and 2D visualization

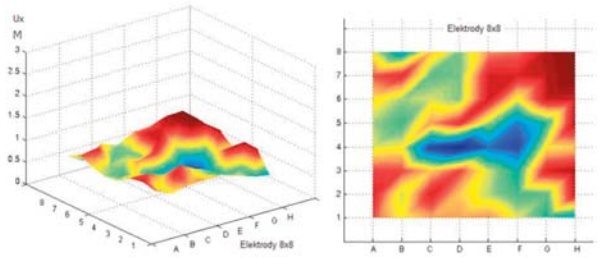

Fig. 9 A voltage chart measured on B position in 3D and 2D visualization

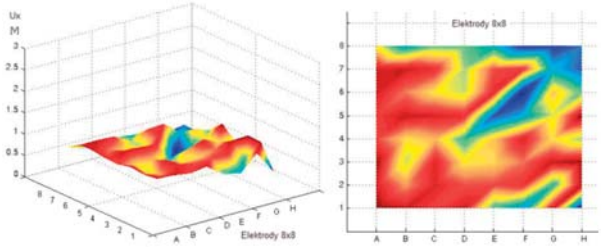

Fig. 10 A voltage chart measured on C position in 3D and 2D visualization

We continued with the measurement in a diagonal positioning of the probe. We placed the electrodes on the C position (Fig. 7.) and the area with a lower measured voltage Ux moved into the right upper quadrant of chart (Fig. 10.). After performing these measurements we located the active point No.4 on the Li meridian in the centre of the B position (Fig. 7.).

7. Comparison of Measured Results

For quite a long time, people believed that the active point of a meridian was a pipeline like a blood vessel or nerve fiber and the active point was like neuroganglion or hole, and expected that we would find them through dissection one day [1]. Unfortunately, this belief failed to be proven by anatomy or histology after half a century of research. On the other hand, however, the objective existence of active points and meridians was proved by means of electronic measurement with excellent reproducibility. Then, we have to ask what the meridians and active points look like – from the data from electronic measurement and whether they are similar to invisible pipelines or knots or holes. From Fig. 11, we can see the shape of the active point measured by the American scientist Becker [5], electronically. The picture shows that the active points are not similar to nerve knots or holes with a clear boundary, but more like a small and invisible hill or hole without clear borders.

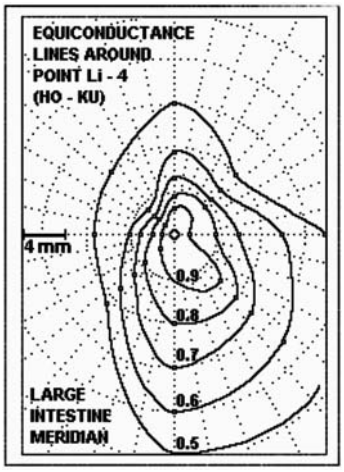

Fig. 11 The shape of active point No.4 on Li meridian from [1], [5]

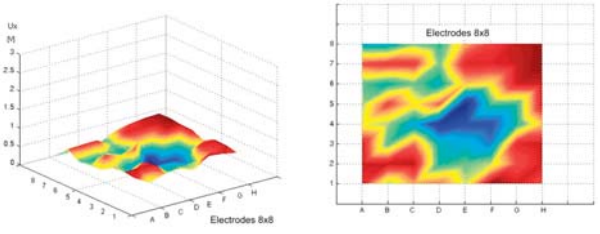

Fig. 12 Voltage chart measured on position of active point No.4 on Li meridian in 3D visualization and 2D visualization.

Our measurement also confirmed these investigations. Here we offer for comparison the following chart on active point surface

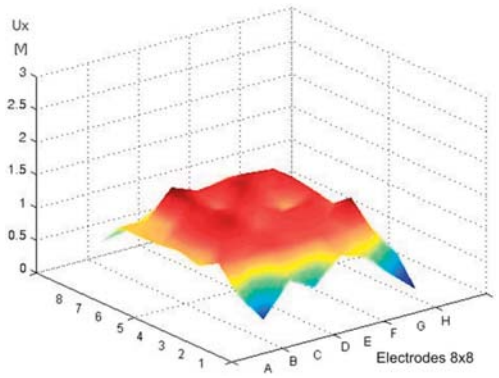

Fig. 13 Voltage chart measured on position of non-active point in 3D visualization

achieved by measuring device (Fig.12), the dark blue color represents the center of an active point, the pale blue color its a narrower border and boundary yellow color is its contour.

We can also see a non active point (Fig. 13) measured for comparison with the active one.

8. Conclusion

Methods and electronic measuring devices used for measuring of 3D voltage charts of human body surface offer a wide space for practical research and can be useful in medicine, diagnostics and therapeutic process as well.

Acknowledgment

The paper was created as a part of a research and education process at the Department of Radio and Electronics, FEI SUT in Bratislava, Slovak Republic and is supported by the Grant VEGA 1/0903/11.

References

[1] ZHANG, C. L.: Skin Resistance vs. Body Conductivity: On the Background of Electronic Measurement on Skin, In: *Subtle Energies and Energy Medicine,* 2003, Vol. 14; Part 2, pp. 151–174.
[2] ONDREIOV, I. M.: *Experimental Impedance Chart Meter of Skin,* Graduation theses, FEI SUT, Bratislava, 2010.
[3] GOGOLA, D. et al.: *Design and Realization of USM Interface for Experimental Scanner of Impedance Chart from Surface of Human Body,* Team project, Bratislava, FEI SUT, 2009.
[4] RUZICKA, R.: *Acupuncture in Theory and Practice,* Nadas, Praha, 1985.
[5] BECKER, R. O. et al.: Electrophysiological Correlates of Acupuncture Points and Meridi-ans, *Psychoenergetic System,* New York, 1979.
[6] ROSELL, J., COLOMINAS, J., RIU, P., PALLAS-ARENY, R., WEBSTER, J. G.: Skin Impedance from 1 Hz to 1 MHz, *IEEE Transactions on Biomedical Engineering,* 35, 649–651, 1988.
[7] SHANG, Ch.: The Mechanism of Acupuncture - Beyond Neurohumoral Theory", In: *Medical Acupuncture. A Journal for Physicians by Physicians,* 1999.
[8] REILLY, J. P.: Electrical stimulation and electropathology, *Cambridge University Press* : Cambridge, 1992.

Marta Horakova – Iveta Vadovicova *

DETERMINATION OF PREDICTIVE FACTORS OF CHOLEDOCHOLITHIASIS IN CASES OF ACUTE BILIARY PANCREATITIS

Choledocholithiasis (bile duct stones) may bring about biliopancreatic obstruction that eventually develops into acute biliary pancreatitis, which could become a serious, life threatening disease. Because stones have the propensity to move spontaneously from the bile duct, it is all-important to determine as accurately as possible, whether biliopancreatic obstruction is still present or not. The aim is to avoid, wherever possible, any invasive and costly diagnostic and therapeutic procedures while preventing serious risk to the patient. In this paper, by retrospective analysis of patients with acute biliary pancreatitis, we examine laboratory and other parameters, obtained by quick and easy to implement non-invasive methods, for to determine predictive factors of biliopancreatic obstruction. Our results indicate that the definite predictive parameter for choledocholithiasis is previous cholecystectomy and the dilation of the bile duct. Supporting predictive factors are bilirubin and alanine aminotransferase.

Key words: acute biliary pancreatitis, endoscopic retrograde cholangiopancreatography, Chi-square tests.

Abbreviations: ABP, acute biliary pancreatitis; ALP, alkaline phosphatase; ALT, alanine aminotransferase; AST, aspartate aminotransferase; Bi, bilirubin; CBDS, common bile duct stone; EPS, endoscopic papilosphincterotomy; ERCP, Endoscopic retrograde cholangiopancreatography; EUS, endoscopic ultrasonography; GMT, gamma-glutamyl transferase; IOC, intraoperative cholangiography; MRCP, magnetic resonance cholangiopancreatography; N, reference value; NS, not significant; ROC, Relative Operating Characteristic; USG, ultrasonography.

1. Introduction

Gallstone (cholelithiasis) disease is a very common condition involving roughly 15% of the population in Europe. In 10% to 15% of cases, cholelithiasis is complicated by the presence of common bile duct stones. Gallstone migration through the biliary tract can cause acute pancreatitis [1]. In many cases biliopancreatic obstruction is transient because the offending stone passes rapidly into the duodenum; otherwise persisting obstruction occurs due to the continued presence of a main bile duct stone or to ampullary edema following stone passage [2]. Biliary pancreatitis can be presumed when abdominal USG confirms gallblader or bile duct stones and, in particular, when serum hepatic transaminases are acutely increased in the initial presentation, and alcohol is reliably excluded [3]. Early therapeutic ERCP reduces complications among acute pancreatitis patients who have biliary obstruction [1, 4]. Because stones have a propensity to move spontaneously from the bile duct, the important question to be answered in all cases of ABP is whether or not a calculous biliary obstruction is still present. Answering this question conditions subsequent management, including the need for ERCP and EPS or surgical procedures, IOC, choledochotomy or non-invasive tests, MRCP, and EUS [1]. Employing non-invasive, widely used and readily available tests, we endeavoured to establish predictive factors-predictors, which would predict the presence of common bile duct stone in patients with ABP with the highest probability.

2. Patients and methods

Our aim was to examine in patients with ABP the relationships between persistent CBDS and values of their laboratory parameters, and with dilation of their bile duct to find significant associations.

For this purpose we retrospectively, in two stages, statistically evaluated the database of total 130 consecutive patients with ABP referred from Martin Faculty Hospital, Internal Gastroenterology Clinic, Martin, Slovakia in the years 1999–2008.

Stage 1. Patients from 1999 to 2003, had received early ERCP (within 48 hours) at the time when we had not had the possibility to perform MRCP and EUS regularly. These patients, group I, $n = 76$, (20 men and 56 women) mean age 60.1 ± 16.3 years (range 24 – 92) were used to determine predictors for CBDS. Analysis was performed on the whole group.

* **Marta Horakova[1], Iveta Vadovicova[2]**
[1] Internal Gastroenterology Clinic, Martin Faculty Hospital, Martin, Slovakia, E-mail: martahorakova@zoznam.sk
[2] Department of Mathematics, Faculty of Science, University of Zilina, Slovakia,

We studied following factors: age, dilation of the common bile duct, and laboratory parameters, specifically Bi, ALT, which had been done to all the patients prior to ERCP, as well as GMT, AST, ALP and dependence of CBDS occurrence from previous cholecystectomy. Pathologic laboratory values were considered to be higher than the reference values (N): *Bi* > 22.2 μmol/l, *AST* > > 0.66 μkat/l, *ALT* > 0.66 μkat/l, *GMT* > 0.82 μkat/l, *ALP* > 2.6 μkat/l, *AMS* > 3.7 μkat/l. The presence of CBDS and the common bile duct diameter were determined by ERCP or by IOC in patients where ERCP was unsuccessful. In ERCP we considered the bile duct dilated when the diameter was 10 mm or more. Prior to ERCP we employed ultrasound to determine the common bile duct diameter. With ultrasonography, we considered the bile duct dilated when the diameter was more than 7 mm (9 mm and more after cholecystectomy).

The associations between the presence of CBDS and bile duct dilation or the values above the mentioned laboratory parameters or previous cholecystectomy were investigated by dividing patients into two sub groups: with CBDS and without CBDS. Their quantitative data (values of laboratory parameters) were compared using Student's *t*-test. For each significant variable on the *t*-test, using ROC curve, we determined the cut-off value as a multiple of the normal value of the relevant parameter. Thus we obtained two categorical variables, which were compared by the χ^2 test of independence, and logistic regression. Using χ^2 test of independence we also investigated the association between occurrence of CBDS and dilation of common bile duct or previous cholecystectomy. For small groups of patients we used Fisher's exact test; logit confidence intervals for the odds ratio was calculated using the method of Alan Agresti [5]. We considered p-values ≤ 0.05 as statistically significant.

Because the prevalence of choledocholithiasis increases with age, [1], and an interaction appeared between the age and other predictors, the multivariate analysis was performed separately for patients older and younger than 70 years.

3. Results

The prevalence of choledocholithiasis in patients ≤ 70 years old with ABP (52 patients, mean age 51.8 ± 12.1 years) was 36.5% (19/52), in patients > 70 years old (24 patients, mean age 78.3 ± 5.9 years) was 54.2% (13/24).

We determined the following significant associations:

Bile ducts dilation. The probability of the presence of a stone in the bile ducts if the bile ducts are dilated was 66.7% (28/42), in the absence of bile duct dilation the probability of CBDS occurrence was 11.7% (4/34), sensitivity 87.5%, specificity 68.2%, $p <$ < 0.001.

Bilirubin. Bilirubin is examined on all patients with ABP. We did not find a statistically significant association between the Bi level and CBDS occurrence even after dividing patients by age. Therefore, we explicated some other medical factors, which could have influenced the value of Bi, hence adversely affected achievement while determining the association between persisting CBDS and increased level of Bi. It was established that if we from the tested group of patients excluded all these with acute cholecystitis and cholangitis (diagnoses with increased value of Bi) a significant association would exist between the CBDS occurrence and bilirubin level in the whole patients group, not divided by age, with dilated bile ducts. The probability of CBDS occurrence for bilirubin level >1.5N is 81.8% (18/22) and for bilirubin level < 1.5N is 50% (6/12). Sensitivity 75%, specificity 60%, $p = 0.05$.

ALT. We found a statistically significant association between CBDS occurrence and ALT activity only after dividing the whole patients group into two subgroups according to their age. In patients ≤ 70 years old with dilated bile ducts and 3N < ALT < 7N or ALT > 12N CBDS is present in 81.3% (13/16) and in 20% (2/10) for other values of ALT. Sensitivity 86.7%, specificity 72.7%, $p < 0.004$.

For the patients ≤ 70 years old without acute cholecystitis with not dilated bile ducts we found an association between the CBDS occurrence and bilirubin level together with ALT activity. For Bi > 1.5N occurring with an ALT > 8N CBDS is present in 33.3% (4/12) and in 0% (0/9) for Bi < 1.5N or ALT < 8N. Sensitivity 100%, specificity 52.9%, p = 0.08 (NS).

As for patients with bile ducts dilation with CBDS occurrence we found the dependence of ALT activity on age. The median of ALT for these patients ≤ 50 years old is 10.6 μkat/l and for patients >50 years old median of ALT is 2.9μkat/l. The mean difference is statistically significant, $p < 0.05$.

We did not find a statistically significant association between the ALT activity and CBDS occurrence at patients >70 years old. Even patients with dilated bile ducts had CBDS also in the case of ALT < 3N, while ALT > 3N is one of symptoms by ABP.

GMT. A bile duct stone is present in 100% (8/8) of patients >70 years old with dilated bile ducts and GMT >5N, and in 25% (1/4) with GMT < 5N and with dilated bile ducts.

Sensitivity 88.9%, specificity 100%, $p = 0.02$.

We did not find a statistically significant association between the GMT activity and CBDS occurrence at patients ≤ 70 years old; but, not everybody in this group had GMT examined before ERCP.

Previous cholecystectomy. By patients with previous cholecystectomy CBDS was present in 81.8% (9/11). Sensitivity 28.1%, specificity 95.5%, $p = 0.005$.

Stage 2. The results we obtained by studying the associations between CBDS and laboratory parameters, previous cholecystectomy, [6], and dilated bile duct on the group I, were verified on the control group of patients with ABP treated in the MNF hospital in Martin in the years 2004–8, group II, which consisted of 54 patients (19 men and 34 women) mean age 63.5 ± 16.3 years (range

CBDS significant predictors for patients with ABP Table 1

Patients	Predictor	% CBDS	Odds ratio (95% CI)	pValue
entire group	previous cholecystectomy	81.8	8.0 (3.5 to 18.2)	0.005
entire group	bile duct dilation	66.7	15.0 (4.5 to 48.8)	< 0.001
without acute cholecystitis with bile duct dilation	Bi $>$ 1.5N	81.8	4.2 (0.9 to 18.3)	0.05
age $\leq$ 70 years with bile duct dilation	3N $<$ ALT $<$ 7N or 12N $<$ ALT	81.3	17.3 (5.2 to 34.0)	0.004
age $>$ 70 years with bile duct dilation	GMT $>$ 5N	100	57.6 (7.6 to 435.4)	0.002

24–86). By using *t*-test, and χ^2 – "goodness of fit" test, respectively, we found that the difference in age composition in both groups I and II, and the difference between observed and expected probabilities of CBDS occurrence depending on bile duct dilation, values of ALT, Bi and previous cholecystectomy in the group II, resp., is not significant. The value of test criteria χ^2 equals $1.041 < < \chi^2_{0.05}(3) = 7.81$.

Comparison of observed and expected probabilities of CBDS occurrence for the group II Table 2

Patients	Predictor	observed % of CBDS	expected % of CBDS
entire group	previous cholecystectomy	66.7	81.8
entire group	bile duct dilation	78.9	66.7
without acute cholecystitis with bile duct dilation	Bi $>$ 1.5N	71.4	81.8
age $\leq$ 70 years with bile duct dilation	3N $<$ ALT $<$ 7N or 12N $<$ ALT	100	81.3

4. Discussion

Bilirubin and ALT were tested for every patient before ERCP. Bilirubin level was influenced by the presence of acute cholecystitis and by the presence of acute cholangitis, while patients with acute cholangitis also had acute cholecystitis. Even without detectable common bile duct obstruction, acute cholecystitis often causes mild elevations in the serum bilirubin concentrations. The elevated bilirubin level may be a consequence of haemathogenous or direct spread infection, which may cause structural and functional abnormalities of the liver. Since the patients with acute cholecystitis had elevated bilirubin levels even when CBDS was not present, the relationship between bilirubin level and CBDS was significant in patients with bile duct dilations after eliminations of patients with acute cholecystitis only.

We found the age to be a factor influencing ALT activity in patients with CBDS and bile duct dilation. Younger patients had higher ALT activity, older patients had elevated ALT activity but of a lesser degree than the younger ones. Two intervals of ALT values, as predictors of CBDS, are probably the result of age-dependent ALT activity as well as of possible spontaneous movement of the stones.

5. Conclusion

ERCP is indicated at patients with suspicion of ABP if biliary obstruction is present and if the presence of ductal stone is suspected. ERCP should have been used selectively because it is difficult, bothersome, expansive and has the potential of causing further pancreatic damage.

By using predictors we had established it is now possible to categorize patients according to the likelihood of CBDS occurrence. Providing predictive factors of biliary obstruction are not present it is useful to perform a less invasive or non-invasive investigation of bile ducts (EUS, MRCP), and ERCP and subsequent sphincterotomy should be indicated only if the presence of CBDS is confirmed by these methods.

Our results manifest that the definite predictive factor for CBDS is previous cholecystectomy and the bile duct dilation. Supporting predictors of these laboratory parameters, which were tested for every patient before ERCP, by patients with dilated bile ducts, influencing the probability of CBDS occurrence are the value of ALT in patients $\leq$70 years old and the level of Bi by patients without acute cholecystitis and cholangitis.

Acknowledgement:
This research has been supported by the Slovak Grant Agency VEGA through the project No. 1/0867/08.

References

[1] PRAT, F., MEDURI, B., DUCOT, B. et al.: Prediction of Common Bile Duct Stones by Noninvasive Tests. *Annals of surgery,* 229, 1999, 3, pp. 362–8.

[2] ORIA, A., CIMMINO, D., OCAMPO, C. et al.: Early Endoscopic Intervention Versus Early Conservative Management in Patients with Acute Gallstone Pancreatitis and Biliopancreatic Obstruction: A randomized clinical trial, *Ann Surg* 245, 2007, (1), pp. 10–17.
[3] NORTON, I.D., PETERSEN, B.T.: Acute and Chronic Pancreatitis Interventional Treatment of Acute and Chronic Pancreatitis, Endoscopic procedures. *Surg Clin North Am*, 79, 1999, 4, pp. 896–911.
[4] MARK, D.H., LEFEVRE, F., FLAMM, C.R.et al: Evidence-based Assessment of ERCP in the Treatment of Pancreatitis. *Gastrointest Endosc,* Supplement to: 56, 2002, 6, pp. 249–54.
[5] AGRESTI, A., LOGIT, O.: Confidence Intervals for the Odds Ratio with Small Samples. *Biometrics* 55, 1999, pp. 597-602.
[6] HORAKOVA, M., VADOVICOVA, I., KATUSCAK, I., JANIK, J., MAKOVNIK, P., SADLONOVA, J.: Consideration of Endoscopic Retrograde Cholangiopancreatography in Cases of Acute Biliary, *Pancreatitis. Bratislava Medical Journal.* Vol. 10, No. 9, 2009, pp. 553–558.

Ivan Rados – Ladislav Schwartz *

THE WORST AVAILABILITY AS A PARAMETER FOR DESIGNING AND REPORTING ON THE NETWORK PERFORMANCES

In the introductory part, the reasons why the availability is important are stated as well as the overview of the papers produced so far dealing with the problem of guaranteed availability. Furthermore, the basic concepts on availability are introduced with the special review of the parallel structure which can actually be applied onto the ring network. The principles of protection of the wavelength channel and optical multiplex section which are used in the ring WDM networks are described. Then the availabilities of different link configurations in relation to its protection are defined: without protection, protection using the same optical cable and protection using completely separated optical cables. Then the availability of the WDM ring was analysed which uses protection of the wavelength channel as well as the protection of the optical multiplex section. Furthermore, the expression for the worst availability of the WDM ring was derived and the number of links of the working path which gives the worst availability was determined. The data on the intensity of failures and the mean time to repair of individual components were taken from different literature. In the analysis we assumed that it is about WDM system with 64 wavelengths. At the end of the paper the answer to the question why the worst availability can be taken as a parameter at projecting WDM networks and for the reporting on the network performances was given.

Key words: WDM, wavelength channel, availability, protection.

1. Introduction

The development of photonic technologies enabled huge transmission speeds over optical fibres. The key technology for this development is WDM which enables hundreds of wavelength channels transmitting data in the Gb/s speeds to be multiplexed in one signal suitable for transmission over optical cable. Exactly due to the large quantity of transmitted data, the network failures can cause big financial losses as well as the service provider's reputation. For that, applying different protection methods in WDM ring structure enables network operators to even, in the event of failures i.e. cable cut, provide to its customers/users normal work and qualitative service. Survival of the service is mostly represented through the availability of the connection which is a probability that the connection will be correct at some point in time. The connection availability depends on the availability of the network components along the path (optical fibres, optical add/drop multiplexors and switches...). In order to provide a quality service to its users, the operators apply different protection methods.

Defined availability in the SLA (Service Level Agreement) usually refers to the average availability of the connection [1]. However, the question is what the average availability means for the service user and if that is good enough to be protected against loss of incomes. If we assume, for example, that the average availability 0.995 in 99% cases , it means that still 1% of unavailability remains which for the big users who are transferring big data quantities (i.e. reda Tb/s) can mean significant loss of incomes and perturbation of the service quality.

In this paper we shall focus on the protection of the wavelength channel and optical multiplex section with 4 threads in the ring WDM network and by deriving the expressions for availability for both types of protection, we shall prove that the same expression is received in which only the availability of the optical link is changed depending on the protection we use.

We shall also introduce the term "the worst availability" and compare average and the worst availability in order to be able to conclude what big users should request from the operators through the SLA contract.

2. Availability Theory

where G network consists of N nodes and N links connecting those nodes.

Availability $A_{st}(G)$ between two terminals is a probability that there is at least one path which is composed of correct links and nodes between s and t in G.

If the nodes are ideal, then only $m = |E|$, remains as a subject to failure where each link $k = 1, 2, ..., m$ matches variable x_{lk} and x represents a set of variables which represent links [2]:

* **Ivan Rados[1], Ladislav Schwartz[2]**
[1] Department of Transmission Systems HT d.d., Mostar, Bosnia and Herzegovina, E-mail: Ivan.Rados@hteronet.ba
[2] Faculty of Electrical Engineering, University of Zilina, Slovakia

$$x \equiv (x_{l1}, x_{l2}, ..., x_{lm}) \quad (1)$$

The aim is to calculate availability between two terminals s and t which is presented by a polynomial function of x elements having the characteristic that the availabilities of links p_{lk} replace corresponding variables x_{lk} which gives the numerical value which is exactly the availability between two terminals [3].

$$A_{st}(x) = A_{st}(x_{l1}, x_{l2}, ..., x_{lm}) \quad (2)$$

To complete the algebra formulation, two operators on polynomial will be introduced:
- $\otimes$, this operator is applied on the serial connection of two or more elements
- $\oplus$, this operator is applied on the parallel connection of two or more elements

Where S represents a set of all polynomials which can come into existence by the combination of operators $\otimes$ and $\oplus$ so that the minimal value of the polynomial is 0 and the maximal is 1.

For polynomials $f, g, h \in S$ following axioms are applicable [9]:

$$f \otimes f = f \qquad f \oplus f = f$$

$$f \otimes 1 = f \qquad f \oplus 0 = f$$

$$f \otimes 0 = 0 \qquad f \oplus 1 = 1$$

$$f \otimes g = g \otimes f \qquad f \oplus g = g \oplus f$$

If the operator $\otimes$ is applied on the serial structure, for instance of two elements whose failures are independent, the availability of such structure is equal to the product of availability of each single element.

$$As = x_1 \otimes x_2 = \Pi_{i=1}^{2} x_i = x_1 \cdot x_2 \quad (3)$$

It is generally applicable for the parallel structure of two elements

$$A_p = x_1 \oplus x_2 = x_1 + x_2 - (x_1 \otimes x_2) \quad (4)$$

If the failures of elements are independent the following applies:

$$A_p - x_1 \oplus x_2 = x_1 + x_2 - (x_1, x_2) \quad (5)$$

If x_1 and x_2 are mutually exclusive which means that $x_1 \otimes x_2 = 0$, we have

$$A_p = x_1 \oplus x_2 = x_1 + x_2 \quad (6)$$

To establish the connection between two nodes and network availability, we define P_{st} to consist of all simple paths P_i between s and t in the network G

Also, we define the *path value* $v(P_i)$ by the "product" of the link variables along the path P_i [2]:

$$v(P_i) = \otimes\{x_{lk}: k \in P_i\} = \otimes \Pi_{k \in P_i} x_{lk} \quad (7)$$

The availability between two terminals $A_{st}(x)$ is the "sum" of path value $v(P_i)$ taken over all the simple paths from s to t.

$$A_{st}(x) = \oplus v(P_i),\ P_i \in P_{st} = \oplus \Sigma_{P_i \in P_{st}} v(P_i) \quad (8)$$

The availability of certain elements (optical cables, nodes elements...) can be calculated by using the expression below

$$A = \frac{MTTF}{MTTF + MTTR} \quad (9)$$

Where *MTTF* (Mean Time to Failure) is mean time till the failure occurs and *MTTR* (Mean Time to Repair) mean time of repair [4].

$$MTTF = 1/\lambda \quad (10)$$

Where λ is a failure rate which is usually expressed in *FIT* (Failure in Time, $1FIT = 1$ failure in 10^9 hours).

Availability can be calculated on the basis of the collected data while the new systems use a probability model.

Unavailability U is probability complementary to availability [12], i.e. $U = 1 - A$.

In reporting about the system/network performances, unavailability U is often expressed as *MDT* (Mean Down Time) in minutes per year, i.e.

$$MDT = 365 * 60 * 24 * u \quad \left(\frac{\min}{god}\right) \quad (11)$$

As an optical network generally consists of cable sections and nodes, an optical fibre failure rate is calculated separately from the node failure rate. The optical fibre failure rate is calculated according to the equation

$$\lambda = \frac{n}{M * T} \quad \left(\frac{l}{kmh}\right) \quad (12)$$

Where n is a number of failures over monitoring time, M the length of installed cable in km and T monitoring period in hours.

3. Availability Analysis of WDM Ring

Since the installation of more SDH line systems between two nodes is very expensive, as the capacities of optical cables exhaust considerably, the need for high transmission capacity system requiring only two fibers has arisen. Such are WDM systems based on wavelength multiplexing which use the wavelength channel protection and optical multiplex section protection.

In order to derive the expression for the availability of the ring using mentioned protections, we shall define different types of links and nodes which are used thereat.

3.1 Link availability

In this paper we shall define three types of links in relation to their protection: without protection (unprotected), protection in the same cable and protection with totally separated cables [5]. The unprotected optical link is comprised of optical cable and mux/demux as can be seen in Fig 1.

All the components of the optical link must be correct so that the connection can be functional. The most often cause of an optical link failure is the breakage of optical fibre. Since, in the case of the cable breakage, mostly all the fibres break, we shall suppose that the failures of fibre and cable are fully dependent so that, instead of the availability for fibre we shall take the availability for cable.

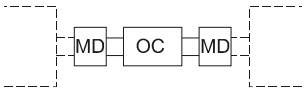

Fig. 1Unprotected link

The availability for link without the protection equals to the availability product of individual components.

$$x_{lk_{up}} = x_{OC} \cdot x_{MD}^2 \tag{13}$$

If optical interfaces are connected to fibres sharing the common cable (Fig. 2), the availability is:

$$\begin{aligned} x_{lk_{cc}} &= x_w \oplus x_p = x_w + x_p - x_w \otimes x_p = \\ &= x_{MD}^2 \cdot x_{OC} + x_{MD}^2 \cdot x_{OC} - \left(x_{MD}^2 \cdot x_{OC} \otimes x_{MD}^2 \cdot x_{OC}\right) = \\ &= 2x_{MD}^2 \cdot x_{OC} - x_{MD}^4 \cdot x_{OC} \end{aligned} \tag{14}$$

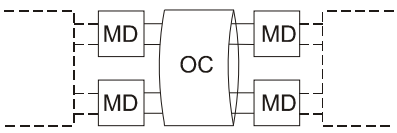

Fig. 2 A span-protected link consisting of two fiber pairs that share a common cable

Although there is product of $x_{OC} \oplus x_{OC} = x_{OC}$, only one member is taken for availability calculation because optical fibres share a common cable which means they have the same failure cause.

If optical interfaces are connected to the optical fibres belonging to completely separated cables (Fig. 3) availability is calculated as:

$$\begin{aligned} x_{lk_{dc}} &= x_w \oplus x_p = x_w \otimes x_p = \\ &= x_{MD}^2 \cdot x_{OC_1} + x_{MD}^2 \cdot x_{OC_2} - \left(x_{MD}^2 \cdot x_{OC_1} \otimes x_{MD}^2 \cdot x_{OC_2}\right) = \\ &= x_{MD}^2 \cdot x_{OC_1} + x_{MD}^2 \cdot x_{OC_2} - \left(x_{MD}^4 \cdot x_{OC_1} \otimes x_{MD}^2 \cdot x_{OC_2}\right) \end{aligned} \tag{15}$$

If the availability of both optical cables is equal, namely $x_{OC_1} = x_{OC_2} = x_{OC}$, the availability of the optical link with separated cables is

$$\begin{aligned} x_{lk_{dc}} &= x_w \oplus x_p = x_w + x_p - x_w \otimes x_p = \\ &= x_{MD}^2 \cdot x_{OC} + x_{MD}^2 \cdot x_{OC} - \left(x_{MD}^4 \cdot x_{OC} \cdot x_{OC}\right) = \\ &= 2x_{MD}^2 \cdot x_{OC} - \left(x_{MD}^4 \cdot x_{OC} \cdot x_{OC}\right) = \\ &= x_{MD}^2 \cdot x_{OC} \cdot \left(2 - x_{MD}^4 \cdot x_{OC}\right) \end{aligned} \tag{16}$$

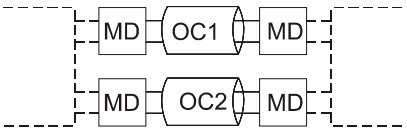

Fig. 3 A diversely-routed link consisting of two fibre pairs that are routed in diversity cables

3.2 Node availability with active components

Signals which are transported inside the ring are added/dropped from the nodes called "*termination*" nodes which are marked *s* and *t*. Nodes in the ring through which the signal only passes from one side to the other are called "regeneration" nodes.

In accordance with that we shall define four node types depending on the trip of the signal through them [6]:
- terminal node is active, x_{nt}
- pass-through node is active, x_{np}
- terminal node with the loop is active, x_{ntlb}
- pass-through node with the loop is active, x_{nplb}

An optical switch with add/drop possibilities is used as the active component. In the case that the node is used as terminal, the wavelength channel passes through the transmitter, receiver and optical switch

$$x_{nt} = x_{TX} \cdot x_{OSW} \cdot x_{RX} \tag{17}$$

For the case of *n* the wavelength channel in terminal node, the availability is

$$x_{nt,n} = x_{TX}^n \cdot x_{OSW} \cdot x_{RX}^n \tag{18}$$

If the node is a pass-through one the wavelength channel passes from east to west side of optical switch so that the availability is

$$x_{np} = x_{OSW} \tag{19}$$

If the terminal node with the loop is active which is the case with the protection of the optical multiplex section, the wavelength channel passes through the transmitter, optical switch and receiver, the availability is

$$x_{ntlb} = x_{TX} \cdot x_{OSW} \cdot x_{RX} \tag{20}$$

But if the pass-through node with the loop is active, the wavelength channel only passes through the optical switch and the following applies:

$$x_{nplb} = x_{OSW} \tag{21}$$

3.3 The availability of the WDM ring with the wavelength channel protection

This type of protection requires two fibres in a ring. Each wavelength channel is being routed on the working path along one side of the ring, and the corresponding dedicated wavelength channel, along the opposite side. Bidirectional wavelength requirements are supported by two wavelength channels; one in each direction.

Two types of dedicated protection are possible: 1+1 and 1:1.

In the ring network which uses the 1+1 wavelength channel protection the wavelength channel is the source node being duplicated and concurrently delivered in both directions of the ring [6];

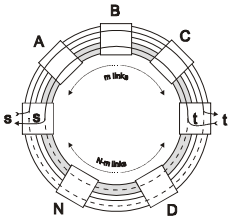

Fig. 4 1+1 wavelength channel protection under conditions without a failure

Under ordinary conditions in the terminal node, the receiver gets two signal copies (with a different delay) and chooses the best one. In the case of failure on the working path, the receiver chooses the signal that it gets from the protection path.

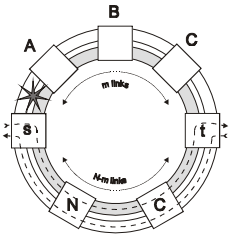

Fig. 5 1+1 wavelength channel protection in the case of a failure on working path

This is so called single ended protection because the switching is carried out only on one (receiving) side. It is important that the working and protection paths do not have components in common, so that one failure would not cause total communication break down, and this means that the component failures on the working and protection paths are fully independent [7].

In 1:1 protection, the wavelength channel on the front side is not permanently duplicated so that the switching is performed dual-ended which requires a protocol to coordinate this dual-ended switching. From the availability point of view, the same availability expression applies as for the 1+1 protection.

If a wavelength channel on the working path P_0 passes the m of optical links between terminal nodes, the availability for the working path is equal to the availability product for optical links and nodes through which this wavelength channel passes [11]

$$\begin{aligned} v_{st}(P_0) &= \otimes\Pi_{k,m\in P_0} x_{lk} x_{nm} = \left[\otimes\Pi_{k\in P_0} x_{lk}\right]\left[\otimes\Pi_{k\in P_0} x_{nm}\right] = \\ &= (x_{nt})^2 (x_{np})^{m-1}\left[\otimes\Pi_{k\in P_0}^{N-m} x_{lk}\right] \end{aligned} \tag{22}$$

In the case of failure on the working path, the wavelength channel passes the N-m of optical links and the N-m−1 of nodes on the protection path P_1 so that the availability for the protection path is (10)

$$\begin{aligned} v_{st}(P_1) &= \otimes\Pi_{k,m\in P_1} x_{lk} x_{nm} = \left[\otimes\Pi_{k\in P_1} x_{lk}\right]\left[\otimes\Pi_{k\in P_1} x_{nm}\right] = \\ &= (x_{nt})^2 (x_{np})^{N-m-1}\left[\otimes\Pi_{k\in P_1}^{N-m} x_{lk}\right] \end{aligned} \tag{23}$$

The availability for the wavelength channel between the s and t nodes is completely determined by these two paths so that the availability for the wavelength channel in the case of 1+1 protection is calculated as the availability of two branches, failures of which are fully independent.

$$A_{st}(\times, m) = v_{st}(P_0) + v_{st}(P_1) - \left[v_{st}(P_0) \otimes v_{st}(P_1)\right] \tag{24}$$

$$\begin{aligned} A_{st}(\times, m) &= (x_{nt})^2 (x_{np})^{m-1}\left[\otimes\Pi_{k\in P_0}^{m} x_{lk}\right] + \\ &+ (x_{nt})^2 (x_{np})^{N-m-1}\left[\otimes\Pi_{k\in P_0}^{N-m} x_{lk}\right] - \\ &- \left\{ \begin{array}{l} (x_{nt})^2 (x_{np})^{m-1}\left[\otimes\Pi_{k\in P_0}^{m} x_{lk}\right] \\ \otimes (x_{nt})^2 (x_{np})^{N-m-1}\left[\otimes\Pi_{k\in P_0}^{N-m} x_{lk}\right] \end{array} \right\} \end{aligned} \tag{25}$$

Although in the equation brackets we have the product of the same two members, we use one member, not the square because of the earlier mentioned axioms which are applied for the operator ⊗; so we have

$$\begin{aligned} A_{st}(\times, m) &= (x_{nt})^2 \left\{ (x_{np})^{m-1}\left[\otimes\Pi_{k\in P_0}^{m} x_{lk}\right] + \right. \\ &\left. + (x_{np})^{N-m-1}\left[\otimes\Pi_{k\in P_1}^{N-m} x_{lk}\right] - (x_{np})^{N-2}\left[\otimes\Pi_{k\in P_0 \cdot P_1}^{N} x_{lk}\right] \right\} \end{aligned} \tag{26}$$

For the unprotected links [12]

$$A_{st}(\times,m) = (x_{nt})^2\{(x_{np})^{m-1}(x_{MD})^{2m}[\otimes\Pi_{k\in P_0}^{m}x_{lk}] + \\ +(x_{np})^{N-m-1}(x_{MD})^{2(N-m)}[\otimes\Pi_{k\in P_1}^{N-m}x_{lk}] - \\ -(x_{np})^{N-2}(x_{MD})^{2N}[\otimes\Pi_{k\in P_0\cdot P_1}^{N}x_{lk}]\} \quad (27)$$

If we assume that optical links have the same length, their availability is the same, i.e.

$$x_{lk} = x_l, \forall k$$

In this case, the availability between the *s* and *t* nodes is

$$A_{st}(\times,m) = (x_{nt})^2[(x_{np})^{m-1}(x_{MD})^{2m}(x_l)^m + \\ +(x_{np})^{N-m-1}(x_{MD})^{2(N-m)}(x_l)^{N-m} - (x_{np})^{N-2}(x_{MD})^{2N}(x_l)^N] \quad (28)$$

3.4 The availability of the WDM ring with optical multiplex section protection

With this type of protection optical interfaces are connected on two or four optical threads which can be in the same cable or belong to the completely separated cables. We shall limit here to four, even though the same analysis stands for two threads only that the ring capacity in that case is twice smaller [8].

In the figure below the state of the optical ring with the protection of the optical multiplex section in case of no failure is presented. With OMS-SPRing-4 optical interfaces are connected to optical fibres sharing a common conduit and to those which are routed in separate conduits.

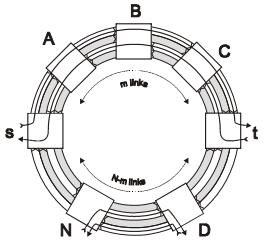

Fig. 6 WDM ring with optical multiplex section protection with 4 fibres under conditions without a failure

In a case of rupture of the optical cable, for instance between two "pass-through nodes", as a reaction to the failure the loop is formed in them and the signal is redirected to other two protection threads [9].

In addition to the working path there are several restoration paths with OMS-SPRing 4, depending on the failure place. All the failures, single or multiple, owing to which the transport signal inside the ring can be restored in less than 60 ms need to be considered in this analysis. If we suppose that there are *x* failures, availability of OMS-SPRing 4 can be written as

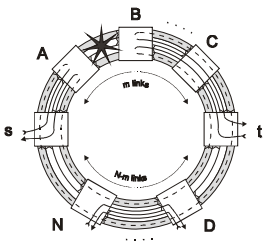

Fig. 7 WDM ring with optical multiplex section protection with 4 fibres in the case of a failure on working path

$$A_{st}(\times,m) = v_{st}(P_0)\oplus[\oplus\Sigma_{i=1}^{x}v_{st}(P_1)] \quad (29)$$

Where $v_{st}(P_0)$ is working path availability, $v_{st}(P_1)$ is availability of one of *x* restoration paths and the mark $\oplus$ represents "sum". Although the number of failures which can be restored can be high it can be demonstrated that the "sum"of all the restoration paths reduced to one path, which means:

$$v_{st}(P_{Am}) = [\oplus\Sigma_{i=1}^{x}v_{st}(P_1)] \quad (30)$$

Where $v_{st}(P_{Am})$ is the availability of the worst restoration path P_m which is the case when all the working path links and nodes are faulty. If we put the availability of the worst restoration path into the expression for OMS-SPRing 4, we obtain

$$A_{st}(\times,m) = v_{st}(P_0)\oplus v_{st}(P_{Am}) \quad (31)$$

Whereat

$$v_{st}(P_{Am}) = v_{st}(P_1)$$

which means that the same expression is obtained for the availability between two terminals using protection of the wavelength channel. Detailed analyses can be found in [10]

4. Worst Terminal Pair Availability

In order to obtain the worst availability regarding the number of links, it is necessary to derive this expression for availability under *m*

$$A_{st}(\times,m) = (x_{nt})^2[(x_{np})^{m-1}(x_{MD})^{2m}(x_l)^m + \\ +(x_{np})^{N-m-1}(x_{MD})^{2(N-m)}(x_l)^{N-m} - (x_{np})^{N-2}(x_{MD})^{2N}(x_l)^N] \quad (32)$$

When equation (32) derive by m and equalise to zero, than

$$\frac{d}{dm}[(x_{np})^{m-1}(x_{MD})^{2m}(x_l)^m + \\ +(x_{np})^{N-m-1}(x_{MD})^{2(N-m)}(x_l)^{N-m} - (x_{np})^{N-2}(x_{MD})^{2N}(x_l)^N] = 0 \quad (33)$$

After simple derivation we obtain the expression

$$\left[(x_{np})^{m-1}(x_{MD})^{2m}(x_l)^m + (x_{np})^{N-m-1}(x_{MD})^{2(N-m)}(x_l)^{N-m} \cdot \right.$$
$$\left. \cdot m(x_{np})^{-L} + 2m(x_{MD})^{-1} + m(x_l)^{-1}\right] = 0 \quad (34)$$

After arranging we obtain

$$m - 1 = N - m - 1, \Rightarrow m = N/2$$

$$2m = 2(N - m), \Rightarrow m = N/2$$

$$m = N - m, \Rightarrow m = N/2$$

This is valid for even number. Since m has to be whole number, this expression cannot be applied for uneven number N and the following is used

$$m = \frac{N-1}{2}$$

Examine is about the minimum or maximum. We have to determine second derivation of this expression and determine whether it is > 0 or < 0

$$\left[(x_{np})^{m-1}(x_{MD})^{2m}(x_l)^m + (x_{np})^{N-m-1}(x_{MD})^{2(N-m)}(x_l)^{N-m} \cdot \right.$$
$$\left. \cdot m(x_{np})^{-L} + 2m(x_{MD})^{-1} + m(x_l)^{-1}\right] = 0 \quad (35)$$

By simple calculation, it is possible to demonstrate that the second derivation is >0 and that it is about the minimum or, in other words, the worst availability which is obtained for $m = N/2$ for even number of nodes and

$$m = \frac{N-1}{2}$$

for odd number of nodes.

5. Numerical Results

In order to calculate the availability for a WDM system we need to know the nodes and optical links availability. For availability calculation, in general, one needs to know the intensity of failures for the individual components, the data of which are shown in Table 1, and are taken from different literature and published works [6].

Availability data for optical components (W = 64) Table 1

Component/Device	Symbol	Failure rate rarateRate(FIT)
Line Amplifier	LOA	3200
Multiplexer	MUX	25xW
Demultiplexer	DEMUX	25xW
Optical Switch	OSW	1000
Fix Transmitter	TX	186
Fix Receiver	RX	70
Cable (per km)	OC	100

NOTE: W is the number of wavelength channels

MDT (min/year) for a node with active components Table 2

	MDT
MTTR = 6 h	λ = 64
Terminal	3.22
Pass-through	0.000018

We shall calculate the availability for different number of nodes, from 6 to 10 which is a common size of rings in realistic networks and equal link length of 20 km. For MTTR equipment and cables 6 and 12 hours is taken, which is also common in practice.

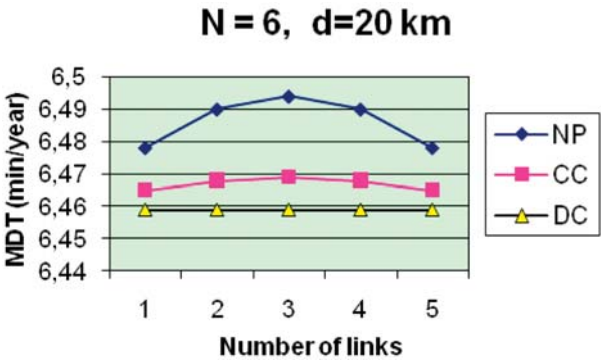

Fig. 8 MDT (min/year) for N = 11 and d = 20 km

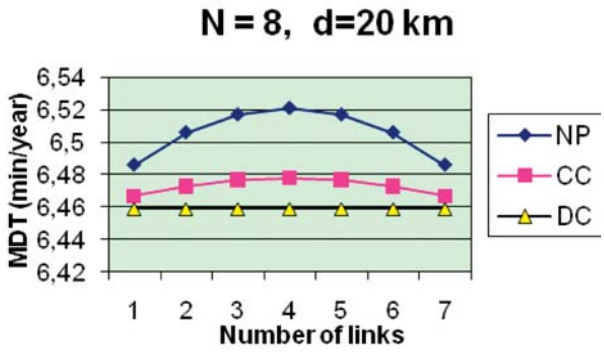

Fig. 9 MDT (min/year) for N = 12 and d = 20 km

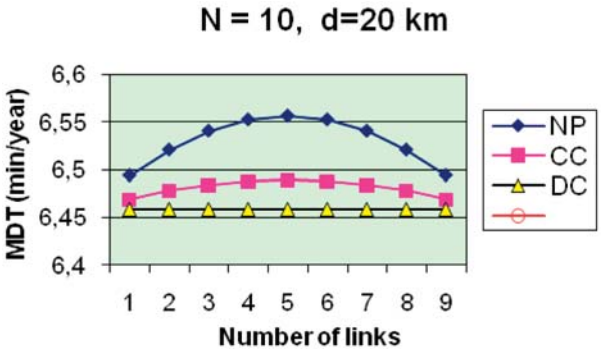

Fig. 10 MDT (min/year) for N = 12 and d = 60 km

As can be seen in the previous graphs, the obtained worst availability expressed over MDT is in accordance with the earlier derived expression for the number of links of the working path, so for example, for the ring with different number of nodes which is unprotected, we have:

- $N = 6$, $m = N/2 = 3$, MDT = 6.494
- $N = 8$, $m = N/2 = 4$, MDT = 6.521
- $N = 10$, $m = N/2 = 5$,MDT = 6.557

It can also be seen that with the increment of the number of nodes, unavailability is increased with the same length of links. Also, by applying protection, the number of unavailable minutes per year is decreased: i.e. for $N = 6$, MDT for the case of protection through the same cable in comparison with the case without protection is decreased by 0.38% and for the case of totally separated cables, the difference is increased to 0.54%. The difference between the worst availability and the availability which is obtained for the certain number of links of the working path is decreased by applying protection: i.e. if we observe MDT for $N = 8$ unprotected, the difference between the worst availability which is in this case for 4 links of the working path and availability for 1 link of the working path is 0.035 min/year while for the case of protection through the same cable that difference is 0.011 min/year and for the case of totally separated cables, the difference is zero-meaning that the availability is always equal, notwithstanding the number of links of the working path. Also this difference is increasing by the increment of the number of nodes, so if we suppose the same length of links for the ring-unprotected, the biggest difference from 0.063 min/year ($N = 10$), 0.035 min/year ($N = 8$) to 0.016 min/year ($N = 6$). For the cases with protection those differences are even smaller. Therefore, we can conclude that all the availabilities between two terminals, notwithstanding the number of links of the working path, are approximately equal for a given ring and that the availability between two terminals for a given ring notwithstanding protection can be presented through the worst availability.

6. Conclusion

The analysis of the results on different WDM rings shows that the worst availability is obtained in accordance with the earlier derived expression for the number of links of the working path and that is $m = N/2$ for the even number of links and $m = N - 1/2$ for uneven number of links of the working path. It is also to note that with the premise of the same length of links, the unavailability is increasing with the increment of the number of nodes in the ring. Also by applying different methods of protection, the unavailability in relation to the case without protection is decreasing and it is the smallest in the case when totally separated cables are used for protection. Due to small differences between the worst availability and the availability between two terminals notwithstanding the number of links of the working path presuming that the links are of the same length, the availability between two terminals can generally be presented through the worst availability and as such can be used as a parameter when projecting new or when reporting on the performances of the existing networks.

References

[1] MELLO, A.A., PELEGRINI, J.U., RIBERIO, R.P., SCHUPKE, D.A., WALDMAN, H.: *Dynamic Provisioning of Shared-Backup Path Protected Connections with Guaranteed Availability Requirements*, International Workshop on Guaranteed Optical Service Provisioning, Boston, USA, 2005

[2] DOUGLAS, S.R.: Network Reliability and Algebraic Structures, *Oxford University Press* : New York, 1991,

[3] JONCZY, J.: *An algebraic Approach to Network Reliability,* Institute of Computer Science and Applied Mathematics, University of Berne, 2008

[4] TRSTENSKY, D., SCHWARTZ, L., TRUNKVALTER, M., BAROS, R.: *Reliability of Telecommunication System by Various Repair Regime,* Int. Conference ELEKTRO 2004, Advances in Electrical and Electronic Engineering, No. 2, Vol. 3/2004, ZU, Zilina, pp. 25–26, ISSN 1336-1376

[5] WILSON, M.R.: The Quantitative Impact of Survivable Network Architecture on Service Availability, *IEEE Communications Magazine,* May 1998, pp.122–127,

[6] RADOS, I.: Availability Models for Wavelength Channel Protection in WDM Ring Networks, *J. of Electronics and Electrical Engineering,* No. 8(88), 2008, pp.81–86, Kaunas University of Technology

[7] MELLO, A.A., QUITERIO, G.S., SCHUPKE, D.A., WALDMAN, H.: *Specification of SLA Survivability Requirements for Optical Path Protected Connections*, Optical Fiber Communications Conference (OFC), Anaheim, 2006,

[8] ZHANG, J., ZHU, Z., ZANG, H., MUKHERJEE, M.: *Service Provisioning to Provide Per-Connection-based Availability-Guarantee in WDM Mesh Networks,* Optical Communications Conference (OFC), 2003,

[9] MYKKELTVEIT, A., HELVIK, B.E.: *On Provision of Availability Guarantees Using Shared Protection*, Optical Network Desing and Modeling (ONDM), 2008,

[10] RADOS, I.: *Availability of the optical bidirectional self-healing ring with four fibres with the Multiplex Section ProtectionAvailability,* SoftCOM 2008, Split.

Zdena Kralova – Julius Zimmermann *

SLOVAK-ENGLISH VOCALIC APPROXIMATION

The article is focused on the quality of English pronunciation of Slovak native speakers reflected in the formant structure of their short English vowels compared to the reference formant values of short English and Slovak vowels. The primary objective is to detect the level of phonic approximation within the system of English short vowels.

Key words: Pronunciation. Slovak. English. Short vowels.

1. Introduction

Besides the dominating behaviorist and structuralist theories of the Second Language Acquisition a new concept of the second language (L2) acquisition was formulated in the 1960s – the theory of interlanguage [1–5]. Some other names used for the interlanguage phenomenon are: transitive competence [1], approximative system [4], idiosyncratic dialect [6], multicompetence [7], transmitting or the third system [8].

The theory of interlanguage considers a foreign language competence to be a process of an autonomous language code creation which gradually (successively or continually) approximates to the foreign language quality in the process of qualitative and quantitative improvement [9]. Thus the interlanguage is a synchronic profile of a diachronic process of L2 acquisition/learning.

Interlanguage (current language competence of an individual) has some features of an idiolect and a dynamic character, therefore a mistake is considered part of language development [10]. Ideally, the interlanguage consists of less and less features of the mother tongue (L1) and of more and more features of the foreign language. The transitive intercode should reflect the potential quality of a L2 competence in 1–100% interval [8]. But, in fact, stagnation and fossilization are much more frequent.

Early trends in the Second Language Acquisition research considered mistake a negative phenomenon and the L2 sounds produced by a non-native speaker were evaluated as correct or incorrect discrete entities. Today, mistakes are thought as a continuum of approximations towards L2 sounds which is influenced by the current language competence more than by the language interference [11].

The Phonological Translation Hypothesis [12] analogically claims that the dominance of L1 sound system is a more probable reason of non-authentic L2 pronunciation than restrictions resulting from the neuro-physiological maturity of an individual. The Upper Limit/Level Hypothesis [13] similarly says that there exists a maximum limit of similar L1 and L2 sounds approximation, where the speakers mix L1 and L2 quality of phones (Merger Hypothesis) [14], but usually do not reach the authentic pronunciation of a native speaker.

Apart from the presupposition that each non-native speaker has an upper limit of approximation to the target level of pronunciation [13], some experiments [14–16] proved the possibility of continuous improvement in L2 phonic competence. Thus the phonetic categories should be gradually optimized and created before the equivalent phonological categories are created. According to L. J. Dickerson [16] the most significant pronunciation deviations are being eliminated first in this process. The close approximations seem to be the most persistent ones. According to the theory of language interference [17], the interlingual identification of sounds significantly contributes to the upper limit of approximation.

Phonological differences between L1 and L2 are not the only ones (or the most important) determinants of L2 sound production quality. The learners must acquire a new complex of articulatory gestures and modify the existing phonetic models, while they often produce the scale of sound variants for one phoneme – a continuum of approximations to the prototype L2 sounds. The phonic interference thus inhibits the approximation to the target system via similarity and difference of elements. The interference is one of the interlanguage phenomena and one, but not the only, reason of non-authentic L2 pronunciation.

2. Methodology

We focused on the quality of English pronunciation of Slovak speakers and its reflection in the formant structure of short vowels.

* **Zdena Kralova[1], Julius Zimmermann[2]**
[1] Department of English Language and Literature, Faculty of Humanities, University of Zilina, Slovakia; zdena.kralova@fpv.uniza.sk
[2] Department of Slovak Studies, Slavonic Philologies, and Communication, Faculty of Arts, P. J. Safarik University in Kosice, Slovakia

Our primary objective was to detect the level of the qualitative approximation of the short English vowels produced by Slovak speakers to the English reference values. The Slovak language is considered primary, native, dominant and interfering system (L1) and the English language is the secondary, non-native, non-dominant, interfered system (L2). We recorded spontaneous English monologues of the Slovak speakers. Then we segmented short English vowels from each text and we experimentally analyzed the values of the first and the second formants of seven short English vowels. Then we statistically compared the detected F1 a F2 values and the reference values of the given vowels mentioned in the relevant phonetic publications [18, 19] for the phonic approximation.

Subjects

We worked with the group of 40 Year 1 students (30 female, 10 male) all enrolled in the study program of English Language and Literature at the Faculty of Humanities, University of Zilina, Slovakia. The average age of the respondents was 19, they all were of Slovak nationality, their mother tongue was Slovak and they all reported normal hearing dispositions. Their average English lexical and grammatical competence was at B1 and B2 levels of the Common European Framework of Reference for Languages (CEFR) [20]. Most of them started learning English at the first level of elementary school with a non-native English teacher. Most of them have never stayed in an English-speaking country for a longer period.

Material

The recordings of the English monologues of each of the 40 respondents (average length 3.8 minutes) were the basic research material. To maintain a similar lexis and style of the respondents' utterances we chose an autobiographical topic. We considered spontaneous speech more natural than reading isolated lexical units. Though the canonic (non-coarticulated) form of vowels is the most suitable for the experimental analysis, we tried to simulate the real L2 performance in which the speaker concentrates more on the content than on its phonetic form. The dialogue with a native speaker would have corresponded with real communication better, but for the practical reasons we chose a one-way type of communication.

Because of the great formant variation of each individual and a relatively high contextual variability (transgresivity) of vowels it was necessary to respect the specificity of the speaker and to define the resulting data according to several measurements of several speakers. Concerning the type of text it was not always possible to keep the context compatibility and the preceding and following segmental environment in all analyzed units [e.g., 21]. The input data for the experimental analysis were segmented from the corpus of spoken texts in English. We selected each of the seven short English vowels /*I*/, /*e*/, /*æ*/, /Λ/, /*D*/, /ʊ/, /*ə*/ in five different manifestations from each text.

Procedure

a) We recorded the spontaneous English monologues of each respondent using a condenser microphone.
b) We segmented the short vowels from the texts.
c) The segments were experimentally analyzed in the Speech Analyzer system.
d) The results of the experimental analysis were statistically analyzed.

3. Results

We chose the formants of short English vowels as the locus of the English phonic competence dynamics. The selected segments were experimentally analyzed, in the Speech Analyzer program (Version 2.7) SIL International. JAARS – ITS, Waxhaw, NC.

The units of the corpus were analyzed by oscillography, spectrography and spectral analysis. In our phonetic research we applied the following procedure:

a) we displayed an oscillogram, wide-band sonagram and LPC spectrum in the Speech Analyzer program (Figure 1);
b) we marked the place in the given oscillogram, where the biggest alternation of the amplitude, frequency and acoustic wave was observed and we manually segmented the given segment via audio-correlation and visual-correlation methods;
c) we made a spectral analysis of the given segment and we read F1 and F2 from the LPC spectrum;
d) we calculated the mean values from the five measured F1 a F2 values of each analyzed sound of each respondent.

The data from the experimental analysis were statistically characterized by the parameters of position and parameters of variability (Table 3).

Parameters of position:

$\bar{x}$ – arithmetic average of the data (mean);
$\tilde{x}$ – median (medium value, which divides the statistical set into two equal parts);

Parameters of variability:

σ_x – standard deviation (absolute measure of variability);
V_x – variation coefficient (relative measure of variability).

Vowels are acoustically characterized by spectral areas defined by the relations of formant frequencies in two-dimensional (F1/F2) spectral structure in Hz. Their mutual articulatory and acoustic discreteness is lower than that of the consonants. The variation interval of the formants is rather big. A person is not able to create an absolutely identical articulatory position twice and the variance also depends on the characteristics of the neighbouring sounds.

The mean values of the formants of the English vowels produced by the respondents (A) are shown in Table 3. When displaying the vowels in the formant scheme the average values of formants are used. The variation of formant values was rather low (under 50%) except F2 [*ə*] (Vx = 55%). The reference values of the English (A^0) and Slovak (S^0) vowels used are cited from relevant linguistic publications [18, p. 100; 19, pp. 204–209] and are shown in Table 2.

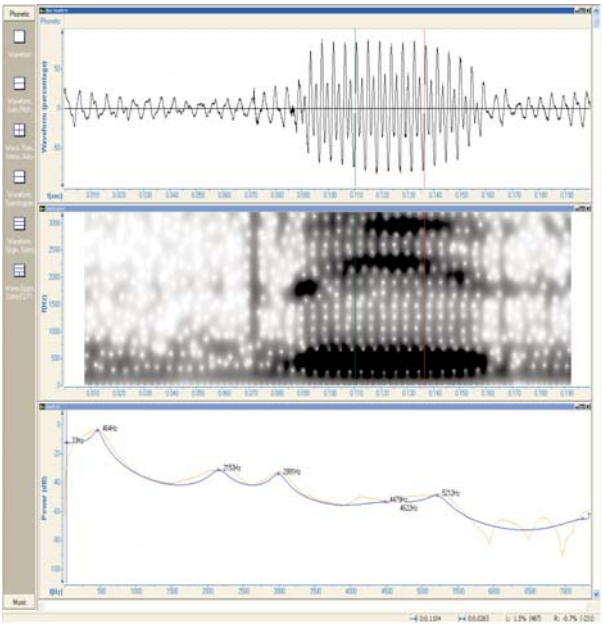

Fig. 1 Experimental analysis (a sample)

We observed a higher approximation of the produced vowels to the Slovak reference values than to the English reference values which can be seen in the formant scheme (Fig. 2). This is an obvious and expected result. The Slovak language as the dominant system significantly influences the production of the secondary (English) system elements. The interlanguage interference, especially at the intermediate level of L2 competence, is the dominant feature of the whole L2 performance.

System of Slovak and English short vowels — Table 1

	Front	Central	Back
High	/i/, /I/		/u/, /ʊ/
Mid	/e/, /e/	/ə/	/o/
Low	/æ/	/ä/, /a/, /Λ/	/D/

Reference values of F_1 and F_2 — Table 2

S^0	F_1	F_2	F_3	A^0	F_1	F_2	F_3
/i/	280	1916	2656	/I/	360	2220	2960
/e/	452	1718	2365	/e/	600	2060	2840
/ä/	700	1510	2300	/æ/	800	1760	2500
/a/	682	1315	2293	/Λ/	760	1320	2500
/o/	481	1084	2194	/D/	560	920	2560
/u/	326	967	2059	/ʊ/	380	940	2300
				/ə/	560	1480	2520

Experimental values of F_1 and F_2 (A) — Table 3

A	/I/		/e/		/æ/		/Λ/		/D/		/ʊ/		/ə/	
	F_1	F_2	F_1	F_2	F_1	F_2	F_1	F_2	F_1	F_2	F_1	F_2	F_1	F_2
1	308	1492	355	1702	689	1666	779	966	407	1009	281	982	301	1615
2	257	2279	478	2055	723	1680	793	1432	426	1296	368	1233	732	2003
3	253	1789	329	1838	495	1270	365	912	492	1091	318	1118	517	1227
4	306	2369	507	1995	388	1258	511	1478	388	1186	450	877	457	1873
5	318	2348	505	1938	989	1566	563	1430	457	1009	353	809	581	1744
6	264	1854	386	1943	668	1446	758	1497	381	963	465	882	397	1766
7	323	1456	518	1692	689	1593	904	1430	421	1570	486	914	711	2110
8	323	1310	410	2151	775	1744	806	1370	632	1197	409	1133	497	1830
9	235	1780	458	1689	474	1572	891	1357	721	1589	480	831	732	1852
10	234	2052	399	1157	495	1462	409	1379	571	981	366	790	366	926
11	283	1922	492	2133	797	1465	493	1138	651	861	317	903	454	2175
12	377	2098	372	1562	603	1400	507	1745	633	993	297	676	475	2369
13	314	2345	513	2028	732	1538	785	1177	492	1246	407	994	383	1016
14	358	2220	367	1842	632	1690	419	1311	399	1054	366	824	432	1637
15	354	2380	375	1634	538	1852	327	1195	581	1140	417	727	430	7809
16	359	1968	465	1818	517	1787	499	1428	253	713	274	834	280	1400
17	394	1940	480	1827	495	1481	886	1727	509	1163	443	1140	489	1744
18	296	2205	467	1800	603	1538	689	1721	543	1153	388	1191	603	2089

A	/I/		/e/		/æ/		/Λ/		/D/		/ʊ/		/ə/	
	F_1	F_2	F_1	F_2	F_1	F_2	F_1	F_2	F_1	F_2	F_1	F_2	F_1	F_2
19	298	2249	555	1749	770	1636	758	1384	368	1099	372	895	624	1830
20	329	2203	489	1725	452	1486	568	1329	504	1224	361	752	668	1680
21	359	1172	515	1890	431	1873	676	1291	382	1053	394	803	581	1723
22	359	2185	412	2331	452	1529	716	1259	326	891	315	876	495	1744
23	330	2325	576	1162	668	1809	579	1564	570	1150	354	764	646	1809
24	317	2114	436	1948	942	1670	780	1394	531	771	346	933	397	1830
25	338	2218	569	1791	560	1766	637	1410	562	786	453	965	388	1830
26	360	2233	503	1474	689	1615	993	1715	506	1135	390	897	383	1787
27	262	1489	465	1830	345	1916	702	1223	742	1070	469	934	646	1895
28	302	1543	508	1626	814	1461	542	1334	263	1303	364	1103	350	1030
29	270	1437	512	1614	732	1292	865	1338	262	1279	335	882	397	1314
30	300	1718	615	1802	775	1658	796	1300	698	1078	397	1121	711	2046
31	236	1592	592	2037	668	1852	827	1336	458	1235	449	1111	475	1787
32	332	2367	610	1959	603	1530	472	1224	577	1408	504	1094	754	1960
33	349	1996	517	1707	474	1464	526	1030	512	1214	338	819	301	1615
34	332	1646	744	2072	646	1560	408	1392	502	1246	369	1390	511	1744
35	426	1185	550	1289	861	1532	472	900	358	966	336	1046	380	1890
36	318	1578	886	1823	747	1420	876	1362	490	944	420	824	377	1016
37	308	2059	366	2039	431	1227	463	1512	590	1060	479	1087	517	1787
38	316	1590	615	1869	760	1555	624	1200	420	1295	374	955	383	1003
39	352	1899	619	2023	643	1787	637	1542	626	984	358	989	454	1744
40	268	1969	433	2147	417	1205	380	1352	435	1240	388	1120	388	1916
$\bar{x}$	**315**	**1914**	**499**	**1818**	**630**	**1571**	**642**	**1352**	**491**	**1116**	**386**	**955**	**492**	**1854**
$\tilde{x}$	**317.5**	**1968.5**	**497.5**	**1828.5**	**644.5**	**1557.5**	**637**	**1359.5**	**497**	**1117**	**373**	**923.5**	**466**	**1787**
σ_x	**44.18**	**355.34**	**108.48**	**253.62**	**155.05**	**182.65**	**177.87**	**200.36**	**122.16**	**190.37**	**58.69**	**157.01**	**132.20**	**1023.86**
Vx	**0.14**	**0.19**	**0.22**	**0.14**	**0.25**	**0.12**	**0.28**	**0.15**	**0.25**	**0.17**	**0.15**	**0.16**	**0.27**	**0.55**

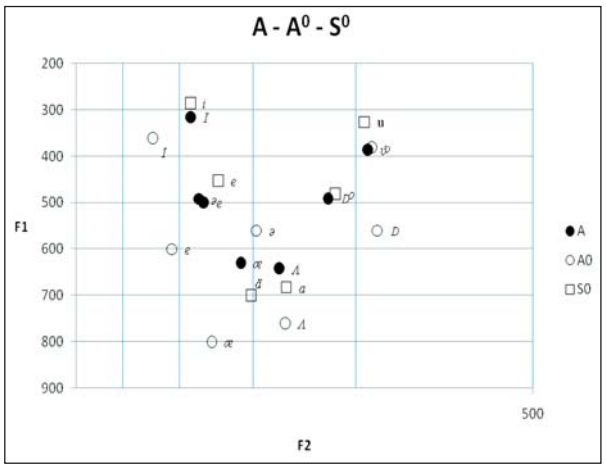

Fig. 2 Values F_1 a F_2 (A - A^0 - S^0)

4. Conclusions

In the experiment we applied the synthesis of the theoretical analysis and we detected the causal relations of the parameters by the statistical analysis of the variables. The consistency of repeated measurements of each text is verified by an adequate variance of measurements (V_x). To provide the internal validity of measurements we used the statistical analysis of variance. To increase the external validity of measurements, i.e., to generalize the research results, we performed the experiment in fairly natural conditions – in the school environment and we used the research material reflecting natural communication.

Content validity results from the fact that the results of vocalic formant measurement of individual respondents represent an overall level of their pronunciation. The criteria validity was evaluated according to the correspondence of experimental analysis and the reference values of the phonemes.

From the percipient's point of view, the auditive impression of a "good" or "bad" pronunciation is created by the complex of many subsegmental, segmental, plurisegmental and suprasegmental phonic phenomena. Some studies [e. g., 11] proved that the number of segmental substitutions highly correlates with marking the utterance as unidiomatic (non-native), though it does not mean that the substitutions are the only criterion. They are probably perceived and identified very easily, but the listener's impression of one`s pronunciation is created by the complex of many interrelated factors [22].

References

[1] CORDER, P. S.: The Significance of Learner's Errors, *IRAL*, No. 4, pp. 161–170, 1967.
[2] SELINKER, L.: Language Transfer, *General Linguistics*, No. 2, pp. 67–92, 1969.
[3] SELINKER, L.: Interlanguage, *IRAL*, No. 3, pp. 209–231, 1972.
[4] NEMSER, W.: Approximative Systems of Foreign Language Learners, *IRAL*, No 2, pp. 115–123, 1971.
[5] RICHARDS, J.: Error Analysis and Second Language Strategies, *Language Sciences*, No. 17, pp. 12–22, 1971,
[6] CORDER, P. S.: Idiosyncratic Dialects and Error Analysis, *IRAL*, No. 2, pp. 147–160, 1971.
[7] COOK, V.: *Second Language Learning and Language Teaching,* London : Edward Arnold, 1991.
[8] HRDLICKA, M. *To the Problems of Foreign Language Code Acquisition,* Casopis pro moderni filologii, No. 1, pp. 36–43, 2004.
[9] FLEGE, J. E.: *Phonetic Interference in Second Language Acquisition,* Bloomington : Indiana University, 1979.
[10] GONDOVA, D.: Using Activities as a Way of Proceduralization of Learners' Language Knowledge, *Communications. Scientific Letters of the University of Zilina*, Vol. 12, 2010, No. 3, pp. 30–34.
[11] MALA, E.: Influence of English on the Slovak Language, In: *Inonarodne sociokulturne fenomeny a cudzojazycne vzdelavanie.* Nitra: FEM SPU, 2004.
[12] FLEGE, J. E.: The Phonological Basis of Foreign Accent: A Hypothesis, *TESOL Quarterly,* No. 4, pp. 443–455, 1981.
[13] FLEGE, J. E., HILLENBRANDT, J. 1984. Limits on Pronunciation Accuracy in Adult Foreign Language Speech Production, *J. of the Acoustical Society of America,* No. 3, pp. 708–721.
[14] FLEGE, J. E.: The production of "new" and "similar" phones in a foreign language: Evidence for the effect of equivalence classification, *Journal of Phonetics,* No. 1, pp. 47–65, 1987.
[15] ASHER, J. J., GARCIA, R.: The optimal age to learn a second language, *The Modern Language Journal*, n. 5, pp. 334–341, 1969.
[16] DICKERSON, L. J.: *Internal and External Patterning of Phonological Variability in the Speech of Japanese Learners of English: Toward a Theory of Second-language Acquisition,* Chicago: University of Illinois, 1974.
[17] WEINREICH, U.: *Languages in Contact*, New York : Linguistic Circle of New York,1953.
[18] GIMSON, A. C. *An Introduction to the Pronunciation of English,* Newcastle upon Tyne : Athenaeum Press, 1989.
[19] KRAL, A., SABOL, J.: *Phonetics and Phonology (in Slovak)*, Bratislava: Slovenske pedagogicke nakladatelstvo, 1989.
[20] *Council for Cultural Co-operation: Common European Framework of Reference for Languages,* Olomouc: Univerzita Palackeho, 2002.
[21] SABOL, J., ZIMMERMANN, J.: *Statistics. Exact methods in Linguistics and Literary Science (in Slovak),* Presov : Filozoficka fakulta UPJS Presov, 1986.
[22] LELAKOVA, E.: Application of Field and Matrix Theory on Lexico-semantic Analysis of English Nouns of Happiness, *J. of Interdisciplinary Philogy,* Vol. 1, 2010, No. 2, pp. 19–46.

COMMUNICATIONS – Scientific Letters of the University of Zilina
Writer's Guidelines

1. Submissions for publication must be unpublished and not be a multiple submission.
2. Manuscripts written **in English language** must include **abstract** also written in English. The submission should not exceed **10 pages** with figures and tables (format A4, Times Roman size 12). The **abstract** should not exceed 10 lines.
3. Submissions should be sent: **by e-mail** (as attachment in application MS WORD) to one of the following addresses: *komunikacie@uniza.sk* or *holesa@uniza.sk* or *vrablova@uniza.sk* or *polednak@fsi.uniza.sk* **with a hard copy** (to be assessed by the editorial board) **or on a CD** with a hard copy to the following address: Zilinska univerzita, OVaV, Univerzitná 1, SK-010 26 Zilina, Slovakia.
4. Abbreviations, which are not common, must be used in full when mentioned for the first time.
5. Figures, graphs and diagrams, if not processed by Microsoft WORD, must be sent in electronic form (as GIF, JPG, TIFF, BMP files) or drawn in contrast on white paper, one copy enclosed. Photographs for publication must be either contrastive or on a slide.
6. References are to be marked either in the text or as footnotes numbered respectively. Numbers must be in square brackets. The list of references should follow the paper (according to **ISO 690**).
7. The author's exact **mailing address of the organisation where the author works, full names, e-mail address or fax or telephone number,** must be enclosed.
8. The editorial board will assess the submission in its following session. In the case that the article is accepted for future volumes, the board submits the manuscript to the editors for review and language correction. After reviewing and incorporating the editor's remarks, the final draft (before printing) will be sent to authors for final review and adjustment.
9. The deadlines for submissions are as follows: September 30, December 31, March 31 and June 30.

COMMUNICATIONS

SCIENTIFIC LETTERS OF THE UNIVERSITY OF ZILINA
VOLUME 13

Address of the editorial office:
Zilinská univerzita
Office for Science and Research
(OVaV)
Univerzitna 1
SK 010 26 Zilina
Slovakia
E-mail: komunikacie@nic.uniza.sk,
pavel.polednak@fsi.uniza.sk

Each paper was reviewed by two reviewers.

Journal is excerpted in Compendex and Scopus

It is published by the University of Zilina in
EDIS – Publishing Institution of Zilina University
Registered No: EV 3672/09
ISSN 1335-4205

Published quarterly

Single issues of the journal can be found on:
http://www.uniza.sk/komunikacie